

Fine Structure of Metric Type IV Radio Bursts Observed with the ARTEMIS-IV Radio-Spectrograph: Association with Flares and Coronal Mass Ejections

C. Bouratzis · A. Hillaris · C.E. Alissandrakis ·
P. Preka-Papadema · X. Moussas · C. Caroubalos ·
P. Tsitsipis · A. Kontogeorgos

Received: 23 September 2013 / Accepted: 17 June 2014 / Published online: 9 July 2014
© Springer Science+Business Media Dordrecht 2014

Abstract Fine structures embedded in type IV burst continua may be used as diagnostics of the magnetic-field restructuring and the corresponding energy release associated with the low-corona development of flare or coronal mass ejection (CME) events. A catalog of 36 type IV bursts observed with the SAO receiver of the ARTEMIS-IV solar radio-spectrograph in the 450–270 MHz range at high cadence (0.01 sec) was compiled; the fine structures were classified into five basic classes with two or more subclasses each. The time of fine-structure emission was compared with the injection of energetic electrons as recorded by hard X-ray and microwave emission, the soft X-ray (SXR) light curves and the CME onset time. Our results indicate a very tight temporal association between energy release episodes and pulsations, spikes, narrow-band bursts of the type III family, and zebra bursts. Of the remaining categories, the featureless broadband continuum starts near the time of the first energy release, between the CME onset and the SXR peak, but extends for several tens of minutes after that, covering almost the full extent of the flare–CME event. The intermediate drift bursts, fibers in their majority, mostly follow the first energy release, but have a wider distribution than other fine structures.

Keywords Radio bursts · Dynamic spectrum · Meter-wavelengths and longer · Association with flares · Coronal mass ejections

New eyes looking at solar activity: Challenges for theory and simulations.
Guest Editors: Silja Pohjolainen and Marian Karlický

C. Bouratzis · A. Hillaris (✉) · P. Preka-Papadema · X. Moussas · C. Caroubalos
University of Athens, 15784 Athens, Greece
e-mail: ahillaris@phys.uoa.gr

C.E. Alissandrakis
University of Ioannina, 45110 Ioannina, Greece

P. Tsitsipis · A. Kontogeorgos
Technological Educational Institute of Lamia, 35100 Lamia, Greece

1. Introduction

Solar metric radio bursts provide a unique diagnostic of the development of flare or coronal mass ejection (CME) events in the low corona; their onset and evolution coincides with an extended opening of the magnetic field, accompanied by energetic-particle acceleration and injection into interplanetary space as well as shocks (*e.g.* review by Pick and Vilmer, 2008). Their signatures at metric–decimetric and longer waves trace disturbances that propagate from the low corona to interplanetary space.

The complexity of these processes is reflected in a diversity of forms in dynamic spectra, which exhibit a variety of fine structures in time and frequency; these are characterized by a wide range in period, bandwidth, amplitude, and temporal and spatial signatures. The fine structures may be used to study in detail the magnetic-field restructuring and the corresponding energy release associated with solar flare/CME events (*e.g.* reviews by Benz, 2003; Nindos and Aurass, 2007). A number of morphological taxonomy schemes, mostly in the microwaves and the decimetric frequency range, have been presented (Bernold, 1980; Slottje, 1982; Güdel and Benz, 1988; Allaart *et al.*, 1990; Isliker and Benz, 1994; Jiříčka *et al.*, 2001; Fu *et al.*, 2004), of which the most recent are also the most comprehensive.

In this work we examine fine structures observed during type IV solar radio events observed with the ARTEMIS-IV solar radio-spectrograph from the beginning of 1999 until the end of 2005; to these we added two well-observed events with rich fine structure recorded in 2010. Some of these events were first cataloged in Caroubalos *et al.* (2004). Our study concentrates on a statistical analysis of the fine structures and their association with the various phases of the flare/CME phenomenon, which might be useful for understanding details of the evolution of the solar energetic phenomena through their radio signatures. In developing our classification scheme, we have built upon the Ondřejov catalog (Jiříčka *et al.*, 2001; Jiříčka, Karlický, and Mészárosová, 2002; Mészárosová, Karlický, and Jiříčka, 2005), which was based on data in the 0.8–2.0 GHz range.

In Section 2 we discuss the instrumentation and data selection. The results of our morphological analysis and classification are given in Section 3, the relative timing of fine structures with respect to the flare evolution is discussed in Section 4, and the conclusions are presented in Section 5.

2. Observations and Data Selection

The basic data used in this study are the high- and medium-resolution dynamic spectra recorded by the ARTEMIS¹–IV solar radio-spectrograph at Thermopylae (Caroubalos *et al.*, 2001, 2006; Kontogeorgos *et al.*, 2006). It consists of a 7 m parabolic antenna that covers the metric range; to this, a dipole aerial adapted to the decametric range was added in October 2002. Two receivers operate in parallel: a sweep frequency analyzer (ASG) that covers the 650–20 MHz range in 630 channels with a cadence of 10 samples/sec, and a high-sensitivity multichannel acousto-optical analyzer (SAO) that covers the 270–450 MHz range in 128 channels with a high time resolution of 100 samples/sec. The narrow-band high time resolution SAO recordings are used to analyze the fine temporal and spectral structures and constitute the main data set of this work. The broad-band medium time resolution data of the ASG, on the other hand, are used to detect and analyze radio emission from the base of the corona to $\sim 2 R_{\odot}$.

¹Appareil de Routine pour le Traitement et l'Enregistrement Magnétique de l' Information Spectral.

To study the association of the fine structures with the flare evolution, we used the following data:

- CME data from the LASCO coronagraph (Brueckner *et al.*, 1995) online² event list (Yashiro *et al.*, 2004; Gopalswamy *et al.*, 2009); the CME onset times used in this study were estimated from the LASCO movies using the linear regression by Yashiro *et al.* (2001) and are included in the online LASCO event list. We supplemented this data set with information from the CACTUS³ CME catalog (Robbrecht and Berghmans, 2004; Robbrecht, Berghmans, and der Linden, 2009).
- The NOAA *Solar Geophysical Data* catalogs and soft X-ray (SXR) online⁴ light curves from GOES. The SXR observations provide a fairly accurate estimate of the start of solar flares and a less accurate one of their end time; the corresponding source locations are also included in the NOAA catalog and are used in this work in addition to the EIT images to establish the spatial association of the SXR flare–CME–radio emission (see below).
- Hard X-ray (HXR) light curves were obtained from the RHESSI (Lin, 2001; Lin *et al.*, 2002) archive for the events after the beginning of 2003. For the events prior to 2003 we used data from the MTI/HXRS experiments (Fárník, Garcia, and Karlický, 2001) and BATSE/GRP (Fishman *et al.*, 1982, 1984).
- Microwave data from the *Radio Solar Telescope Network* (RSTN, Guidice *et al.*, 1981) at 4.995 GHz; in a few events the 2.695 GHz channel of the *Trieste Solar Radio System* (TSRS Messerotti, Zlobec, and Padovan, 2001) was used instead.
- Two-dimensional images of the Sun at five frequencies (164, 236.6, 327, 410.5, and 432 MHz) from the *Nançay Radio Heliograph* (NRH) (Kerdran and Delouis, 1997). All five frequencies are within the spectral range of the ASG, while the last three are also within the range of the SAO; they thus supplement the dynamic spectra with positional information on the radio emission. A detailed investigation of the fine-structure positions with respect to the bulk of the type IV emission has not been attempted in this work, but will be the subject of subsequent publications.
- Images from the *Extreme Ultraviolet Imaging Telescope* (EIT) onboard SOHO (Delaboudinière *et al.*, 1995); they were used to obtain information on the position of the associated flare.

The soft X-ray light curves provided the overall time evolution of the flares; the microwave and hard X-ray light curves, which are very good signatures of electron acceleration, were used to estimate the time of the first major episode of energy release. This time was used as a reference for the relative timing of fine structures. To determine the association of the type IV radio events with flare emissions and CMEs we used spatial and temporal criteria as follows (see also Caroubalos *et al.*, 2004, where similar criteria were employed):

- For the type IV flare association: to determine the temporal association we required the overlap, at least in part, of the total duration of the flare with the total duration of the radio emission (see Figure 1 for an example). To determine the spatial association we used positional data from the *Nançay Radio Heliograph* images and movies; we examined coincidence with flares using their position recorded in the NOAA *Solar Geophysical Data* catalogs. If both criteria were satisfied, we classified the association as excellent; if

²http://cdaw.gsfc.nasa.gov/CME_list/.

³<http://sidc.oma.be/cactus/>.

⁴<http://www.swpc.noaa.gov/ftpmenu/indices/>.

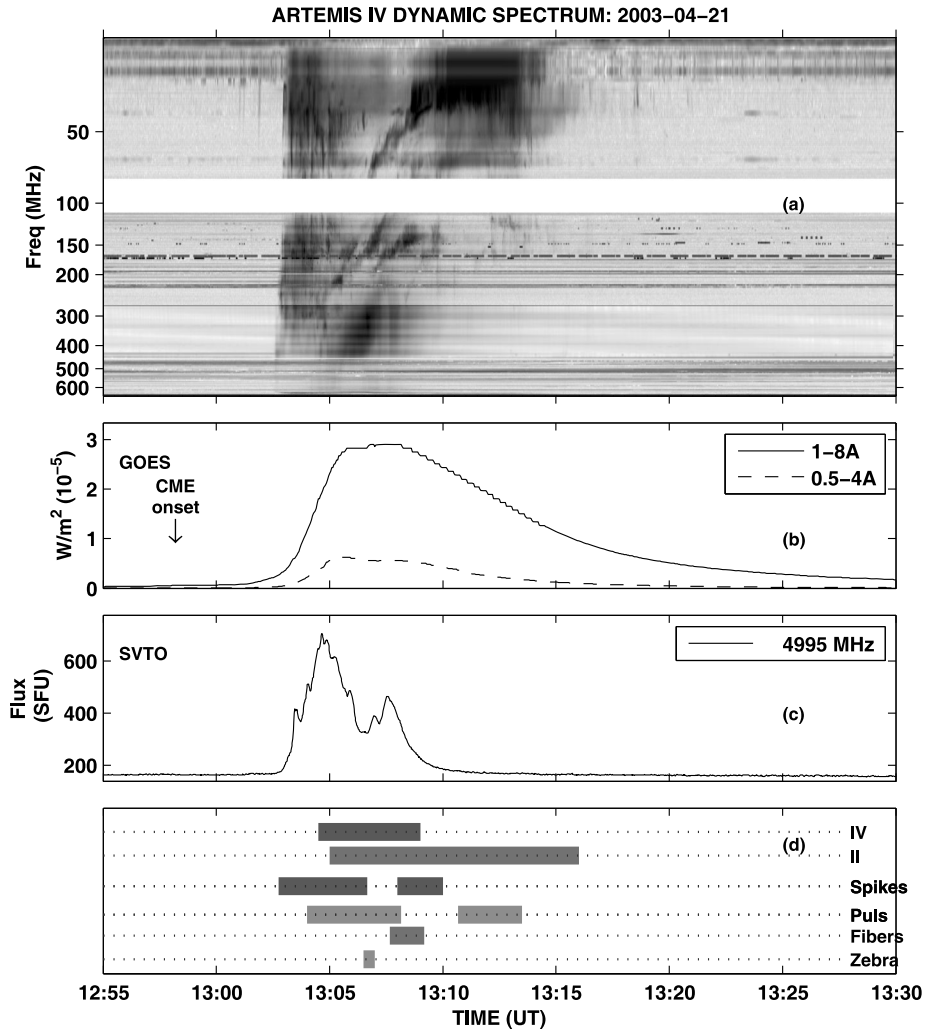


Figure 1 Example of type IV and fine structure–flare–CME temporal relationship from combined data for the 21 April 2003 event. (a): ARTEMIS-IV ASG dynamic spectrum. (b): GOES SXR flux; the CME onset time from the LASCO lists is marked with an arrow. (c): Microwave (4995 MHz) flux from the RSTN San Vito (SVTO). (d): Time range of the type IV, II, spikes, fibers, pulsating, and zebra structures.

we were unable to establish a spatial association because we lacked NRH positional data, the association was characterized as good.

- After establishing the relationship between type IV and SXR flare, we determined the time of the first peak of the HXR and/or the microwave bursts, which we treated as the signature of the *first impulsive energy release*. This was used as a reference for comparing the relative timing of the fine structure.
- For the CME–flare association: from the time–height diagrams in the CME lists we defined a time window of 60 minutes between the CME onset time and the peak of the accompanying SXR flare; we used the flare peak instead of the onset because this is more

easily identifiable. To establish the spatial association, we required that the flare and CME originate in the same quadrant, as schematically depicted in Figure 2. For this we compared the flare location with the CME position angle, which refers to the fastest-moving segment of the CME leading edge, and the angular width; the latter was only used for non-halo CMEs.

For twelve events the spatial criterion failed to lead to acceptance or rejection of association, either because we lacked positional data for the radio burst or the flare, or because there were more than one accompanying flares as candidates for association. These events were not eliminated from the data set, but were only used in deriving the basic statistics of the fine structure parameters.

The basic characteristics of the type IV continuum, the fine structure, the accompanying type II and type III bursts, and the associated flare and CME of the 36 selected events are presented in Table 2. Their dynamic spectra, light curves, and the relative timing of fine structures are given in Appendix B, while four examples of the CME–flare type IV event spatial association, of varying quality, are presented in Figure 2.

3. Morphology and Classification

The 36 type IV bursts selected as described in Section 2 were further examined for the existence of fine structures, which were classified on the basis of their morphology in the SAO dynamic spectra.

Because the various types of fine structure overlapped, we used several high- and low-pass filters on dynamic spectra. The suppression of the continuum background by high-pass filtering in time enhanced fast time-varying spectral structures such as pulsations and fibers. We separated pulsations from other types of structures with medium- to low-frequency variation, such as fibers, by low-pass filtering of the dynamic spectra along the frequency axis; the opposite was obtained with the complementary high-pass filtering, which provides pulsation suppression and facilitates detecting fibers and similar structures (see Figure 3). Occasionally, the fine-structure onset appears to precede the start of the type IV continuum on the synoptic chronological evolution diagrams (*e.g.* Figure 1); this effect results from the above-mentioned processing of the dynamic spectra, which permits detecting fine structure even if the continuum is not detectable because it is too close to the background.

In all events the radio continuum was found to exhibit a combination of three or more types of fine structures embedded within longer or shorter periods of smooth continuum. We classified the fine structures based on phenomenological characteristics, grouping these bursts by the similarity of their form in the dynamic spectra. The criteria jointly employed were bandwidth, duration, drift rate, substructures, impulsive behavior, *etc.* (see the review by Benz, 2003). This work focuses mainly on basic classes of fine structures that have been identified and documented from observations by a number of radio-spectrographs during a very extended period of time; an additional division into subclasses has been known to depend on receiver sensitivity as well as on the time and frequency resolution (see Elgaroy, 1986, for example). Examples of the effect of improved resolution are zebra- and fibers which, at high-cadence observations, turn out to be patterns of dot-bursts (Mészárosová *et al.*, 2008) or spikes (Chernov, Yan, and Fu, 2003) in zebra-like or fiber-like chains. Most of the basic classes examined include more than one subclass corresponding to the Ondřejov classification (Jiříčka *et al.*, 2001) and the earlier catalog by Isliker and Benz (1994). This approach introduces a two-level hierarchy of basic classes and subclasses.

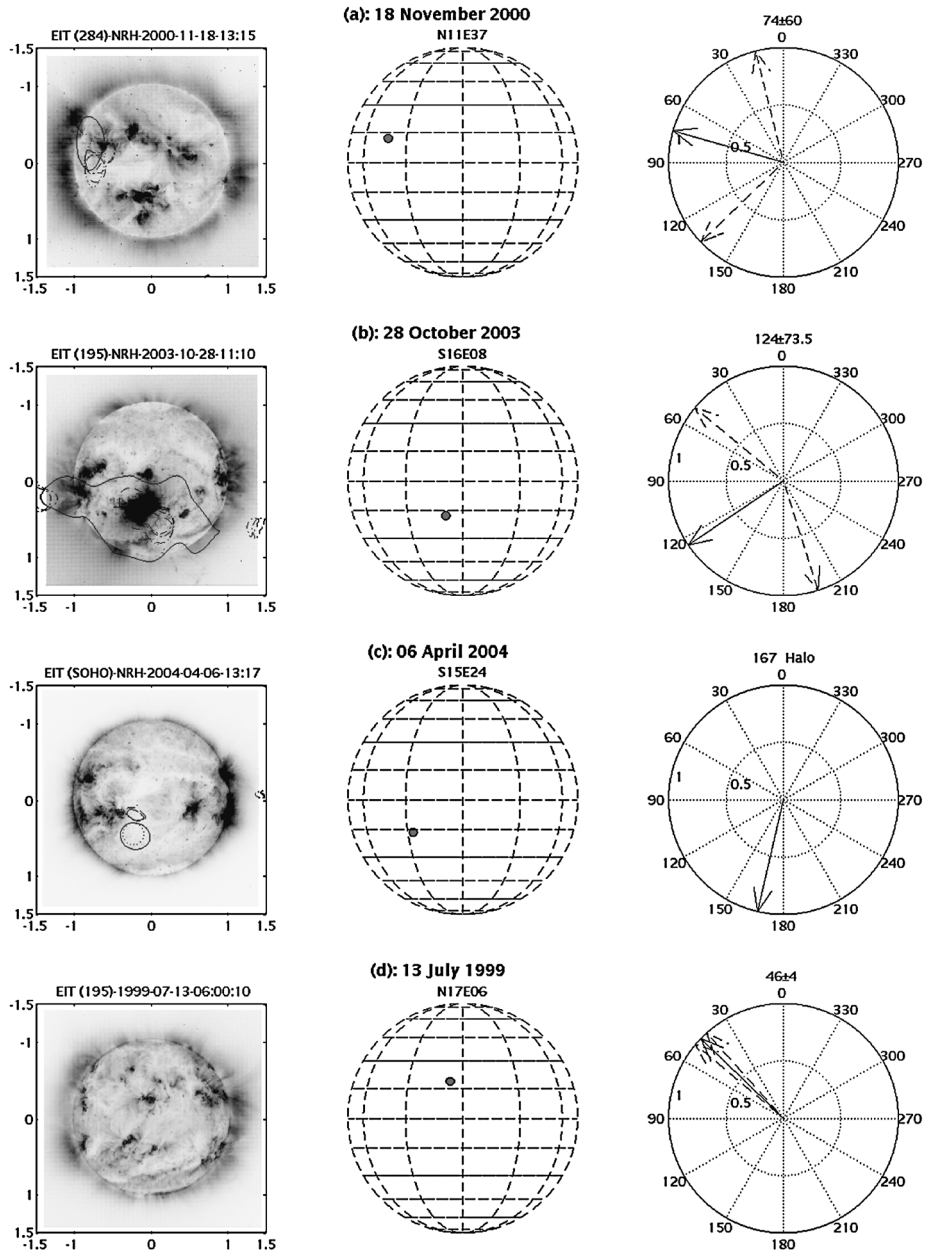


Figure 2 Examples of type IV–flare–CME spatial association from combined data. In the left column the NRH half power contours are overlaid on EIT images. The middle and right columns show the flare position from the NOAA/SGD catalogs and the direction of the CME launch (except for halo); this is marked graphically by the CME position angle and the angular width from the LASCO lists. The events of 18 November 2000 (a) and 28 October 2003 (b) for which excellent spatial association was established among all data sets. (c): The event of 06 April 2004 accompanied by a halo CME exhibits a good association with the active region and the type IV position (see text for details). (d): The event of 13 July 1999 at 06:00 UT, outside the NRH observation window.

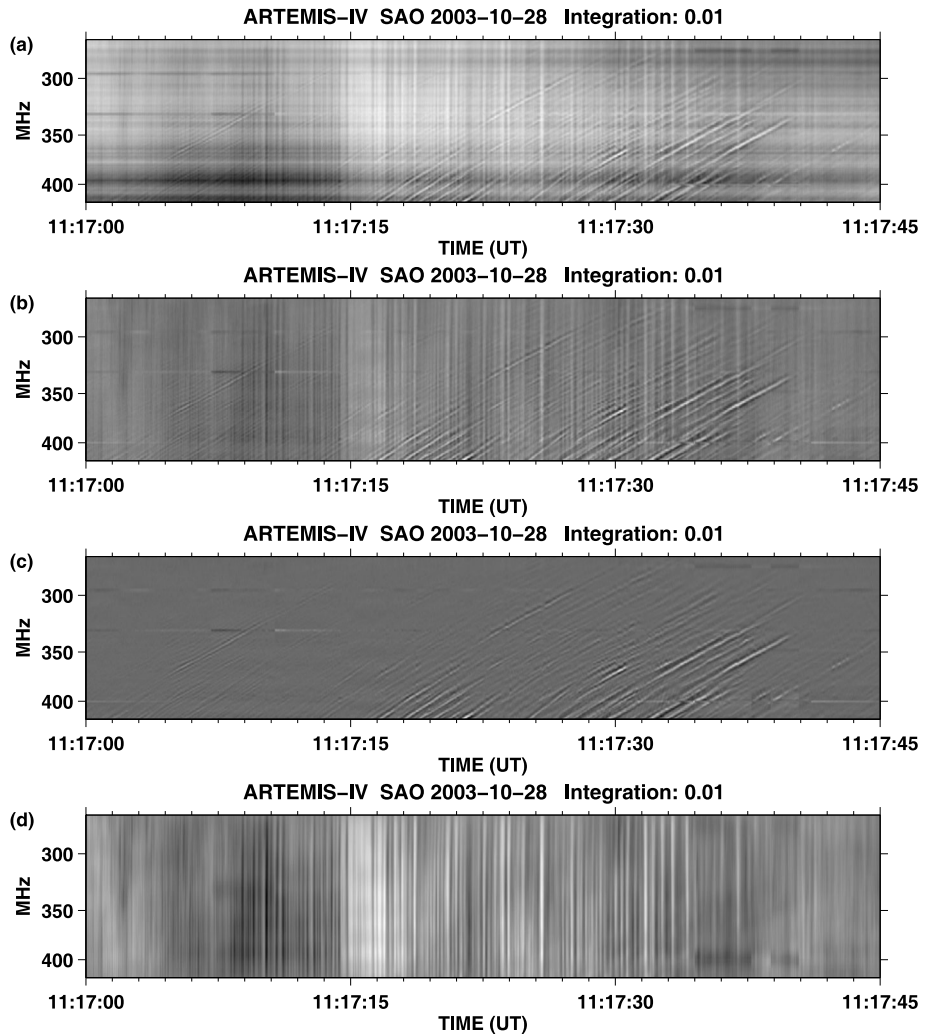


Figure 3 Example of high resolution type IV recording of the ARTEMIS-IV/SAO with fine structure enhancement by means of filtering. (a): The original dynamic spectrum of the type IV continuum. (b): High pass filtering along the time axis reveals underlying pulsations and fibers. These are disentangled by means of high pass filtering along the frequency axis which removes pulsations (c) and low pass filtering along the frequency axis which suppresses fibers (d).

The basic classes of fine structures embedded in the type IV continua we defined are described below.

3.1. Featureless Broadband Continuum

This class of structures, known also as *diffuse continuum*, comprises both featureless segments of type IV bursts and structures of smaller frequency bandwidth and duration, such as *slowly drifting bursts* and *patches*. Our data indicate that long periods of broadband continuum overlap in time with the SXR emission, with embedded intermittent periods of pul-

sation, fiber bursts, spike groups, and zebra bands. Intensity variations within the smooth periods of the type IV bursts that might qualify as patches were recorded as well. On average, the smooth periods without fine structure varied between 0 % to 60 % of the type IV continuum duration; the relatively longest smooth periods were found to increase with the duration of the type IV burst. We note that, although featureless periods have been recorded in the past, our high-cadence data indicate that fine structure may still be revealed at adequately high resolution and sensitivity.

3.2. Pulsating Structures

This class includes drifting and stationary pulsating structures (see review by Nindos and Aurass, 2007); the shortest groups of pulsating structures with durations of about 10 seconds appear as isolated broadband pulses in Jiříčka *et al.* (2001), Jiříčka, Karlický, and Mészárosová (2002), Mészárosová, Karlický, and Jiříčka (2005). The pulsations are considered as the radio-signature of kinetic plasma instabilities, induced by energetic electron populations from quasi-periodic acceleration episodes in reconnecting current sheets (Aurass, 2007).

In our sample 59 periods of pulsations were detected in 33 events; an auto-correlation analysis of their intensity–time profiles indicated periodicities of 0.6–3 sec and individual pulse widths of 0.35–1.3 sec. Their bandwidth exceeds that of the SAO receiver (180 MHz).

3.3. Narrow-Band Bursts

These are reported as narrow-band bursts of the type III family, spikes, dots, and subsecond patches, depending on their shape in the dynamic spectra, (part of the same family are the III(U) and III(J) narrow-band bursts reported by Fu *et al.*, 2004; Bouratzis *et al.*, 2010). They have been interpreted as signatures of small scale acceleration episodes (Nindos and Aurass, 2007). In this basic class we might also include the *sawtooth oscillations* by Klassen, Aurass, and Mann (2001), although these are associated with type II shocks. Figure 4 shows some examples from our data set.

In the ARTEMIS-IV/SAO data set the average duration of individual spikes was found to be ≈ 70 ms; the relative bandwidth of the dynamic spectra was $df/f \approx 2\%$. In a subset of the recorded spikes a positive or negative frequency-drift rate was measurable; typical values were found to be $df/f dt \approx \pm(0.3-0.6) \text{ sec}^{-1}$, similar to the type III frequency-drift rate (see Table 1 of Benz, Csillaghy, and Aschwanden, 1996, where $df/f dt = 0.31 \text{ sec}^{-1}$ at 328 MHz). More often than not, the bursts of this class were grouped in clusters of individual spikes close in time and/or frequency. A particular class of cluster are spike-chains, which exhibit an overall frequency drift; most of them exhibit negative drift $df/f dt \approx -0.021 \text{ sec}^{-1}$, while few drift toward higher frequencies at a rate $df/f dt \approx -0.033 \text{ sec}^{-1}$. The average chain in our data set lasted for 2–20 sec.

3.4. Intermediate-Drift Bursts

These include the typical fibers and the narrow-band *rope-like fibers* (Mann *et al.*, 1989; Chernov, 1990, 2006, 2008); there are also variants of these sub-classes such as the *broad-band fibers* (Chernov *et al.*, 2007) which were observed in the wake of type II bursts. The fiber bursts are thought to be the result of Whistler–Langmuir or Alfvén–Langmuir wave interaction in, mainly, postflare loops; a more recent interpretation (Karlický, Mészárosová,

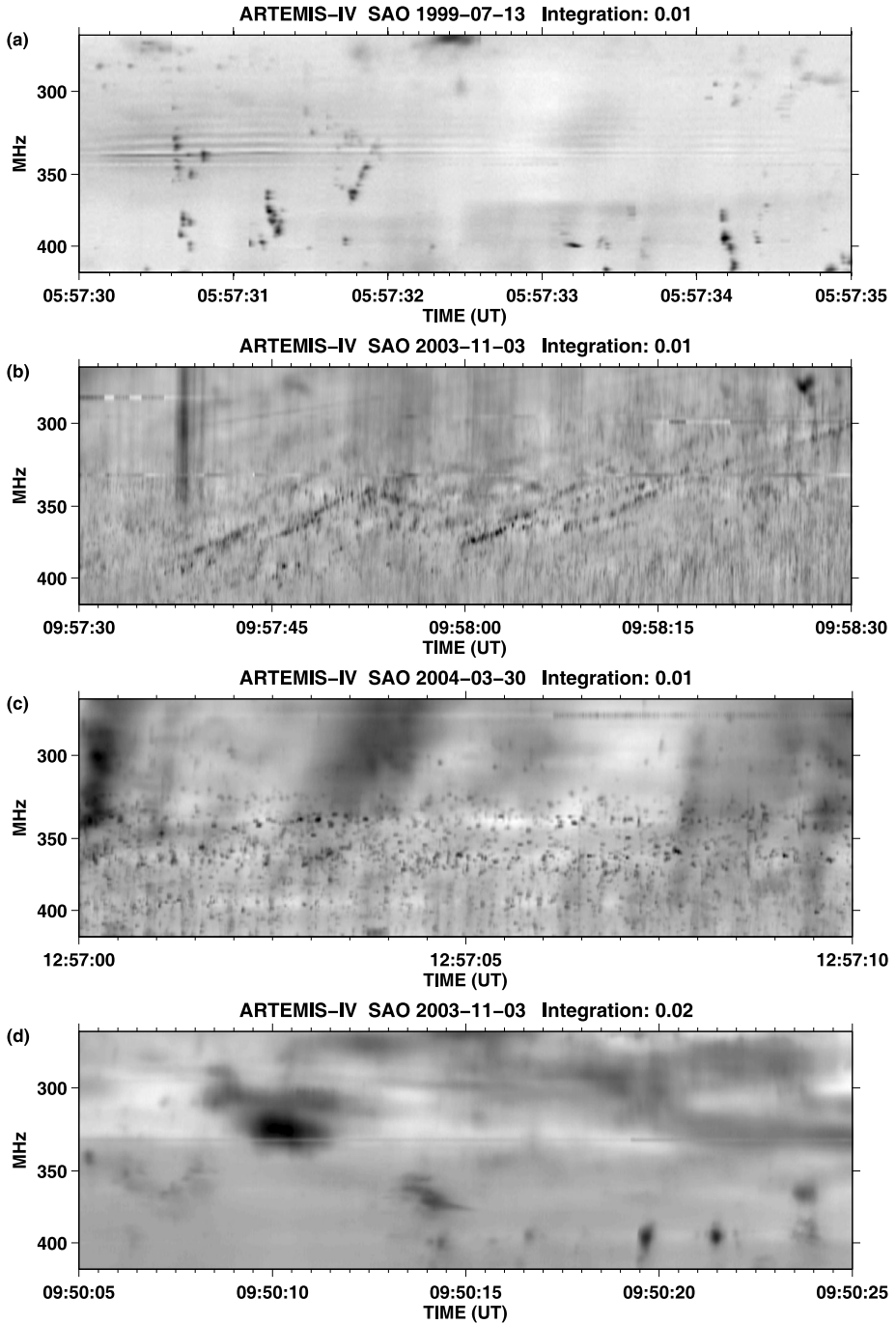


Figure 4 Examples of narrow band bursts observed by ARTEMIS-IV. (a): Spike clusters on 13 July 1999 at 0.01 sec resolution. (b): Spike drifting chains on 03 November 2003. (c): Subsecond narrow band bursts. (d): Example of patch on 03 November 2003.

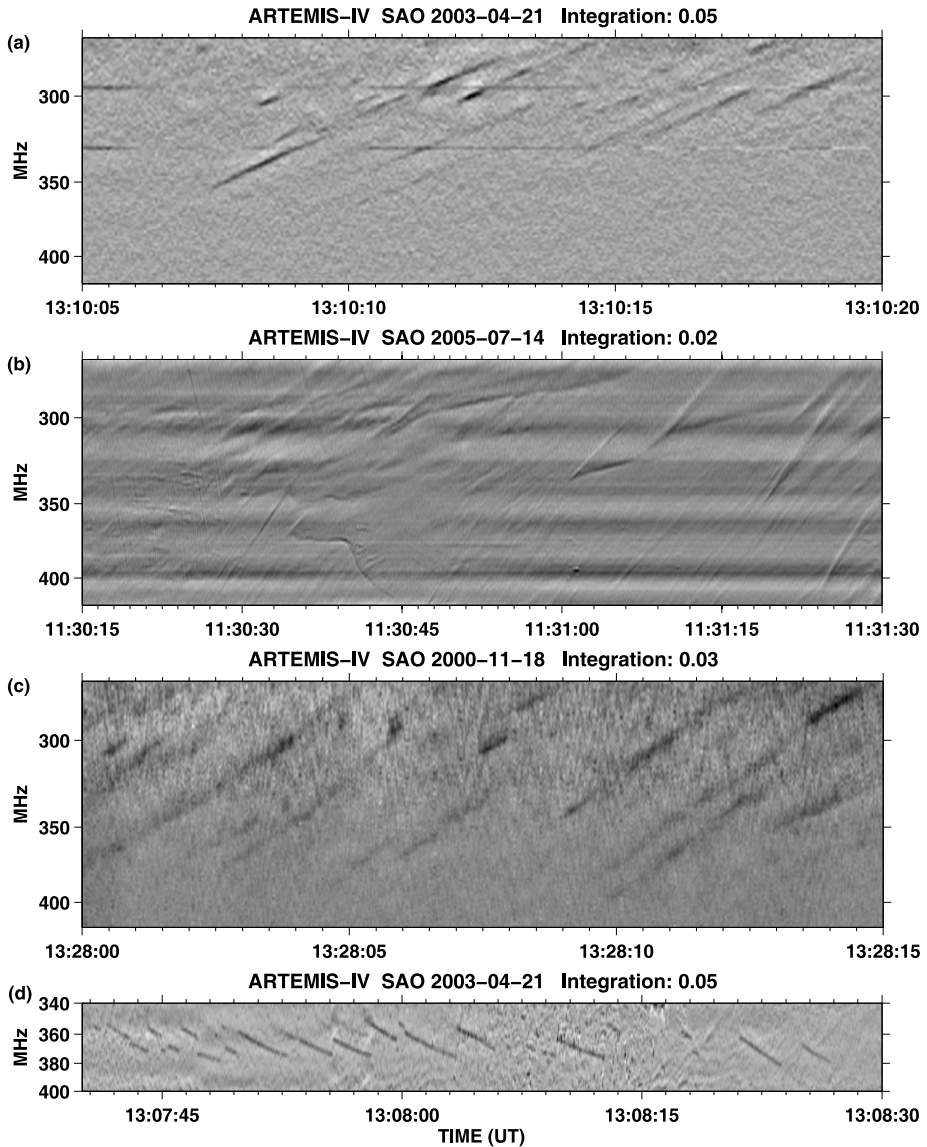


Figure 5 Example of intermediate drift bursts. (a): Fiber bursts. (b): A complex group of fibers observed by ARTEMIS-IV on 14 July 2005. (c): Fast drift structures with drift rate approximately double that of a typical fiber. (d): Ropes.

and Jelínek, 2013) resorts to fast magnetoacoustic wave trains. Because of their origin they qualify as model-dependent magnetic-field diagnostics (see Kuijpers, 1975; Aurass *et al.*, 2005; Rausche *et al.*, 2007).

On average, the fiber bursts recorded by the ARTEMIS-IV/SAO (see examples in Figure 5) exhibit normalized drift rates $df/f dt \approx 0.03 \text{ sec}^{-1}$. Some outliers of the drift-rate distribution reached $\approx 0.4 \text{ sec}^{-1}$, which imply exciting speeds similar to the type III

bursts; these were dubbed fast-drift bursts by Jiříčka *et al.* (2001), Jiříčka, Karlický, and Mészárosová (2002), Mészárosová, Karlický, and Jiříčka (2005). In this work, these outliers were provisionally retained as intermediate-drift bursts.

In our data set nineteen events had multiple groups of fibers, and in two events rope-like fibers were recorded; the fiber-rate period was in the range of 0.46–2.3 sec. The individual fibers lasted for ≈ 0.4 sec and had an instantaneous bandwidth of ≈ 3.5 MHz (consistent with observations of Benz and Mann, 1998, in the 1–3 GHz range); the group extent in frequency was ≈ 40 MHz on average, which corresponds to $df/f \approx 0.11$. Most fibers had negative drift rates of $df/f dt \approx -0.023 \text{ sec}^{-1}$, while those with positive drift reached rates of $df/f dt \approx 0.034 \text{ sec}^{-1}$; the latter always coexisted with fibers of negative drift rate. A comparison of these results with the spike-chain characteristics in Section 3.3 indicates that the fiber frequency drift rates and instantaneous bandwidths are equal to the spike-chain frequency drift rate and the individual spike bandwidth on average.

Finally, groups of fibers with different drift rates were found to overlap in dynamic spectra (see Figure 5 for an example); it is unclear whether these might constitute a separate subclass, or if they originate from different regions; a more detailed analysis employing NRH images may be able to answer this question.

3.5. Emission Bands

These comprise the various subtypes of the zebra family (classic or pulsation-superposed zebra patterns, fiber-associated zebras (Chernov, 2005, 2006), zebras with a drifting emission envelope (Zlotnik *et al.*, 2009)), the rare lace-bursts (first reported by Karlický *et al.*, 2001 see bottom panel of Figure 6 for an example recorded by ARTEMIS-IV), the equally rare single-emission band, dubbed *evolving emission line* (EEL), first reported by Chernov *et al.* (1998) in the decimetric frequency range and by Fu *et al.* (2004), Ning *et al.* (2008) in the GHz range. In the same basic class we include some unusual bursts consisting of short (≈ 2 –4 ms) parallel stripes with a relative delay with decreasing frequency; they are characterized by an overall frequency drift (Oberoi, Evarts, and Rogers, 2009). The zebra-burst emission mechanism has been attributed to a number of different interpretations, some including double plasma resonance (Zlotnik *et al.*, 2003; Aurass *et al.*, 2003), Bernstein modes, or plasma waves trapped in resonators, to mention but a few (see Chernov, 2005; Nindos *et al.*, 2008); the double-resonance interpretation has also been proposed for the lace-bursts (Fernandes *et al.*, 2003; Bárta and Karlický, 2005). Chen *et al.* (2011) have provided observational evidence in support of this interpretation.

Twenty-two events of our dataset exhibited one or more patches of zebra structures; they appeared in almost equal numbers before and after the flare maximum. The energy release episodes indicate a good correspondence between these two; all *patches of zebra bands* were within five minutes of the time of the release episode, provided that the *frequency* of the latter, estimated from the type III feet or the type IV burst high-frequency boundary, was within the SAO range. The majority were pulsation- and fiber-associated zebra (12) within overlapping pulsation- and fiber activity, and we were unable to resolve their association. Five zebra patches appear to be clearly pulsation associated. Seven periods of lace-bursts were also recorded; they were found to coincide in time and frequency, mostly, with pulsations and spikes. Only one EEL was recorded. Examples of zebras, laces, and EEL are shown in Figure 6.

A summary of the fine-structure properties is presented in Table 1.

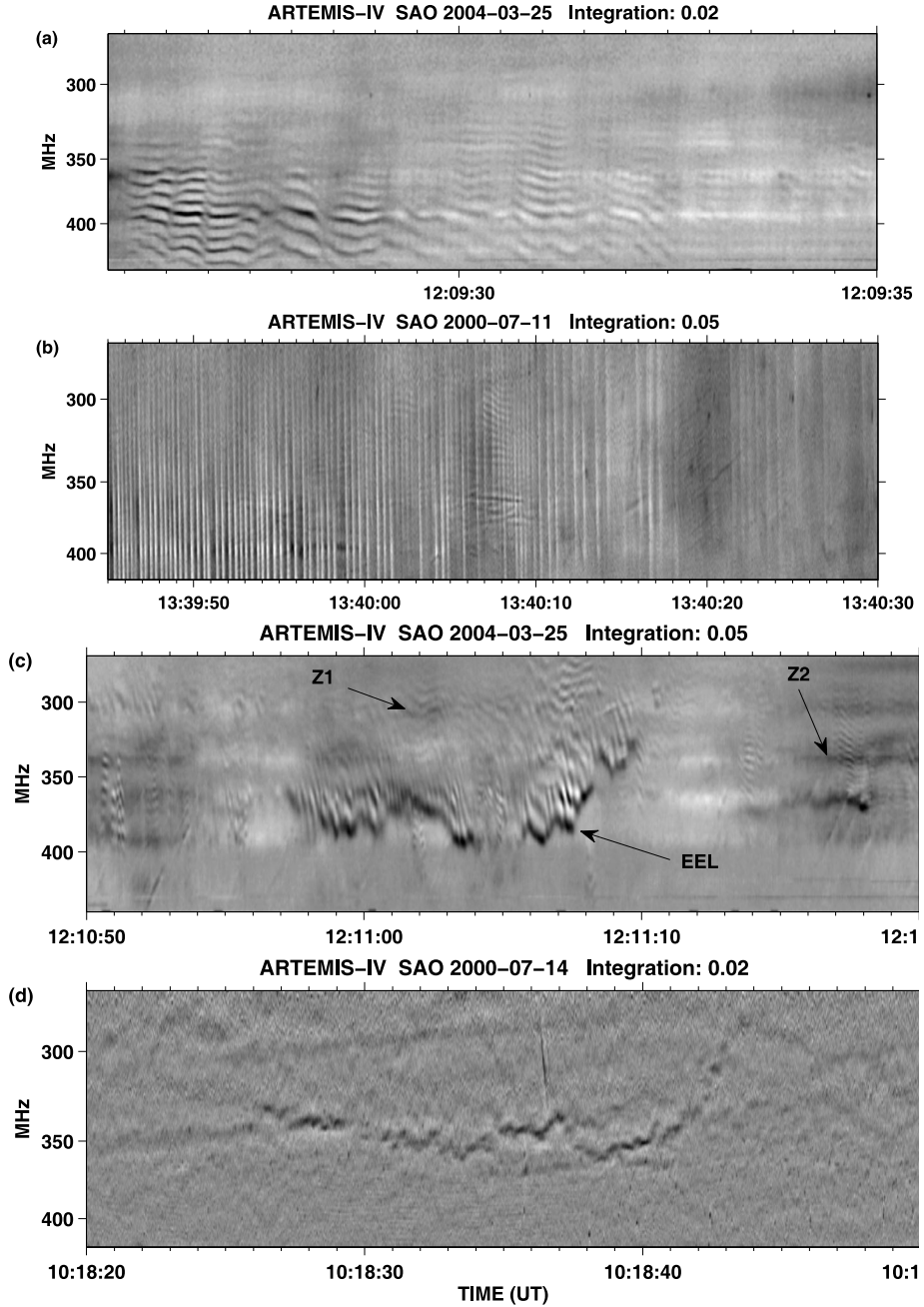


Figure 6 ARTEMIS-IV high-resolution dynamic spectra of emission bands: (a): Zebra structure. (b): Zebra superposed on pulsations. (c): Recording of zebra structures with possible *evolving emission line* (EEL on the figure) at the high frequency limit of the event; Z1 and Z2 mark typical and fiber-associated zebra patterns. (d): Lace burst on 14 July 2000.

Table 1 Summary of the fine-structure properties. The last column gives the median and width of the distribution of the relative timing with respect to the first impulsive energy release.

Category or subcategory	Characteristics	Remarks	T_{md} , FWHM min
Featureless broadband continuum	Lack of fine structure	Part of type IV burst	–
Pulsating structures	Periodicities 0.6–3 sec	Embedded within the type IV burst continuum (moving or stationary)	1.5 (8.0)
<i>drifting stationary</i>	Drift rate $ df/f dr \approx 0.003 \text{ sec}^{-1}$	Part of moving type IV burst	
<i>isolated broadband pulses</i>	Drift rate negligible		
Narrow-band bursts	Duration ≈ 10 seconds	Shortest pulsating structures	6.5 (18.0)
<i>narrow-band type III spikes</i>	Sub-second narrow band bursts, near the time resolution limits of SAO $df/f \approx 10 \%$, $ df/f dr \approx 0.4 \text{ sec}^{-1}$	Including III(U)–III(J) narrow-band bursts	
<i>patches</i>	Individual spike: bandwidth $df/f \approx 2 \%$, duration ≈ 70 ms, $ df/f dr \approx 0.45 \text{ sec}^{-1}$	Often clustered, occasionally organized in fiber-like or type III like sequences	
Intermediate-drift bursts	Bandwidth $f/f \approx 3-4 \%$, drift rate $ df/f dr \lesssim 0.03 \text{ sec}^{-1}$, duration $\approx 1-5$ sec		
<i>fibers ropes</i>	Drift rate between type II–type III bursts $ df/f dr \approx 0.03 \text{ sec}^{-1}$, Bandwidth $df/f \gtrsim 10 \%$		
<i>fast-drift bursts</i>	Similar to fibers, bandwidth $df/f \lesssim 10 \%$ Frequency drift rate up to $ df/f dr \approx 0.4 \text{ sec}^{-1}$	Drift rate similar to type III	6.8 (10.0)
Emission bands	Single band: $df/f \approx 2.5 \%$, duration 1–10 sec; total bandwidth df/f up to 35 %	Most of the emission bands	
<i>zebra</i>			
<i>lace-bursts</i>			
<i>evolving emis. line (EEL)</i>		Only one was recorded	

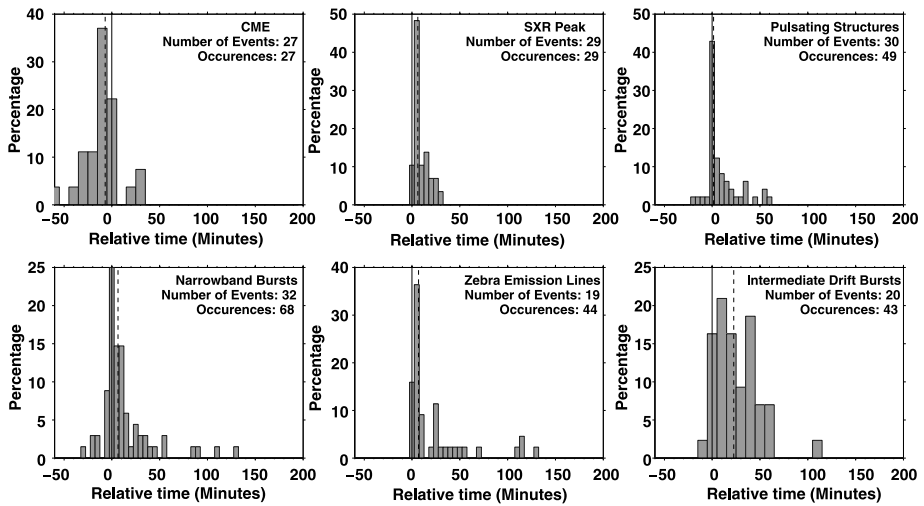


Figure 7 Histograms of the time of occurrence of the CME onset, SXR peak, pulsations, spikes (narrow-band bursts), zebra patterns, and fiber bursts (intermediate-drift bursts) with respect to the time of the first impulsive energy release. Note that the bin size is 10 min for the CMEs and the intermediate-drift bursts and five minutes for the others. Dashed vertical lines mark the distribution median.

4. Relative Timing of Fine Structures

As mentioned in Section 2, the time of *first impulsive energy release*, shown by the first HXR/microwave peak, was used as reference for timing the appearance of fine structures with respect to the evolution of the flare process. Figure 7 shows the distributions of the relative time of occurrence of various fine structures, together with those of the CME onset and SXR peaks. Because each event shows multiple instances of fine structure, we used all of them to compute the histograms. Several events exhibit a composite structure, with clearly distinct HXR/microwave peaks or groups within the same SXR peak and the same type IV burst (see for example event 27, Figure 37). We were unable to identify some of the associated fine structures with a particular HXR/microwave peak; these were not used to compute the histograms in Figure 7.

The CME onset precedes the *first impulsive energy release* by several minutes (Figure 7), in agreement with Zhang *et al.* (2001), Webb and Howard (2012). The histogram of SXR peaks shows a sharp maximum five minutes after the first impulsive energy release, as expected. A more detailed chronological evolution is schematically depicted in Figures 8, 9, and 10; in the latter we have included the times of the standard type III bursts. We note that, in the case of the continuum, determining the onset is threshold dependent, which means that the times reported in the figures and in Table 2 are only approximate values.

Of our 36 events, eight had short periods of broadband diffuse continuum and seven had patches. With very few exceptions, they started between the CME onset and the SXR peak, extending for several tens of minutes after that. This time interval of continuum emission, well past the impulsive phase, was named by Benz *et al.* (2006) *extended decimetric emission*, based on dynamic spectra obtained during the active period in October–November 2003.

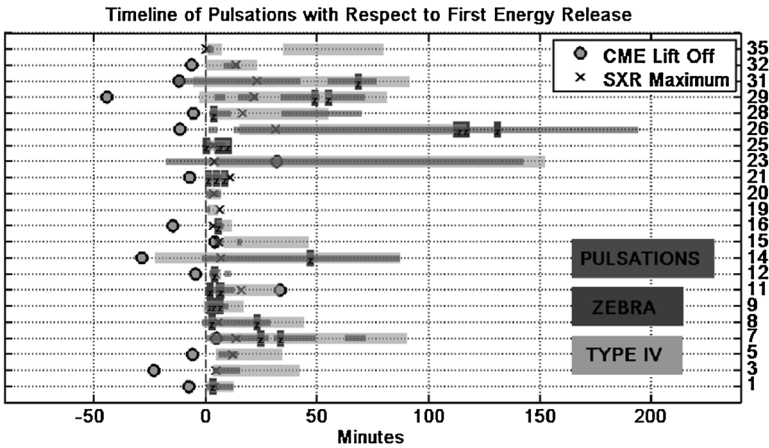


Figure 8 Relative timing of pulsations and zebra stripes associated with the type IV continua (gray); the z labels mark the short periods of zebra stripes. The circles mark the CME onset and the X symbols the SXR flux maximum. Time is in minutes from the first impulsive energy release. The event number is marked at the right (cf. Table 2).

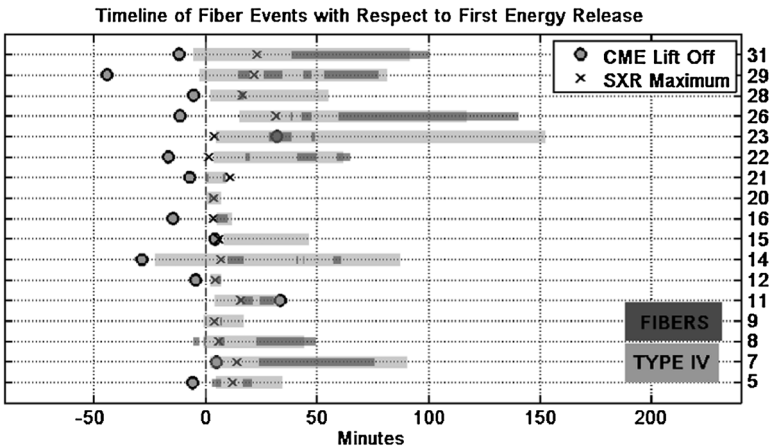


Figure 9 Same as Figure 9 for fiber bursts.

As shown in Figure 7, pulsations show a narrow distribution around the time of the *first impulsive energy release*, with the median of their histogram at 1.5 min and a full width at half maximum (FWHM) of 8.0 min. Their total duration is shorter than that of the continuum, although in event 14 they extended for more than 150 minutes after the flare maximum (Figure 8).

Narrow-band bursts also cluster around the *first impulsive energy release*; their histogram peaks at 0 min, with a median value of 6.5 min and a FWHM of 18.0 minutes. Although they are concentrated mostly around the flare maximum, they occasionally cover longer periods within the flare-decay phase, probably associated with subsequent energy releases. Furthermore, narrow-band fine structures may appear before the impulsive phase of the flare (see for example Aurass, 2007).

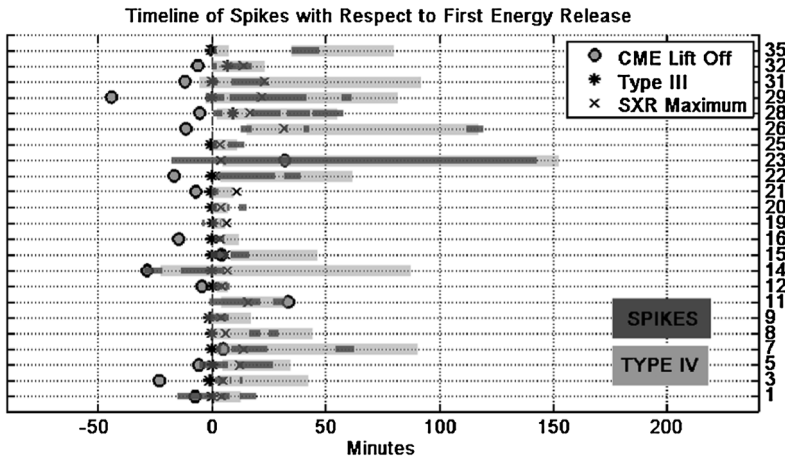


Figure 10 Same as Figure 9 for spike groups and type III (standard type III).

The peak of the histogram for sebra patterns is five minutes after the *first impulsive energy release*, with a median value of 6.8 minutes and a FWHM of 10.0 minutes. The distribution exhibits a secondary peak around 120 minutes because of the contribution of the longest events, which are characterized by secondary energy releases accompanied by zebra patterns. Apparently, the energy release episodes, initial and secondary, provide the energetic electrons required to trigger this type of fine structure within loops (see Zlotnik *et al.*, 2005). Characteristic examples of multiple energy-release episodes are events 13 (26 October 2003, Figure 23) and 19 (30 March 2004, Figure 29) in Appendix B.

Intermediate-drift bursts (fibers), which are known to appear often in postflare loops, (see Chernov, 2006), are the most dispersed of all; their distribution shows two peaks 10 and 40 minutes after the *first impulsive energy release*.

5. Discussion and Conclusions

Using the high time resolution SAO receiver, which operates in the frequency range of 450–270 MHz on the ARTEMIS-IV radio-spectrograph, we observed a number of fine structure bursts embedded in metric type IV radio continua; these were compared with the associated HXR bursts, the GOES/SXR flares, and SOHO/LASCO CMEs to establish a relationship between this type of radio-bursts and the evolution of solar energetic phenomena. Our study started by examining the characteristics of each type of fine structure, such as bandwidth, duration, frequency drift rate, and shape in the dynamic spectrum. This necessitated an appropriate taxonomy because of the diversity of forms; we introduced a two-level hierarchy of basic classes and subclasses.

At the top level, this two-level hierarchy adopted the basic classes of fine structures that have been recognized and documented from multiple observations over a long period of time. The second-level division into subclasses permitted including new and, probably, rare types of bursts alongside the well known; the ensuing subdivisions match, more or less, the Ondřejov taxonomy (Jiříčka *et al.*, 2001), but include other types of fine structure as well. We note at this point that the subdivision into types and subtypes based solely on morphology

and not on the underlying radiation process remains an artificial construct, often dependent on the resolution of observational data. Furthermore, the classes thus defined are rather broad and may, at times, include bursts that are morphologically similar, yet originate from different radiation processes. It is, however, necessary as a background for theoretical work, as already pointed out by Elgaroy (1986) and Benz (2003), although the classification, in particular the second level, remains more or less tentative.

The time of appearance of the type IV fine structures with respect to the evolution of the associated CMEs and flares was examined next. Our data indicate that the type IV continua, in which the fine structures were embedded, were associated with flare eruptions exhibiting spatial scales from the active-region size up to almost one solar radius, thus verifying that bursts accompanied by type IV are usually complex events that probably involve multiple small-scale components. We therefore used the time of the *first impulsive energy release*, shown by HXR and/or microwave time profiles, as a reference for timing the fine structures. This reference time is very near the time of the first appearance of type III emissions, as expected.

In the vast majority of the cases studied, the onset of all fine-structure classes shows a close temporal association with the *first impulsive energy release*, which places their onset between the CME onset and the SXR peak. The closest association was found for the pulsating structures, which show a narrow distribution with a median at 1.5 minutes after the *first impulsive energy release*. Narrow-band bursts (spikes and narrow-band bursts of the type III family) come next, with a histogram median at 6.5 minutes, closely followed by zebra patterns at 6.8 minutes. Intermediate-drift bursts (fibers) are more dispersed; their distribution shows two peaks 10 and 40 minutes after the *first impulsive energy release*.

Pulsations and zebras show the narrowest distribution with a FWHM of 8.0 and 10.0 minutes, respectively, followed by narrow-band bursts with a FWHM of 18.0 minutes. Intermediate-drift bursts are more dispersed, with two peaks in their distribution at 10 and 40 minutes.

More detailed studies of the various fine structures will appear in subsequent publications.

Acknowledgements We would like to thank the anonymous referee, whose comments and suggestions have improved the quality of this work. This work was supported in part by the Special Account for Research Grants of the National and Kapodistrian University of Athens. The LASCO CME catalog is generated and maintained at the CDAW Data Center by NASA and The Catholic University of America in cooperation with the Naval Research Laboratory. SOHO is a project of international cooperation between ESA and NASA. The NRH (*Nançay Radioheliograph*) is operated by the Observatoire de Paris and funded by the French research agency CNRS/INSU. The *Radio Solar Telescope Network* (RSTN) is a network of solar observatories maintained and operated by the US Air Force Weather Agency.

Appendix A: Comprehensive Catalog of the ARTEMIS-IV Recordings

In Table 2 we provide a summary of the metric type IV bursts with fine structure recorded by the ARTEMIS-IV/SAO receiver; accompanying metric bursts and explosive events are included for comparison. Column 3 gives the type of activity (for SXR flares we list the flare class, IV corresponds to type IV continuum). Column 4 gives the extrapolated launch time of CMEs, as specified in Section 3. The location of the flare on the disk and the NOAA active-region number are given in Column 8. In the same column we list the measurement position angle (MPA) of the CMEs with their angular width in parenthesis, as explained in Section 2.

Table 2 ARTEMIS-IV observations: metric radio bursts and associated LASCO CMEs and GOES SXR flares.

#	Date	Activity	Start UT	Max	End	Position of AR-CME
1	30.06.1999	M1.9	11:24	11:30	11:45	S15E00–8603 03 (halo)
		CME	11:18			
		SVTO 4995 MHz	11:26	11:28	11:29	
		IV	11:26	11:38		
		II	11:26	11:28		
		III	11:26			
		Spikes	11:10	11:27		
		Puls.	11:26	11:38		
		Zebra	11:29	11:29		
		Spikes	11:29	11:33		
		Spikes	11:37	11:45		
Note: in the 11:10–11:22 UT interval there are intermittent spike bursts; these become chains and clusters after 11:22 UT by the time of the energy-release episode marked by the San Vito (SVTO) peak.						
2	13.07.1999	C2.9	05:22	05:46	07:00	8628 46 (8)
		CME	05:43			
		IV	05:57	05:59		
		II	06:02	06:05		
		SVTO 4995 MHz	05:57	05:58	06:00	
		III	05:57			
		Spikes	05:55	6:05		
		Puls.	05:57	05:59		
		Zebra	05:57	05:58		
Note: the event started before the ARTEMIS-IV observations. Outside NRH daily observations.						
3	15.04.2000	M4.3	10:09	10:18	10:35	S22E29–8955 93 (176)
		CME	10:04			
		IV	10:16	10:55		
		III	10:12			
		III	10:17			
		Spikes	10:14	10:18		
		Puls.	10:16	10:27		
		Ropes	10:17	10:17		
		Spikes	10:20	10:22		
Note: no HXR or microwave data.						
4	15.04.2000	C1.0	12:13	12:17	12:23	–
		C3.0	13:38	13:43	13:50	S22E29–8955
		M2.2	14:37	14:48	15:00	S23E28–8955
		CME	14:18			165 (43)
		HXRS 45 KeV	14:31	14:34	14:37	
		IV	12:13		14:44	
		III	13:41			
		III	14:40			
		III	15:10			
		HXRS 45 KeV	14:40	14:42	14:44	
		Spikes	11:50		15:10	
		Puls.	14:39		14:43	
		Note: spikes started during the previous flare at 10:14 UT and lasted until the end of the day. There are also several type III bursts during this time interval. A type IV burst was probably still present from the previous flare (event 03), but it is too faint in the dynamic spectrum. NRH data gap.				

Table 2 (Continued)

#	Date	Activity	Start UT	Max	End	Position of AR–CME
5	30.04.2000	C7.7	07:53	08:08	09:30	S11W18–8976 186 (104)
		CME	08:10			
		IV	08:00		08:30	
		SVTO 4995 MHz	07:54	08:01	08:09	
		II	07:55		08:02	
		III	07:56			
		Spikes	07:50		08:01	
		Fiber	07:58		08:02	
		Puls.	08:01		08:10	
		Spikes	08:08		08:22	
		Fiber	08:12		08:16	
		Ropes	08:20		08:20	
		6	11.07.2000	X1.0	12:12	
CME	12:33					
IV	12:36				15:20	
HXRS 45 KeV				12:58		
Spikes	12:38				13:16	
Puls.	12:47				12:48	
Fiber	12:55				12:56	
Puls.	12:56				13:29	
Fiber	13:03				13:04	
Fiber	13:19				13:26	
Spikes	13:22				13:29	
Zebra	13:29				13:29	
Fiber	13:31				13:40	
Puls.	13:32				13:40	
Zebra	13:35				13:35	
Puls.	13:43				13:53	
Fiber	13:48				13:54	
7	14.07.2000	X5.7	10:03	10:24	11:30	N22W07–9077 273 (halo)
		CME	10:15			
		IV	10:12		11:41	
		II	10:11		10:37	
		III	10:10			
		HXRS 45 KeV	10:08		10:15	
		TSRS 2695 MHz	10:10	10:29	10:45	
		III	10:28			
		Puls.	10:10		10:38	
		Spikes	10:11		10:14	
		Spikes	10:18		10:34	

Note: double peak in HXR

Table 2 (Continued)

#	Date	Activity	Start	Max	End	Position of AR–CME
			UT			
		Lace	10:18		10:19	
		Fiber	10:33		11:25	
		Zebra	10:35		10:35	
		Puls.	10:40		10:59	
		Zebra	10:43		10:44	
		Spikes	11:04		11:12	
		Puls.	11:12		11:21	

Note: the type IV burst appears to be in two parts: a structureless drifting continuum starting at 10:12, and a stationary type IV starting at 10:10, which becomes quite pronounced at 10:27 and continues until 10:41. The TSRS 2695 MHz flux exhibits a number of peaks between 10:10–10:45 UT.

8	14.07.2000	M1.7	12:50	12:57	13:10	S09W01–9002 no CME
		TSRS 2695 MHz	12:50	12:52	12:56	
		IV	12:50		13:35	
		Fiber	12:45		12:48	
		Puls.	12:49		13:20	
		Fiber	12:50		12:51	
		Zebra	12:54		12:54	
		Fiber	12:56		12:59	
		Fiber	13:13		13:40	
		Spikes	12:49		12:51	
		Spikes	13:07		13:12	
		Zebra	13:14		13:14	
		Spikes	13:15		13:20	
		9	14.07.2000	M3.7	13:44	
III	13:47					
TSRS 2695 MHz	13:46			13:50	13:51	
Spikes	13:45				13:55	
Puls.	13:49				13:58	
III	13:55					
TSRS 2695 MHz	13:53			13:54	13:56	
IV	13:47				14:05	
Zebra	13:50				13:50	
Zebra	13:51				13:52	
Zebra	13:54				13:54	
Fiber	13:54				13:55	

Note: double peak of TSRS 2695 MHz flux.

10	19.09.2000	M5.1	08:06	08:26	08:42	N14 W46–9165 283 (76)
		CME	08:08			
		IV	08:11		08:27	
		II	08:13		08:20	
		III	08:13			
		Spikes	08:10		08:12	
		Puls.	08:11		08:12	

Note: no HXR or microwave data.

Table 2 (Continued)

#	Date	Activity	Start	Max	End	Position of AR–CME
			UT			
11	18.11.2000	M1.5	13:02	13:25	15:00	N11E37–9235 74 (120)
		CME	13:42			
		HXRS 45 KeV	13:09	13:11	13:12	
		IV	13:13			
		II	13:12	13:17		
		Spikes	13:07	13:30		
		Puls.	13:09	13:21		
		Zebra	13:11	13:11		
		Zebra	13:15	13:15		
		Zebra	13:16	13:16		
		Lace	13:22	13:22		
		Spikes	13:35	13:40		
12	21.04.2003	M2.8	12:54	13:07	13:30	N18E02–10338 355 (163)
		CME	12:58			
		IV	13:04	13:09		
		II	13:05	13:16		
		SVTO 4995 MHz	13:03	13:04	13:10	
		III	13:03			
		Spikes	13:03	13:07		
		Puls.	13:04	13:08		
		Lace	13:05	13:05		
		Zebra	13:06	13:07		
		Fiber	13:07	13:09		
		Spikes	13:08	13:10		
		Puls.	13:11	13:13		

Note: position angle from the CACTUS catalog. SVTO 4995 MHz double peak. AR localization from MDI.

13	26.10.2003	X1.2	05:57	06:54	09:00	S15E44–10486 108 (207)
		CME	06:13			
		IV	07:06	09:10		
		II	06:16	06:30		
		SVTO 4995 MHz	06:12	08:00		
		RHESSI 50–100 KeV	06:09	06:12	06:18	
		Puls.	07:07			
		Spikes	07:11	07:12		
		Lace	07:19	07:19		
		Zebra	07:22	07:23		
		RHESSI 50–100 KeV	08:30	08:32	08:34	
		Puls.	08:35			
		RHESSI 50–100 KeV	08:40	08:41	08:42	

Note: probably multiple event that began before the start time of ARTEMIS-IV; SVTO 4995 MHz flux exhibits multiple peaks. NRH data gap.

Table 2 (Continued)

#	Date	Activity	Start	Max	End	Position of AR–CME	
			UT				
14	28.10.2003	X17.2	09:51	11:10	12:40	S16E08–10486 124 (147)	
		CME	10:34				
		IV	10:40		15:00		
		II	11:03		11:11		
		SVTO 4995 MHz	11:03		11:25		
		III	11:03				
		Spikes	10:33		11:41		
		Spikes	10:49		11:08		
		Puls.	11:01		12:26		
		RHESSI 50–100 KeV	11:06		11:14		11:25
		Lace	11:07		11:09		
		Fiber	11:12		11:20		
		Fiber	11:43		11:44		
		Fiber	11:46		11:47		
		Zebra	11:50		11:50		
		Fiber	12:00		12:03		
Spikes	14:14	14:22					
Note: SVTO 4995 MHz flux exhibits multiple peaks.							
15	03.11.2003	X3.9	09:43	09:55	11:00	N08W77–10488 293 (103)	
		CME	09:53				
		IV	09:57		10:35		
		II	09:51		10:10		
		III	09:49				
		III	09:51				
		RHESSI 100–300 KeV	09:48		09:49		09:55
		SVTO 4995 MHz	09:49		10:20		
		Spikes	09:48		09:48		
		Puls.	09:48		09:49		
		Fiber	09:48		09:48		
		Puls.	09:53		09:57		
		Lace	09:57		09:57		
		Note: SVTO flux exhibits multiple peaks.					
16	04.02.2004	C9.9	11:12	11:18	12:15	S07W49–10547 274 (33)	
		CME	11:19				
		IV	11:19		11:26		
		II	11:16		11:17		
		III	11:14				
		SVTO 4995 MHz	11:14		11:16		11:19
		Puls.	11:16		11:17		
		Fiber	11:19		11:24		
		Puls.	11:19		11:23		
		Lace	11:19		11:19		
		Zebra	11:20		11:20		
		Spikes	11:15		11:20		
Note: NRH data gap.							

Table 2 (Continued)

#	Date	Activity	Start UT	Max	End	Position of AR–CME
17	25.03.2004	C3.7	12:01	12:12	12:20	N01W19–10577 LASCO data gap.
		IV	12:08		12:14	
		SVTO 4995 MHz	12:05	12:06	12:07	
		SVTO 4995 MHz	12:08	12:10	12:12	
		Zebra	12:07		12:08	
		Puls.	12:08		12:13	
		Zebra	12:09		12:09	
		Zebra	12:11		12:11	
		Zebra	12:12		12:12	
		Spikes	12:13		12:15	
Note: NRH data gap; no EIT data, MDI is used to spatially localize the active region. Double SVTO 4995 MHz peak.						
18	30.03.2004	C1.7	05:37	05:41	05:46	N15E05–10582 LASCO data gap.
		IV	05:43		05:49	
		III	05:45			
		RHESSI 12–25 KeV	05:36	05:40	05:47	
		RHESSI 12–25 KeV	06:00	06:05	06:10	
		Puls.	05:43		05:45	
		Puls.	05:47		05:49	
		Spikes	05:48		05:50	
Note: outside NRH daily observations; no EIT data, MDI is used to spatially localize the active region. Multiple HXR peaks in two main groups that probably indicate a double event.						
19	30.03.2004	C5.9	09:41	09:51	09:54	N15E06–10582 LASCO data gap.
		IV	09:45		09:55	
		SVTO 4995 MHz	09:44	09:45	09:46	
		SVTO 4995 MHz	09:51	09:52	09:55	
		III	09:45			
		III	09:51			
		Puls.	09:44		09:47	
		Puls.	09:51		09:55	
		Spikes	09:40		09:41	
		Spikes	09:43		09:46	
		Spikes	09:48		09:49	
		Spikes	09:51		09:55	
Zebra	09:54		09:55			
Note: no EIT Data, MDI is used to spatially localize the active region. Multiple SVTO 4995 MHz peaks in two main groups that probably indicate a double event from the same AR; the second part starts at \approx 09:50 UT.						
20	30.03.2004	C4.7	12:54	13:00	13:06	N15E05–10582 LASCO data gap.
		CME	gap			
		IV	12:56		13:03	
		III	12:56		13:03	

Table 2 (Continued)

#	Date	Activity	Start UT	Max	End	Position of AR–CME
		SVTO 4995 MHz	12:56	12:57	12:58	
		SVTO 4995 MHz	13:00	13:01	13:03	
		Puls.	12:56		13:03	
		Fiber	12:57		12:58	
		Spikes	12:55		12:58	
		Spikes	13:02		13:04	
		Spikes	13:08		13:11	
Note: following type III group at 12:56, there is intermittent type III activity until 13:03 UT. No EIT data, MDI is used to spatially localize the active region. Multiple SVTO 4995 MHz peaks.						
21	06.04.2004	M2.4	12:30	13:28	14:30	S18E15–10588
		CME	13:17			167 (halo)
		IV	13:16		13:26	
		III	13:16			
		SVTO 4995 MHz	13:16	13:23	13:30	
		RHESSI 50–100 KeV	13:19	13:23	13:28	
		Puls.	13:16		13:24	
		Zebra	13:22		13:22	
		Fiber	13:25		13:26	
		Zebra	13:22		13:22	
Note: multiple SVTO 4995 MHz peaks.						
22	13.07.2004	M5.4	08:40	08:48	10:15	N12W52–10646
		CME	08:45			326 (halo)
		IV	08:50		09:48	
		II	08:48		08:57	
		III	08:46			
		SVTO 4995 MHz	08:44	08:47	08:51	
		RHESSI 12–25 KeV	08:39	08:44	08:46	
		Spikes	08:48		09:14	
		Fiber	09:04		09:06	
		Fiber	09:27		09:36	
		Fiber	09:45		09:51	
Note: position angle from CACTUS. Multiple SVTO 4995 MHz peaks in a single group.						
23	20.07.2004	M8.6	12:22	12:32	13:00	N11E34–10652
		CME	13:17			334 (halo)
		IV	07:00		15:00	
		SVTO 4995 MHz	12:25	12:29	12:36	
		II	12:33		12:40	
		Spikes	12:10		14:50	
		Puls.	12:10		14:50	
		Fiber	12:56		13:06	
		Fiber	13:15		13:16	
Note: the CME onset appears on the 195 Å movies at AR 10652 bound northwest across the disk. Because of this nonradial propagation the onset time is somewhat uncertain.						

Table 2 (Continued)

#	Date	Activity	Start	Max	End	Position of AR–CME		
			UT					
24	21.07.2004	C8.9	05:05	05:21	06:35	N05E24–10652 165 (66)		
		CME	05:11					
		IV	05:41				10:55	
		III	07:49					
		III	07:58					
		III	08:15					
		SVTO 4995 MHz	05:15				05:16	05:30
		RHESSI 12–25 KeV	05:10				05:16	05:30
		Puls.	05:42					09:18
		Spikes	05:30					06:30
		Spikes	06:44					06:56
		Spikes	07:17					07:28
		Spikes	07:34					07:45
		Spikes	07:55					08:22
25	14.01.2005	C4.6	12:33	12:41	13:00	S07E05–10718 no CME		
		IV	12:37				12:48	
		II	12:47				12:50	
		III	12:37					
		SVTO 4995 MHz	12:37				12:38	12:40
		III	12:46					
		RHESSI 25–50 KeV	12:35				12:39	12:42
		Puls.	12:37					12:46
		Zebra	12:37					12:37
		RHESSI 25–50 KeV	12:42				12:43	12:55
		Zebra	12:43					12:43
		Zebra	12:44					12:44
		SVTO 4995 MHz	12:45				12:46	12:47
		Zebra	12:47					12:48
		Spikes	12:47					12:52
		Note: multiple HXR peaks.						
26	15.01.2005	M8.6	05:54	06:38	8:30	N16E04–10720 359 (halo)		
		CME	06:03					
		IV	06:21				8:40	
		SVTO 4995 MHz	05:56				06:29	07:10
		Puls.	06:07					06:11
		Spikes	06:18					06:24
		Puls.	06:18					09:20
		Spikes	06:38					06:40
		Fiber	06:44					06:45
		Spikes	06:46					06:49
		Fiber	06:49					06:53
		Fiber	07:05					08:26
		Spikes	07:58					08:05
		Zebra	07:59					07:59
		Zebra	08:00					08:00
		Zebra	08:03					08:03
		Zebra	08:17					08:17
		Note: multiple SVTO 4995 MHz peaks.						

Table 2 (Continued)

#	Date	Activity	Start	Max	End	Position of AR–CME		
			UT					
27	17.01.2005	X3.8	6:59	09:52	11:00	N15W25–10720 334 (halo)		
		CME	09:06					
		IV	08:40				10:46	
		II	09:44				9:48	
		III	09:44					
		RHESSI 100–300 KeV	09:36				09:50	10:30
		SVTO 4995 MHz	09:02				09:29	10:30
		Spikes	09:02					09:09
		Puls.	09:02					10:27
		Spikes	09:13					09:22
		Fiber	09:15				09:54	
		Spikes	09:32				09:34	
		CME	09:43					309 (halo)
		Fiber	09:59				10:49	
		Spikes	10:12				10:38	
		Puls.	10:34				11:20	
		Fiber	11:09				12:02	
		Puls.	11:33				12:02	
		Zebra	09:20				09:20	
		Zebra	10:45				10:45	
Spikes	10:56		11:40					
Zebra	10:58		11:00					
Spikes	11:51		12:01					

Note: two CMEs in close succession with SXR flux rising in two stages (see Hillaris *et al.*, 2011).

28	19.01.2005	X1.3	08:03	08:22	9:00	N15W51–10720 320 (halo)		
		CME	08:08					
		IV	08:07				9:00	
		II	08:11				8:18	
		III	08:14					
		RHESSI 100–300 KeV	08:12				08:26	08:38
		SVTO 4995 MHz	08:12				08:26	09:20
		Spikes	08:05					08:10
		Puls.	08:06					08:16
		Zebra	08:09					08:09
		Spikes	08:12				08:15	
		Fiber	08:20				08:22	
		Spikes	08:22				09:03	
		Puls.	08:39				09:38	
		Spikes	09:22				09:35	
		Fiber	09:53				09:54	
		III	10:24					
		Puls.	10:23				10:25	
		Spikes	10:23				10:28	

Note: multiple SVTO 4995 MHz peaks and probably a double event whose second part started at $\approx 09:15$ UT.

Table 2 (Continued)

#	Date	Activity	Start UT	Max	End	Position of AR–CME	
29	20.01.2005	X7.1	06:36	07:01	07:45	N15W51–10720 288 (halo)	
		CME	06:08				
		IV	06:36		08:00		
		III	06:39				
		II	06:44		06:49		
		III	06:44				
		III	06:57				
		III	07:07				
		RHESSI 25–50 KeV	06:38		06:45		07:27
		SVTO 4995 MHz	06:38		06:49		07:30
		Spikes	06:36				06:44
		II	06:56				06:58
		Puls.	06:42				06:47
		Spikes	06:46				07:20
		Puls.	06:53				07:02
		Fiber	06:53				06:59
		Fiber	07:05				07:13
		Puls.	07:12				07:30
		Fiber	07:22				07:26
		Zebra	07:28				07:28
Fiber	07:32		07:56				
Zebra	07:34		07:34				
Puls.	07:35		07:50				
Spikes	07:35		07:40				

Note: double SVTO 4995 MHz peak.

30	13.07.2005	M5.0	14:01	14:49	18:15	N11W90–10786 303 (halo)	
		CME	14:12				
		IV	13:56		14:23		
		RHESSI 25–50 KeV	14:12				
		SVTO 4995 MHz	14:02		14:18		14:34
		Puls.	13:52				14:12
		Zebra	13:58				13:59
		Fiber	14:03				14:06
		Zebra	14:08				14:08
		Spikes	14:09				14:11
		Puls.	14:16				14:22
		Zebra	14:18				14:18
		Zebra	14:19				14:19
		Zebra	14:21				14:21
		Zebra	14:22				14:22

Note: no EIT data, MDI is used to spatially localize the active region. Activity extends beyond the ARTEMIS-IV observation period.

Table 2 (Continued)

#	Date	Activity	Start	Max	End	Position of AR–CME		
			UT					
31	14.07.2005	X1.2	10:16	10:55	12:00	N11W90–10786 296 (halo)		
		CME	10:27					
		IV	10:26				12:03	
		III	10:32					
		III	10:38					
		RHESSI 25–50 KeV	10:25				10:27	10:29
		SVTO 4995 MHz	10:30				10:35	11:25
		RHESSI 25–50 KeV	11:00				11:04	11:25
		Puls.	10:18					11:14
		Spikes	10:32					10:34
		Spikes	10:40					10:55
		Fiber	11:10					12:12
		Puls.	11:26					11:48

Note: NRH data gap. Multiple SVTO 4995 MHz peaks.

32	30.07.2005	X1.3	06:17	06:35	07:30	N12E60–10792 050 (halo)		
		CME	06:21					
		IV	06:21				06:44	
		II	06:26				06:32	
		III	06:28					
		SVTO 4995 MHz	06:20				06:32	06:45
		RHESSI 100–300 KeV	06:27				06:32	06:45
		Spikes	06:20					06:23
		Spikes	06:26					06:39
		Puls.	06:29					06:36

Note: outside NRH daily observations. Multiple SVTO 4995 MHz peaks

33	22.8.2005	M2.6	00:44	01:33	09:00	S11W65–10798 222 (56)		
		CME	05:09					
		IV	05:43				6:30	
		RHESSI 6–12 KeV	05:50				06:01	06:30
		Spikes	05:40					05:46
		Puls.	05:52					05:54
		Zebra	05:53					05:54
		Zebra	05:59					06:03
		Spikes	06:14					06:14

Note: partial observation of the end of a type IV continuum starting at about 00:44 UT, as reported by the Culgoora radio-spectrograph. Outside NRH daily observations.

34	23.8.2005	M2.7	14:19	14:44	16:08	S11W65–10798 230 (halo)		
		CME	14:45					
		IV	14:26				15:02	
		SVTO 4995 MHz	14:23				14:49	15:20
		RHESSI 50–100 KeV	14:23				14:38	15:10
		Spikes	14:26					15:00

Note: activity extends beyond the ARTEMIS-IV observation period. Multiple HXR and SVTO 4995 MHz peaks.

Table 2 (Continued)

#	Date	Activity	Start	Max	End	Position of AR–CME		
			UT					
35	12.02.2010	M8.3	11:19	11:26	11:28	N26E11–11046 044 (halo)		
		CME	11:18					
		IV	11:26				11:32	
		IV	12:00				12:45	
		II	11:26				11:31	
		III	11:25					
		III	11:29					
		RHESSI 50–100 KeV	11:21				11:26	11:36
		Spikes	11:24					11:25
		Spikes	12:00					12:12
		Puls.	11:25					11:28
36	01.08.2010	C3.2	07:55	08:26	09:35	N20E36–11092 084 (halo)		
		CME	08:27					
		IV	08:06				10:00	
		RHESSI 100–300 KeV	08:00				08:33	08:48
		Puls.	08:00					08:03
		Spikes	08:08					08:09
		Spikes	08:18					08:22
		Puls.	08:16					09:26
		Fiber	08:26					09:36
		Spikes	09:30					09:50
		Fiber	09:47					09:48
Spikes	10:12		10:20					

Note: NRH data gap.

Comments and remarks, when necessary, have been added below the appropriate entries. A collection of observational data, including dynamic spectra, is given in Appendix B.

Appendix B: Details on the ARTEMIS-IV Recordings and Accompanying Data

In Figures 11–46 we present dynamic spectra and other observational data for the 36 events used to compile Table 2 and Figures 9, 8, and 10. They are intended to show the temporal and spatial association of type IV continua and their fine structure with flares, microwave, and HXR bursts and CMEs, as detailed in Section 2. In each figure we list the following:

- The upper panel shows medium resolution dynamic spectra recorded by the ARTEMIS-IV/ASG in the 650–20 MHz range (cadence of 10 samples/sec); in the 270–450 MHz range the ARTEMIS-IV/SAO high sensitivity, high time resolution spectrum is overlaid (sampling rate 100 samples/sec).

Table 3 List of event dates and start–end times.

#	Date	Start UT	End	#	Date	Start UT	End
1	30.06.1999	11:24	11:45	2	13.07.1999	05:22	07:00
3	15.04.2000	10:04	10:55	4	15.04.2000	12:13	14:43
5	30.04.2000	07:53	09:30	6	11.07.2000	12:12	15:20
7	14.07.2000	10:03	11:30	8	14.07.2000	12:50	13:40
9	14.07.2000	13:44	14:30	10	19.09.2000	08:06	08:42
11	18.11.2000	13:02	15:00	12	21.04.2003	12:54	13:30
13	26.10.2003	05:57	09:10	14	28.10.2003	09:51	15:00
15	03.11.2003	09:43	11:00	16	04.02.2004	11:12	12:15
17	25.03.2004	12:01	12:20	18	30.03.2004	05:37	06:10
19	30.03.2004	09:41	09:55	20	30.03.2004	12:54	13:11
21	06.04.2004	12:30	14:30	22	13.07.2004	08:39	10:15
23	20.07.2004	12:10	15:00	24	21.07.2004	05:05	10:55
25	14.01.2005	12:33	13:00	26	15.01.2005	05:54	08:40
27	17.01.2005	06:59	12:00	28	19.01.2005	08:03	10:28
29	20.01.2005	06:36	07:56	30	13.07.2005	14:01	18:15
31	14.07.2005	10:16	12:12	32	30.07.2005	06:17	07:30
33	22.08.2005	00:44	09:00	34	23.08.2005	14:19	16:08
35	12.02.2010	11:18	12:45	36	01.08.2010	07:55	10:20

- Soft X-Ray (SXR) light curves, obtained from the *Geostationary Operational Environmental Satellites* (GOES). The CME onset times are marked with arrows; they were estimated from the LASCO movies using the linear regression and are included in the online LASCO event lists.
- Hard X-Ray (HXR) light curves from the *Reuven Ramaty High Energy Solar Spectroscopic Imager* (RHESSI) archive for events after the beginning of 2003; prior to 2003, HXR data are from the MTI/HXRS and BATSE/GRP experiments.
- Centimetric radio flux; 4.995 GHz radio flux profiles from the *Radio Solar Telescope Network* (RSTN) or, in a few events, from the 2.695 GHz channel of the *Trieste solar Radio System* (TSTS).
- Time-line plot; relative timing of pulsations, fiber bursts, zebra stripes, and spike groups associated with type IV continuum.
- Type IV–flare–CME positions; these include, from left to the right: Nançay Radioheliograph (NRH) half-power contours at 164, 236, 327 MHz, 410 and 432 MHz (when available), overlaid on *Extreme Ultraviolet Imaging Telescope* (EIT) images. When EIT data were not available, MDI images were used to identify the associated active region. The flare position from the NOAA/SGD catalogs is schematically shown in the middle panel for comparison with the direction of the CME launch to the right panel. This is marked graphically in the right panel, which shows the CME measurement position angle (MPA, solid arrow) and, for non-halo CMEs, the angular width (dashed arrow) from the LASCO coronagraph event lists and/or the CACTUS CME catalog.

A concise list of the dates and event start and end times is given in Table 3.

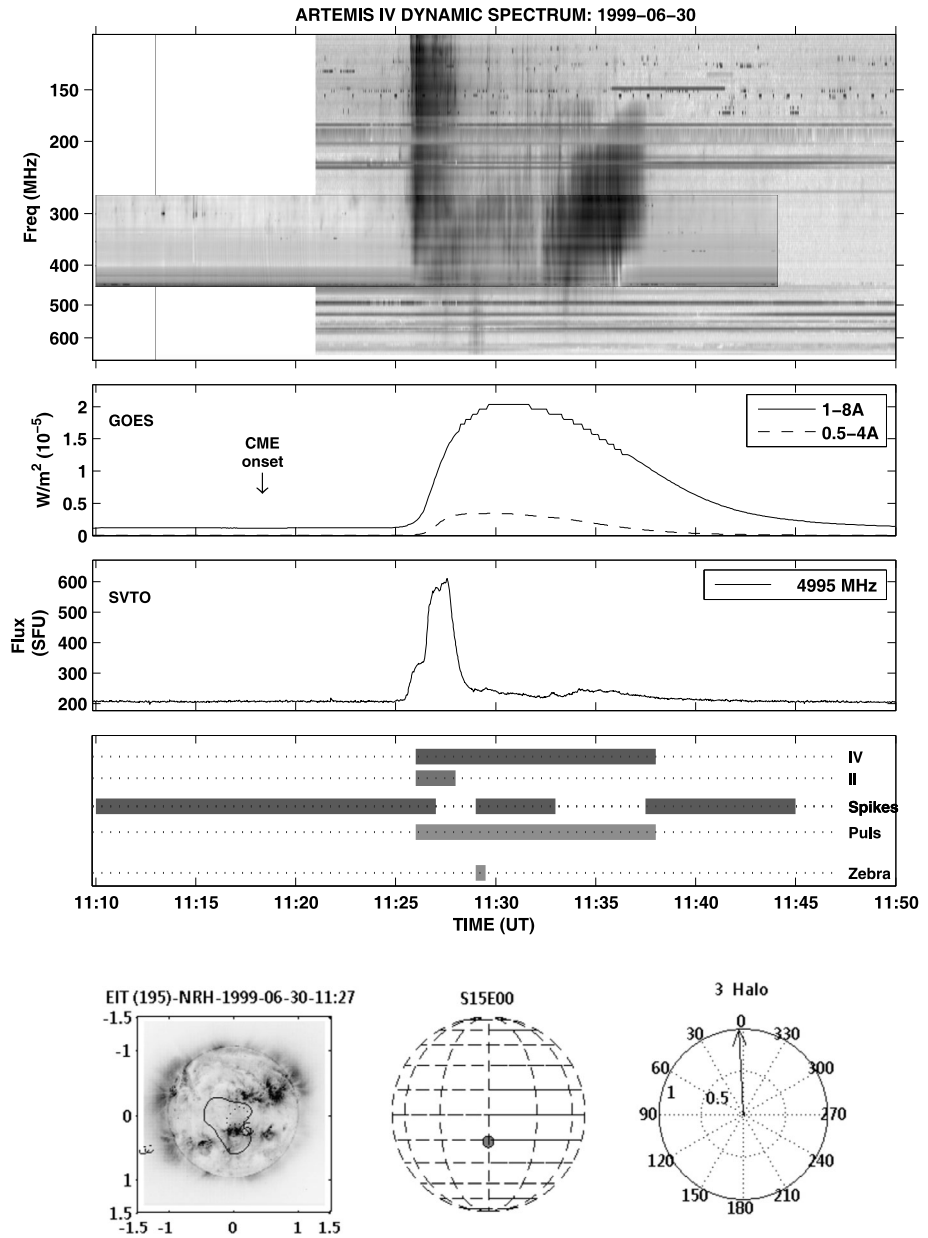


Figure 11 Event 1 on 30 June 1999.

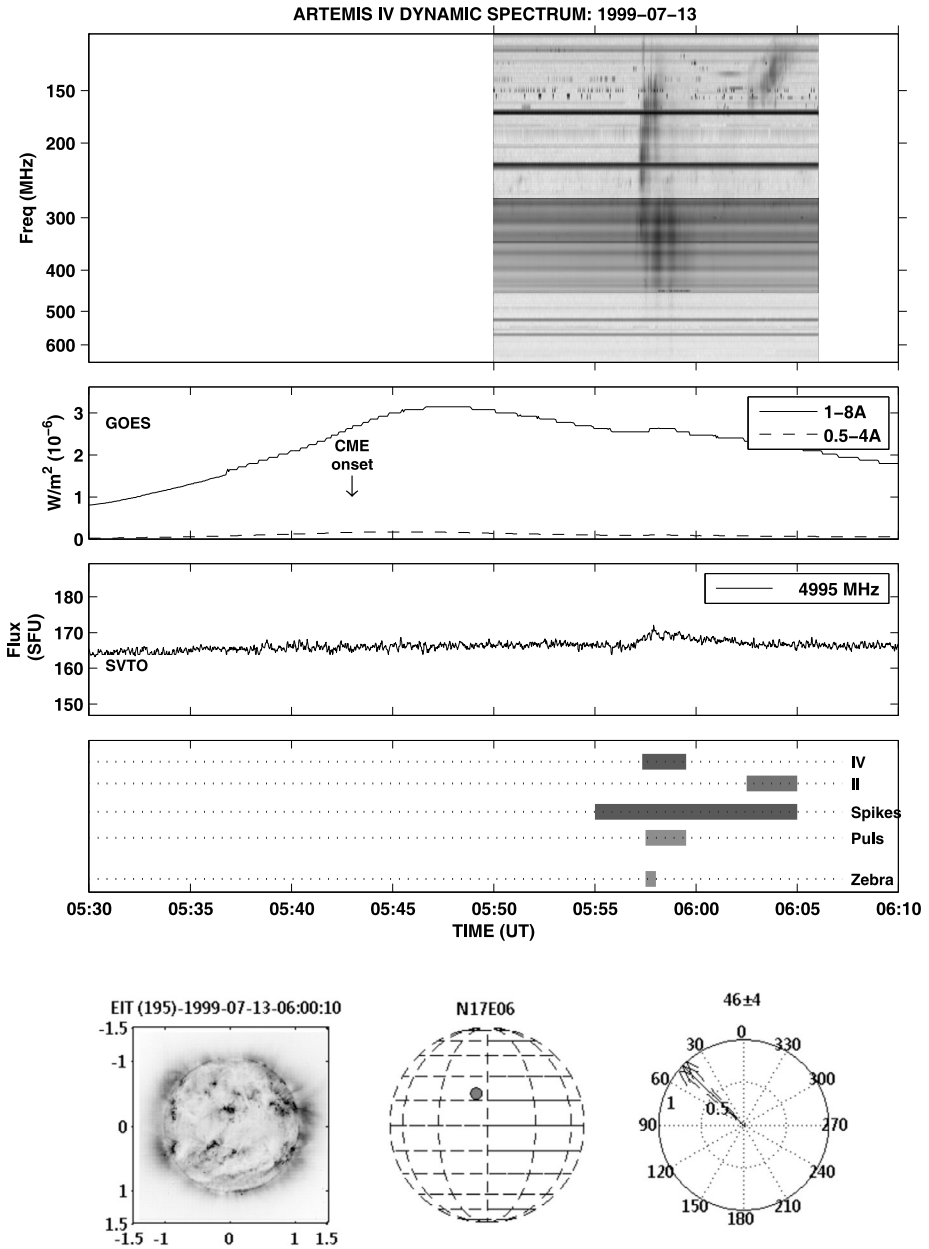


Figure 12 Event 2 on 13 July 1999.

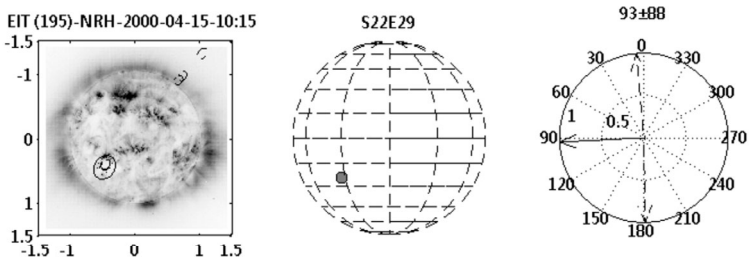
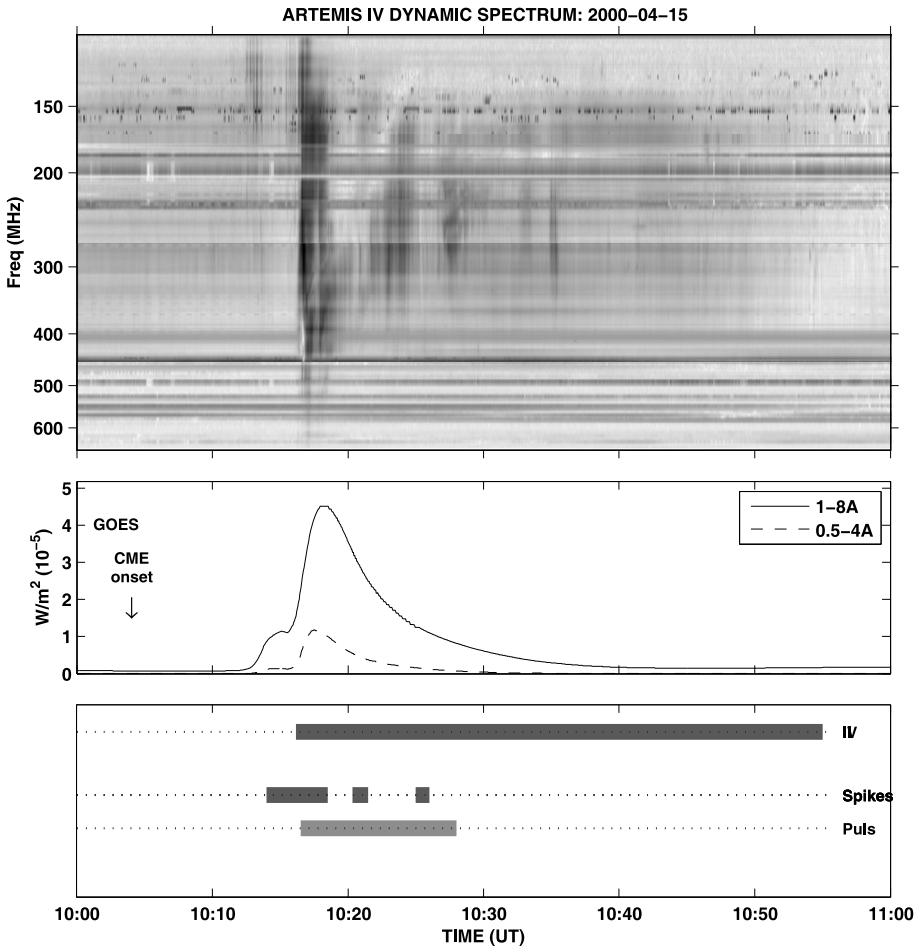


Figure 13 Event 3 on 15 April 2000.

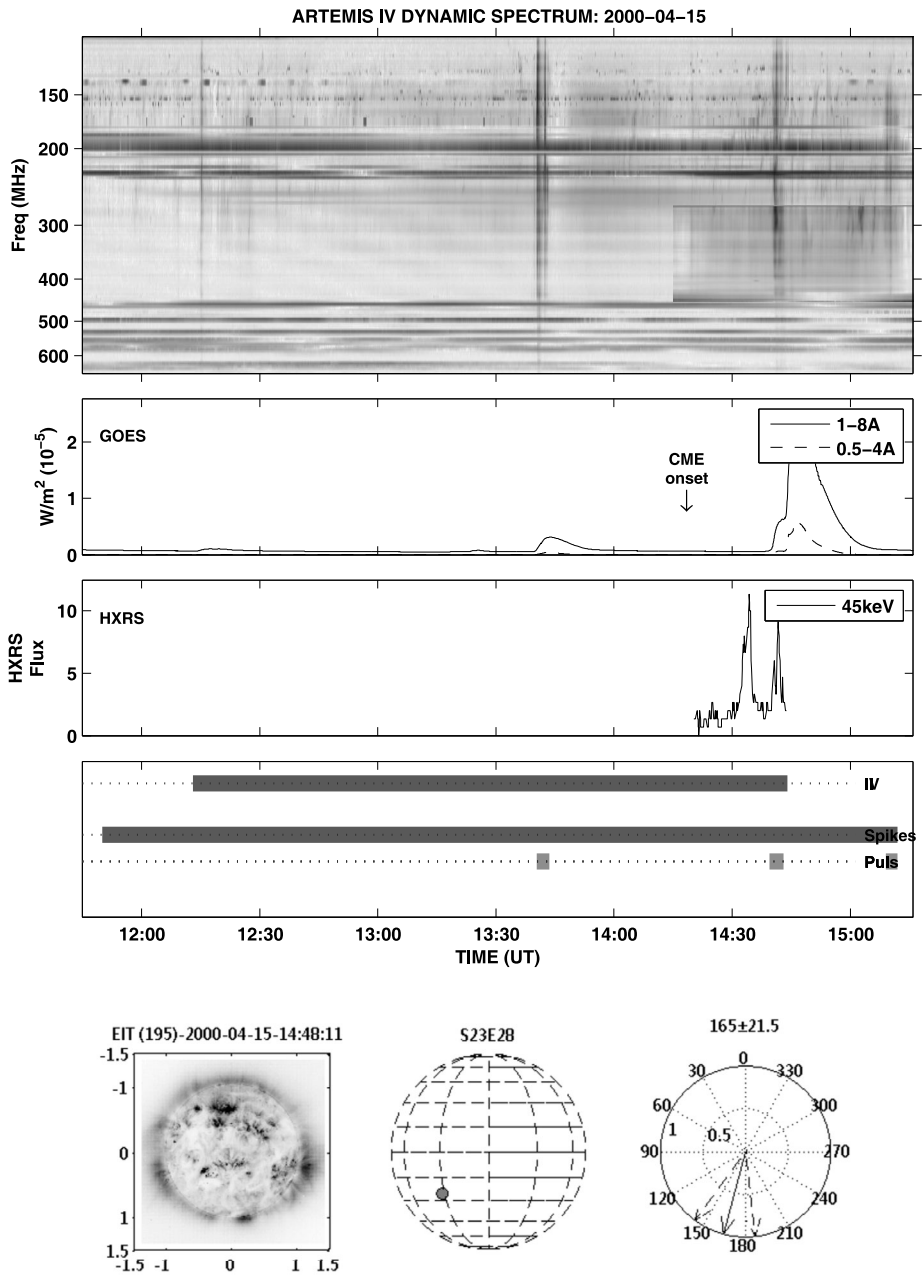


Figure 14 Event 4 on 15 April 2000.

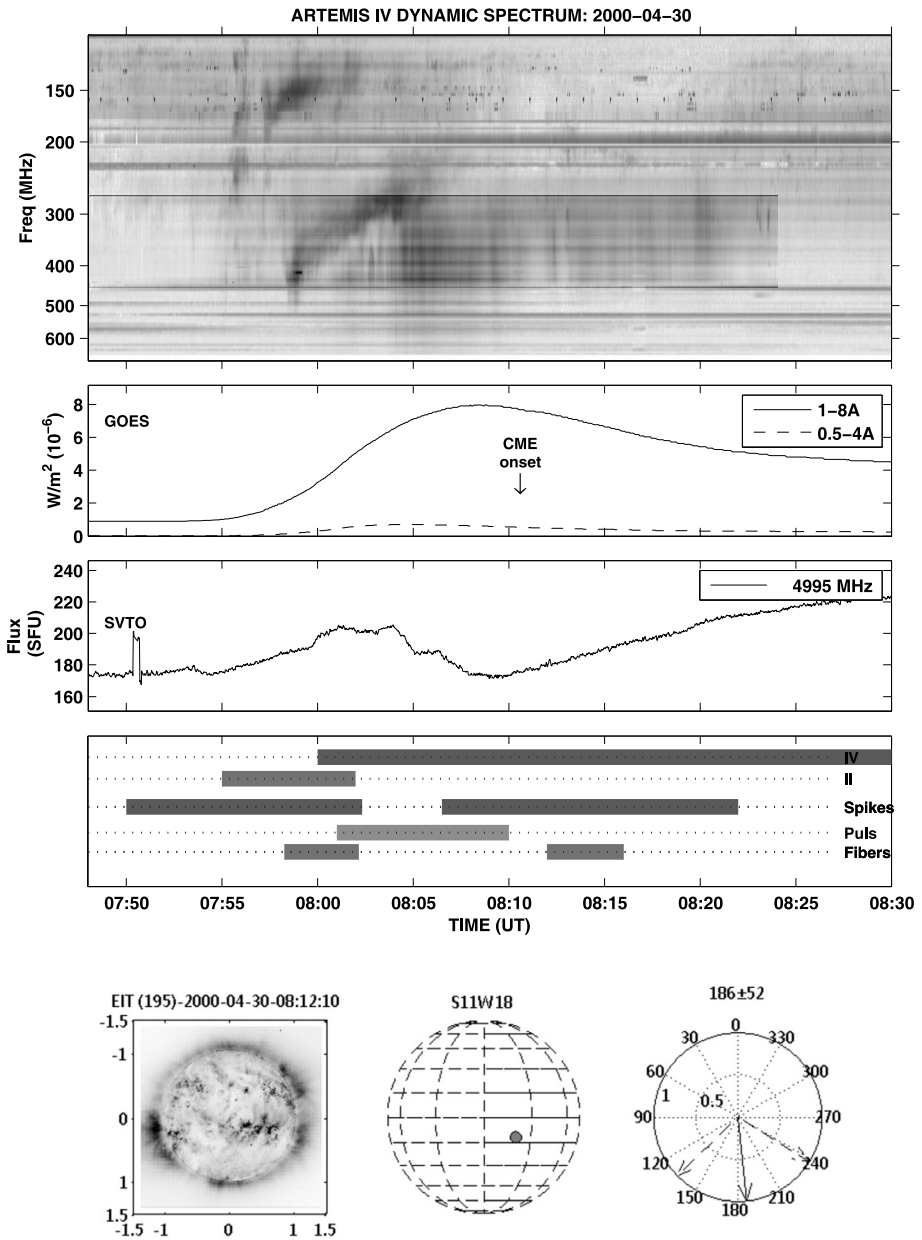


Figure 15 Event 5 on 30 April 2000.

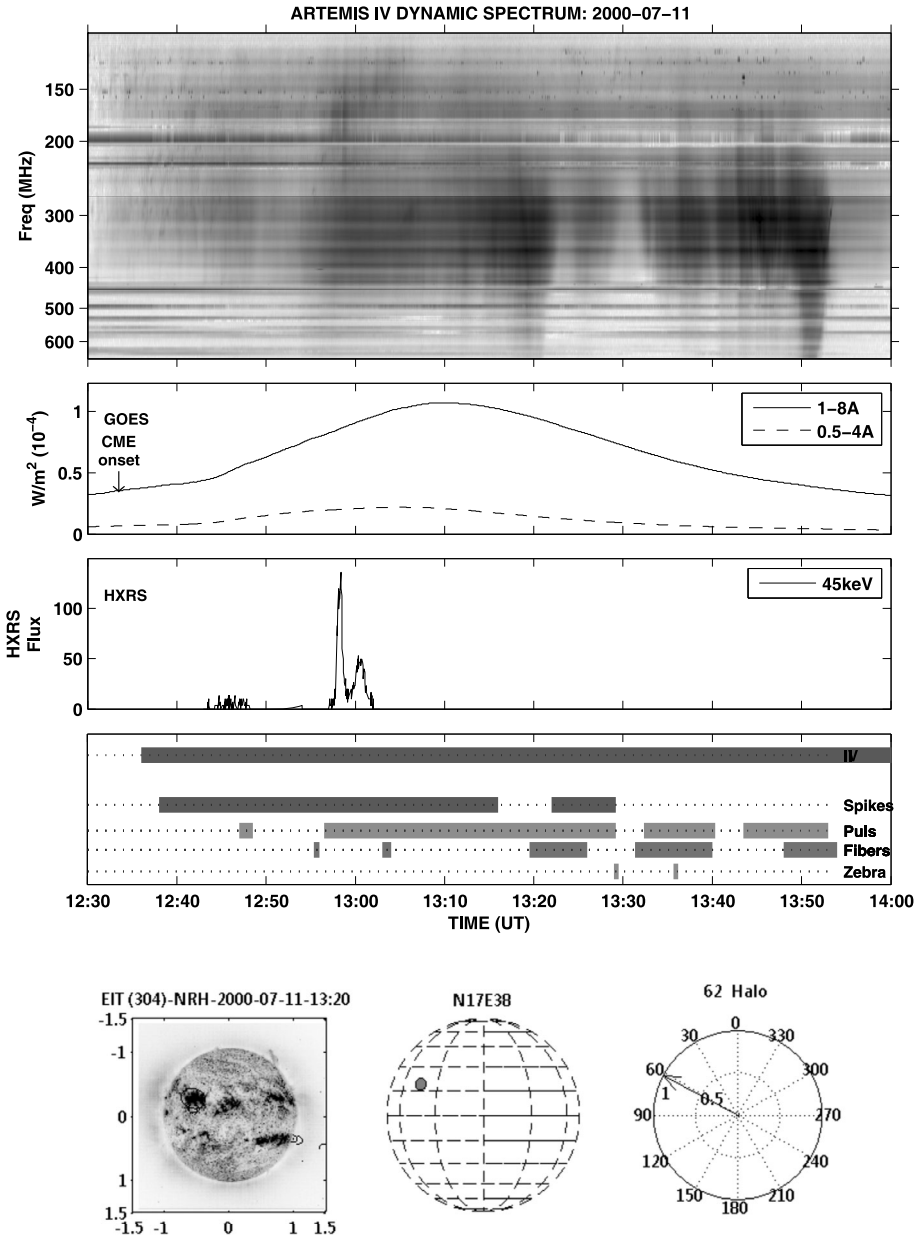


Figure 16 Event 6 on 11 July 2000.

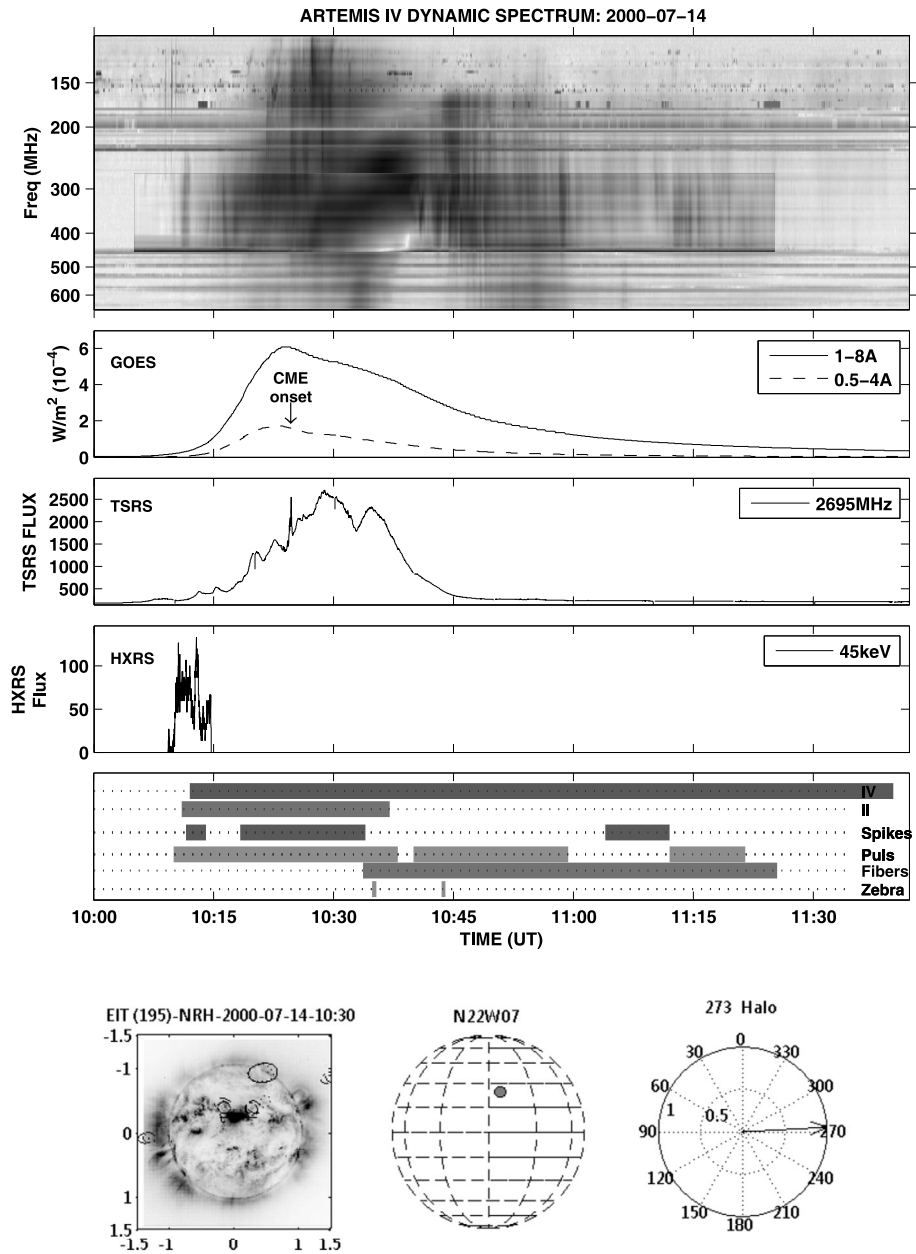


Figure 17 Event 7 on 14 July 2000.

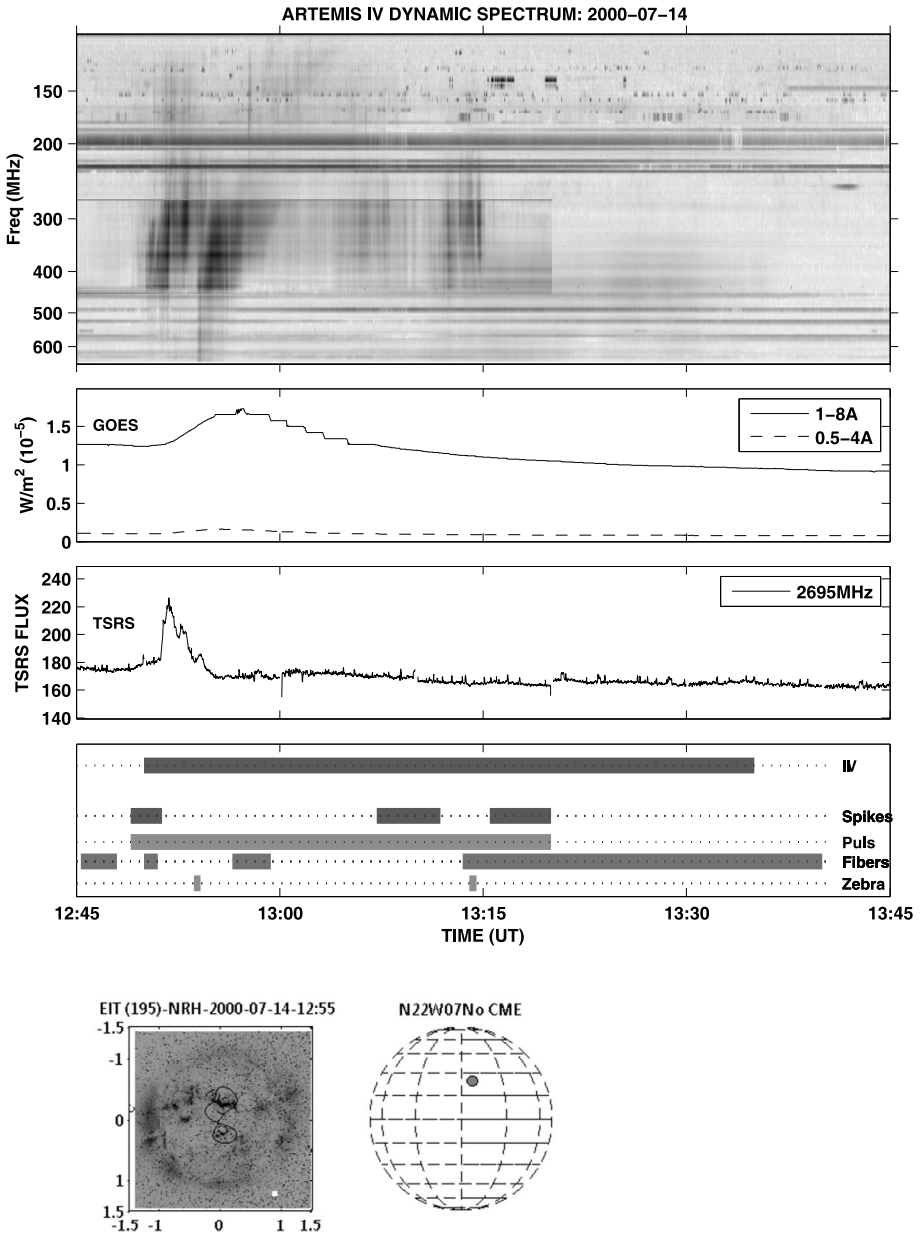


Figure 18 Event 8 on 14 July 2000.

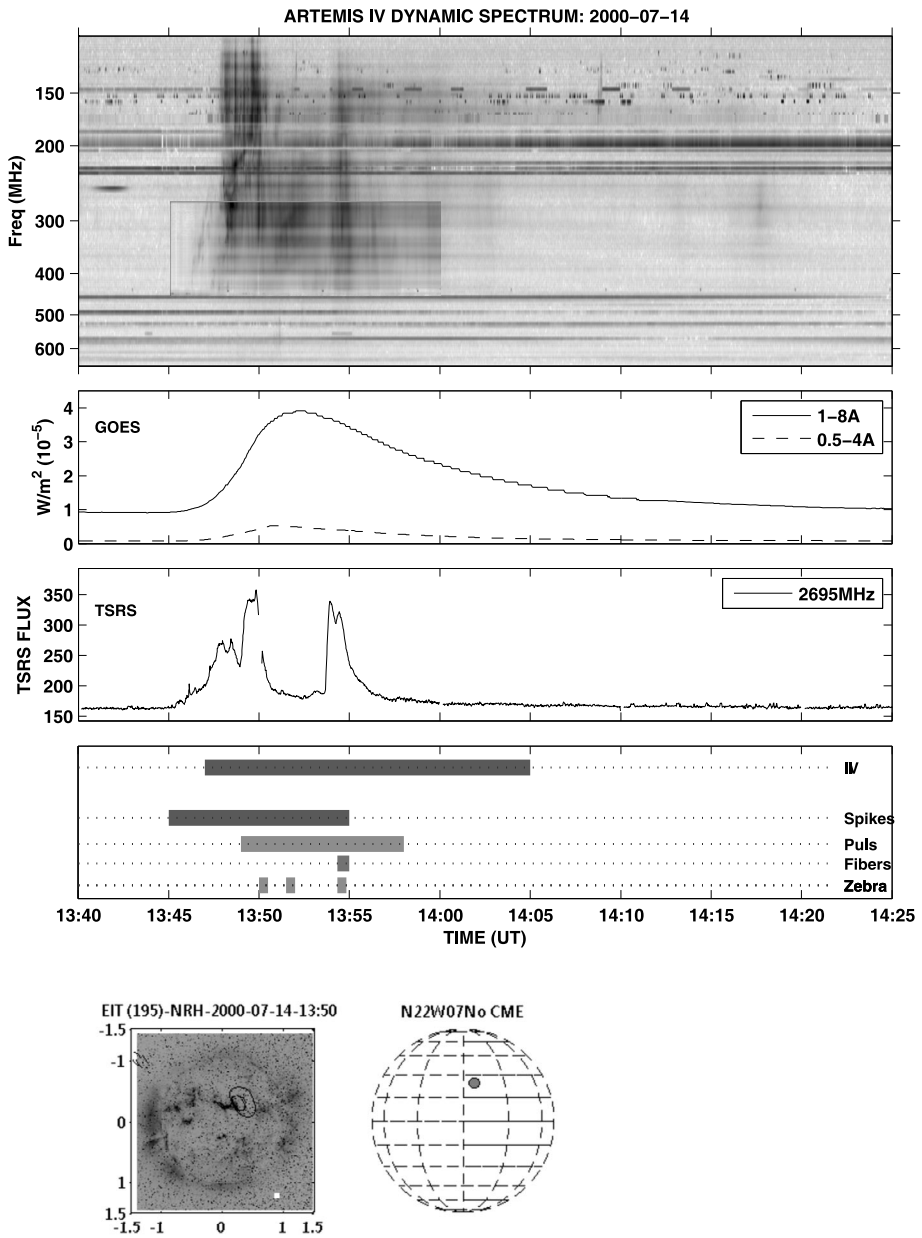


Figure 19 Event 9 on 14 July 2000.

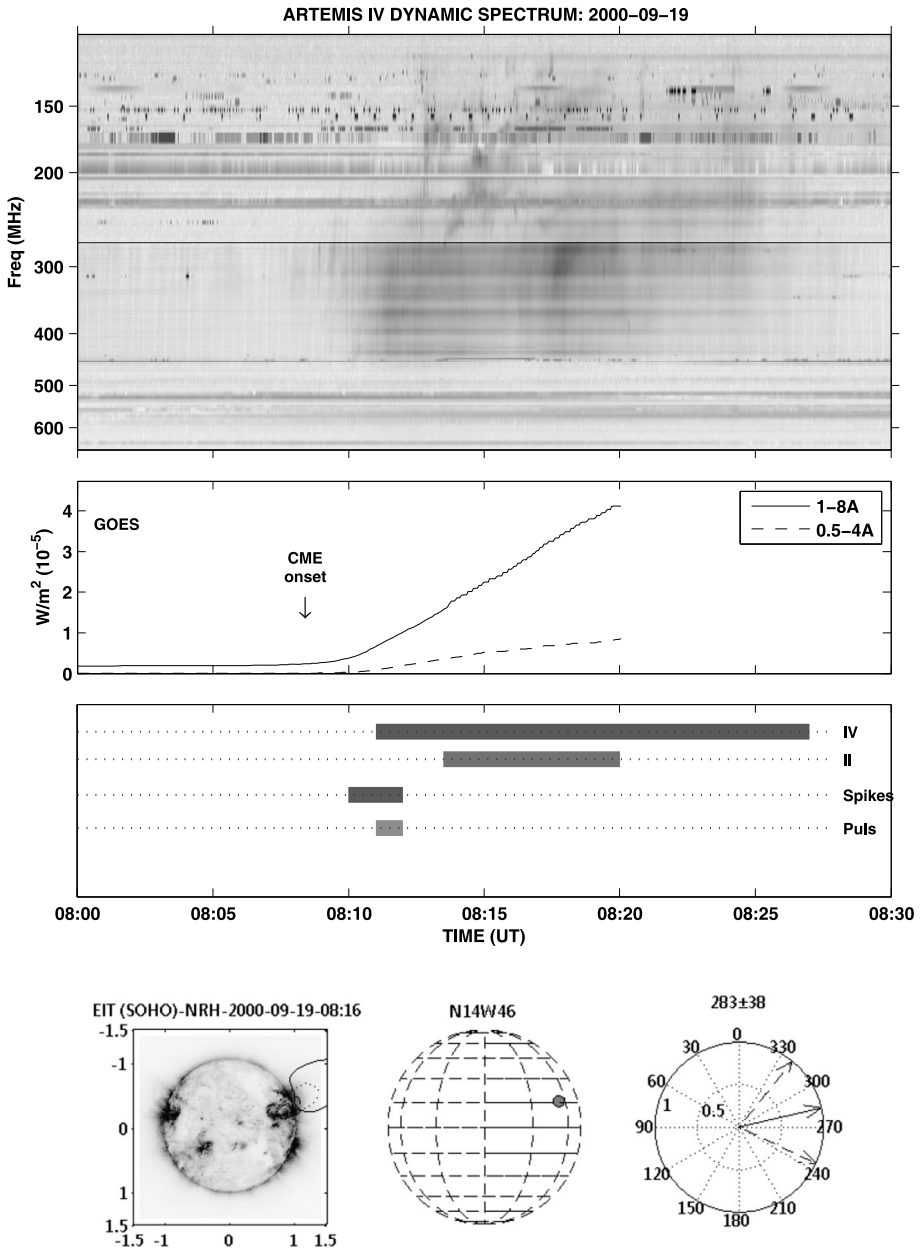


Figure 20 Event 10 on 19 September 2000.

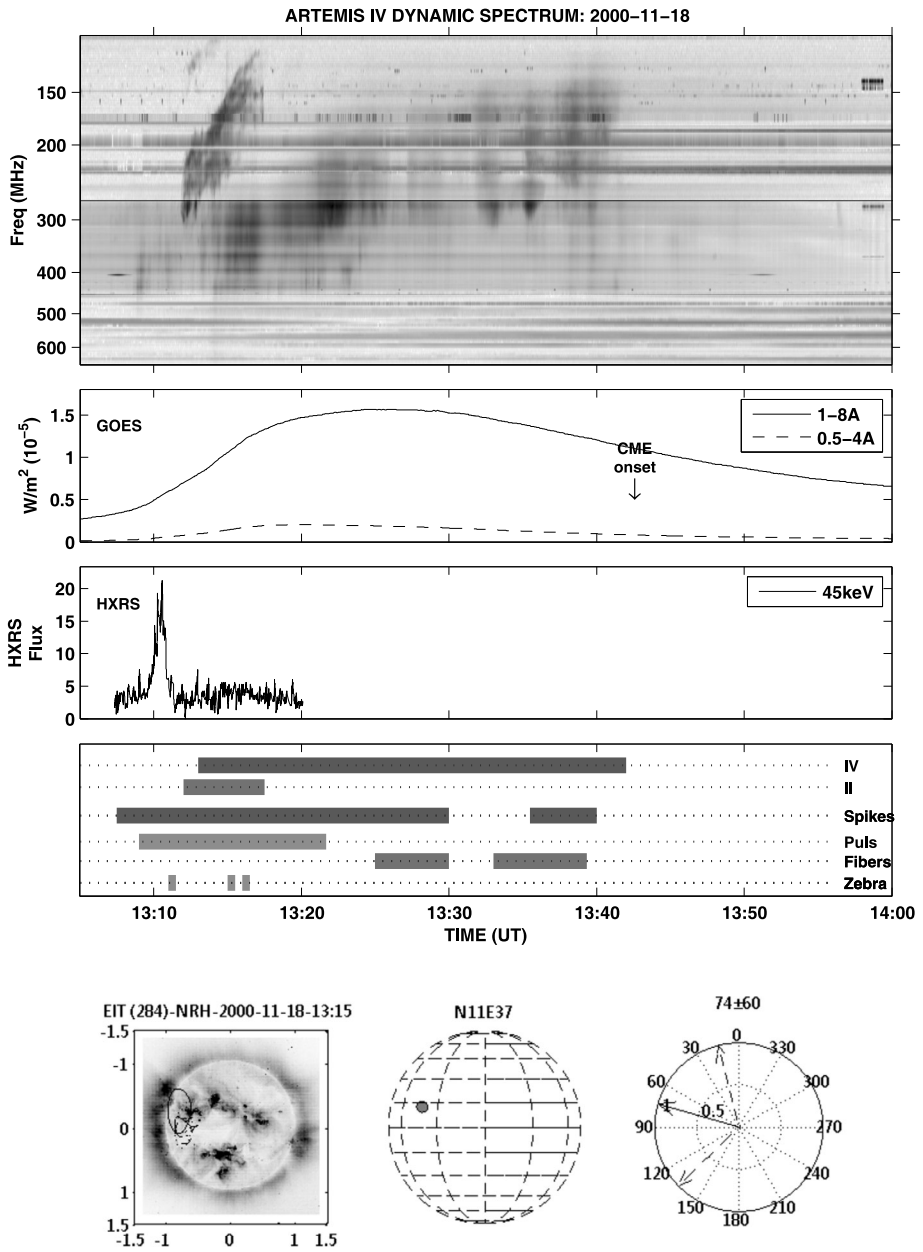


Figure 21 Event 11 on 18 November 2000.

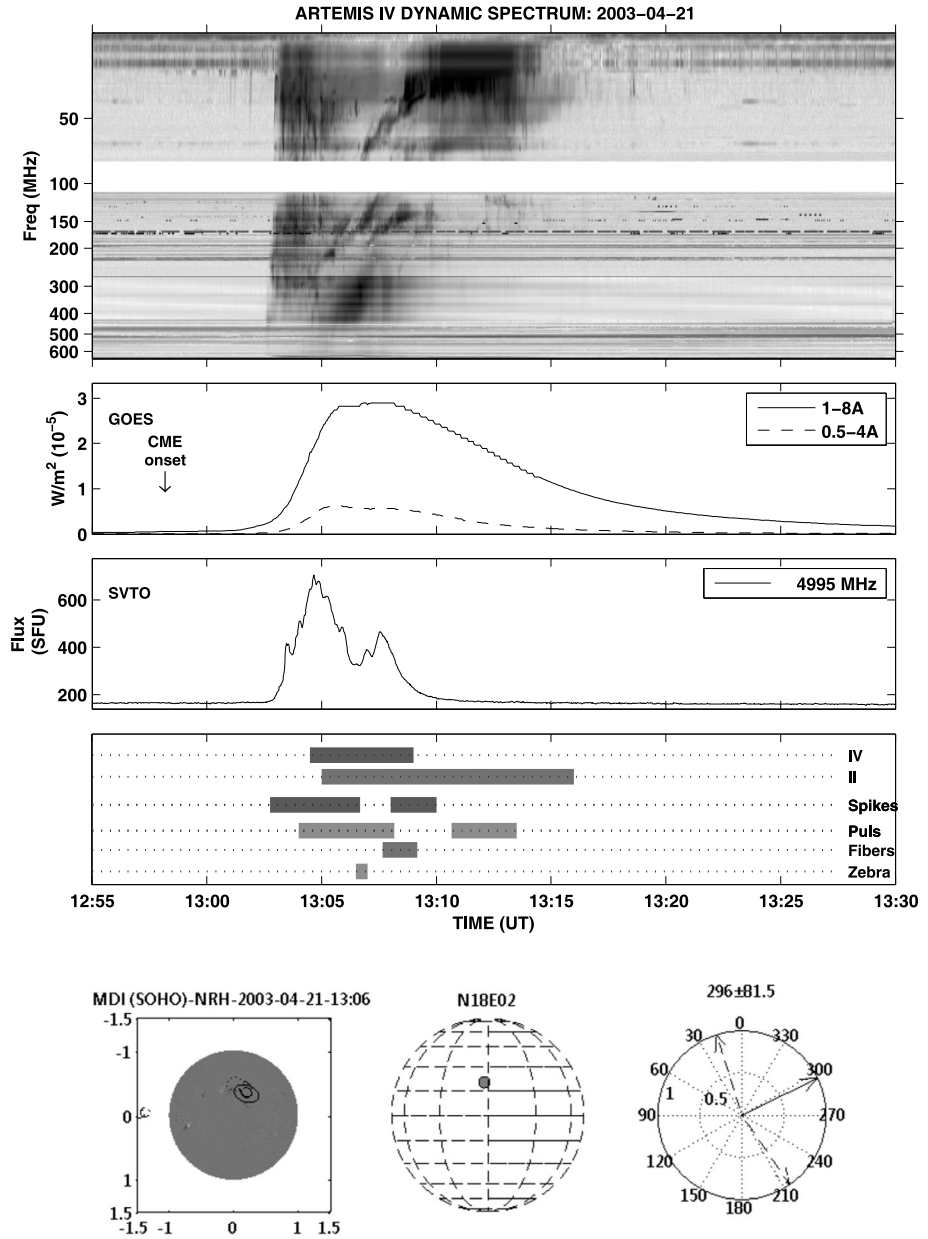


Figure 22 Event 12 on 21 April 2003.

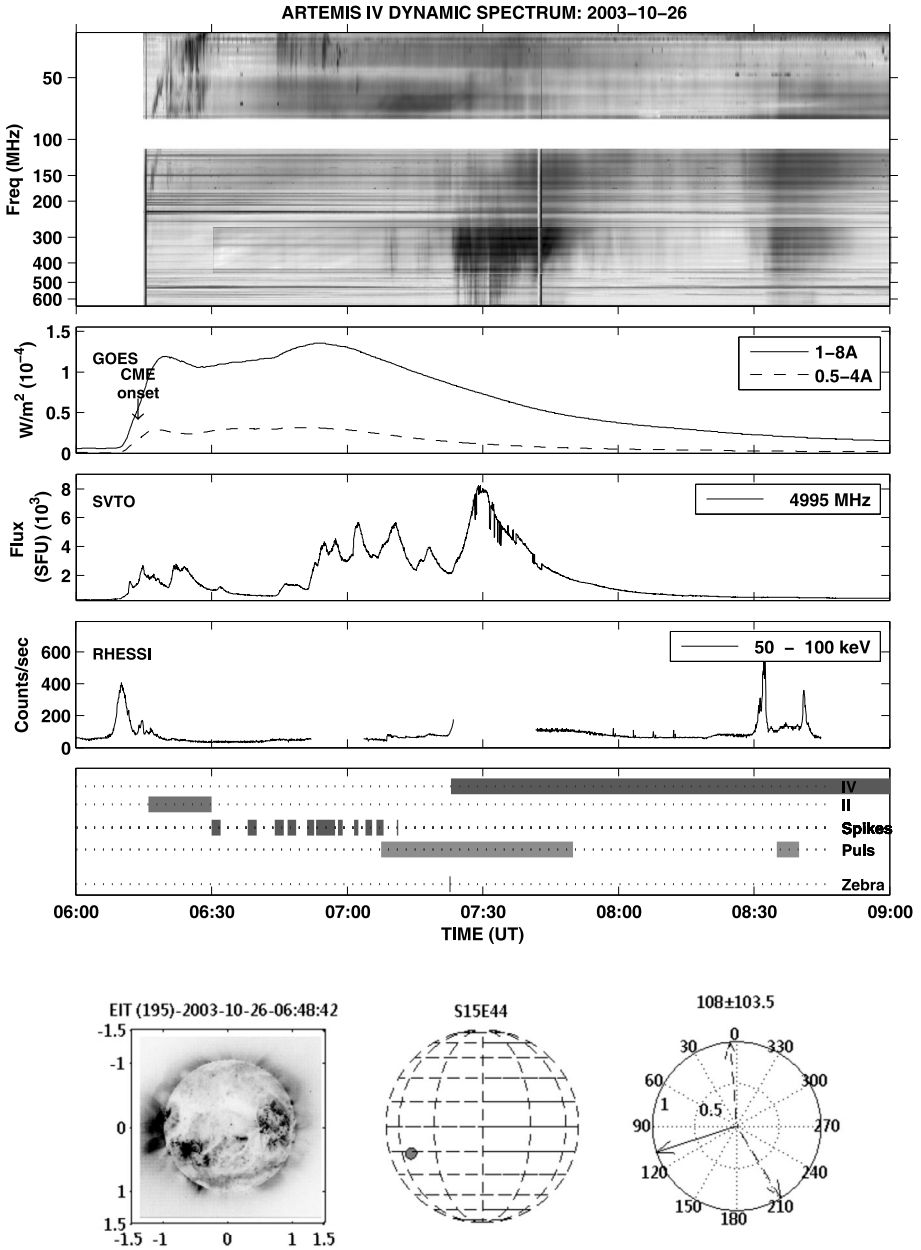


Figure 23 Event 13 on 26 October 2003.

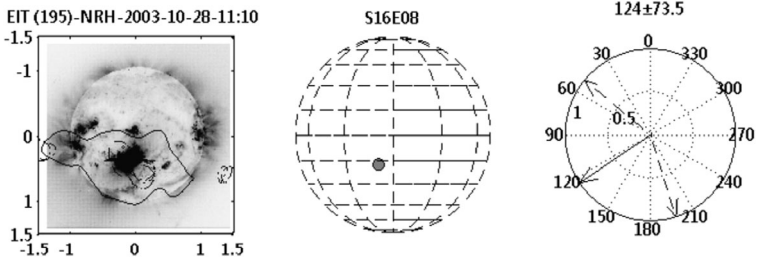
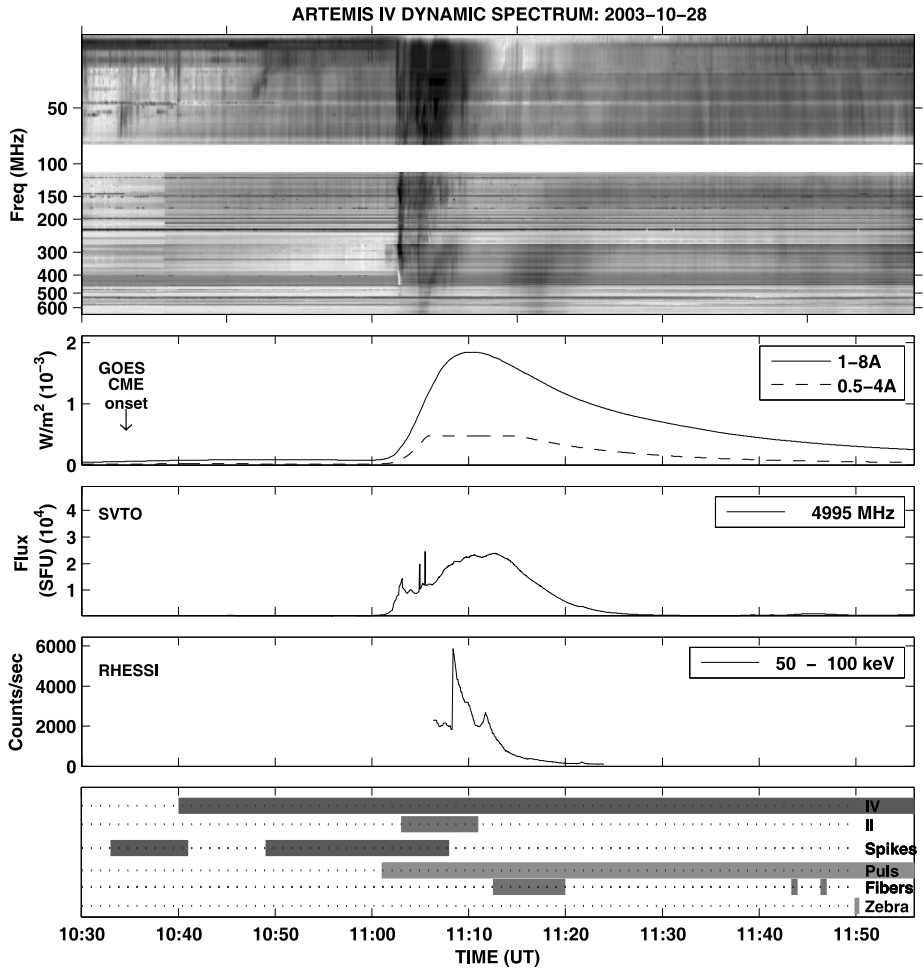


Figure 24 Event 14 on 28 October 2003.

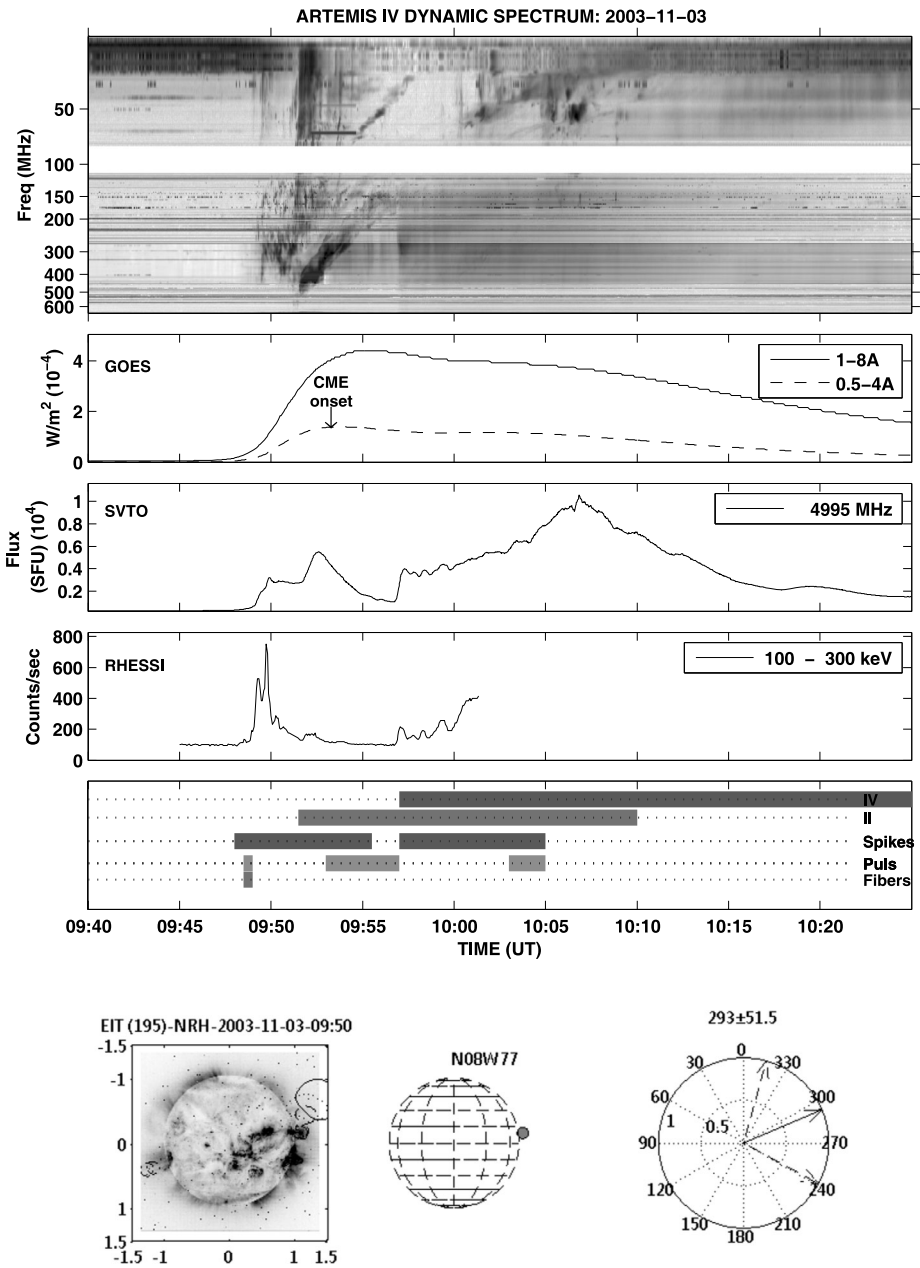


Figure 25 Event 15 on 03 November 2003.

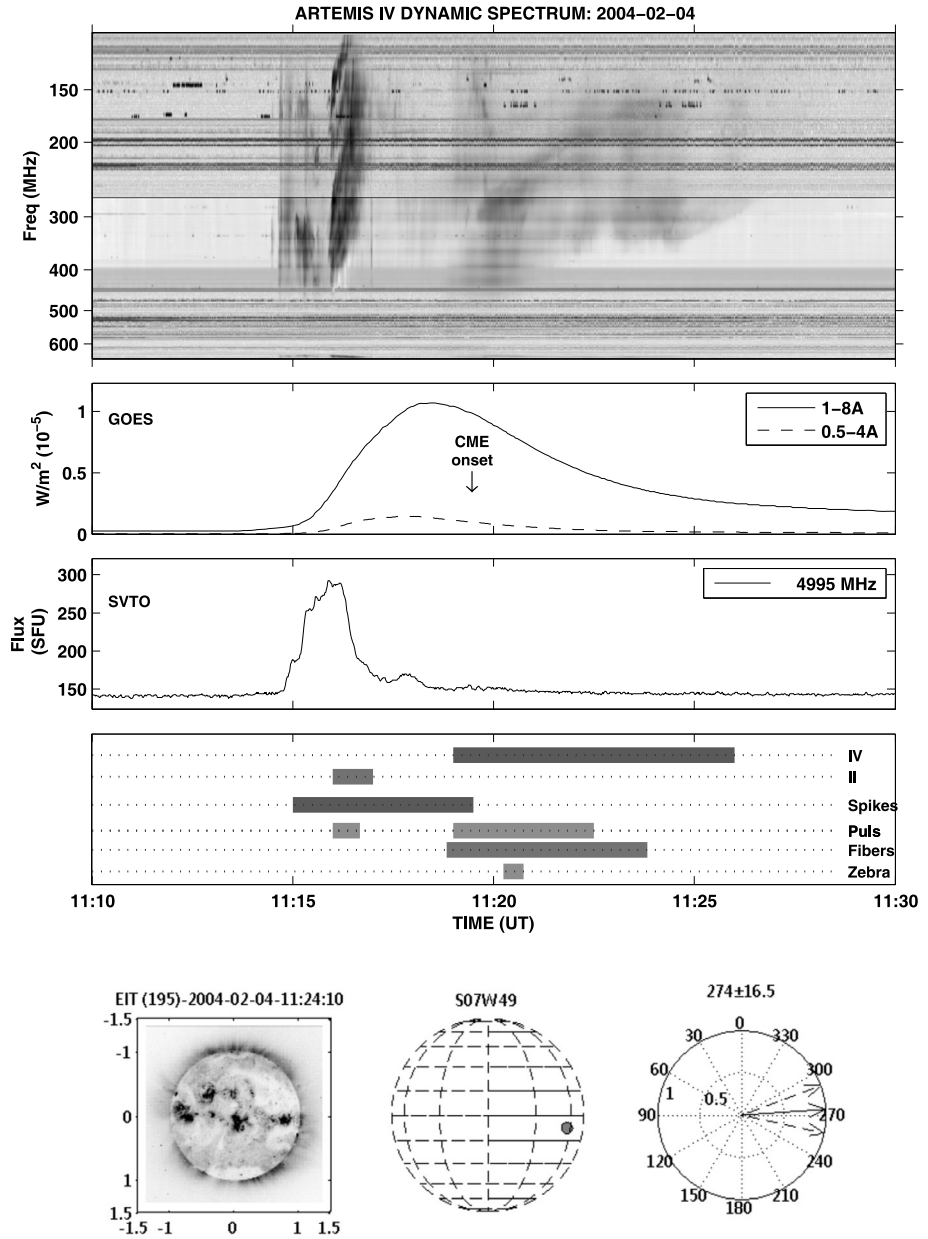


Figure 26 Event 16 on 04 February 2004.

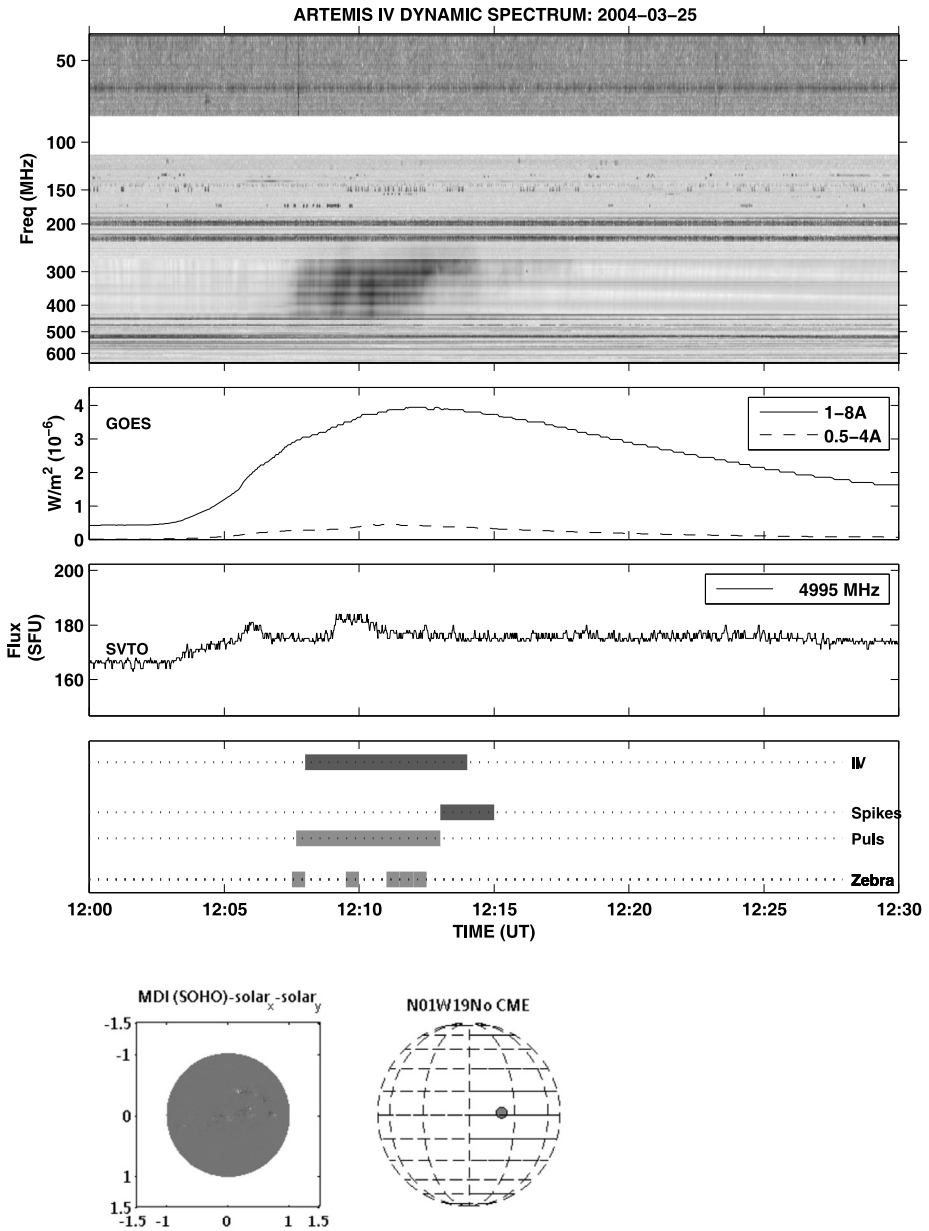


Figure 27 Event 17 on 25 March 2004.

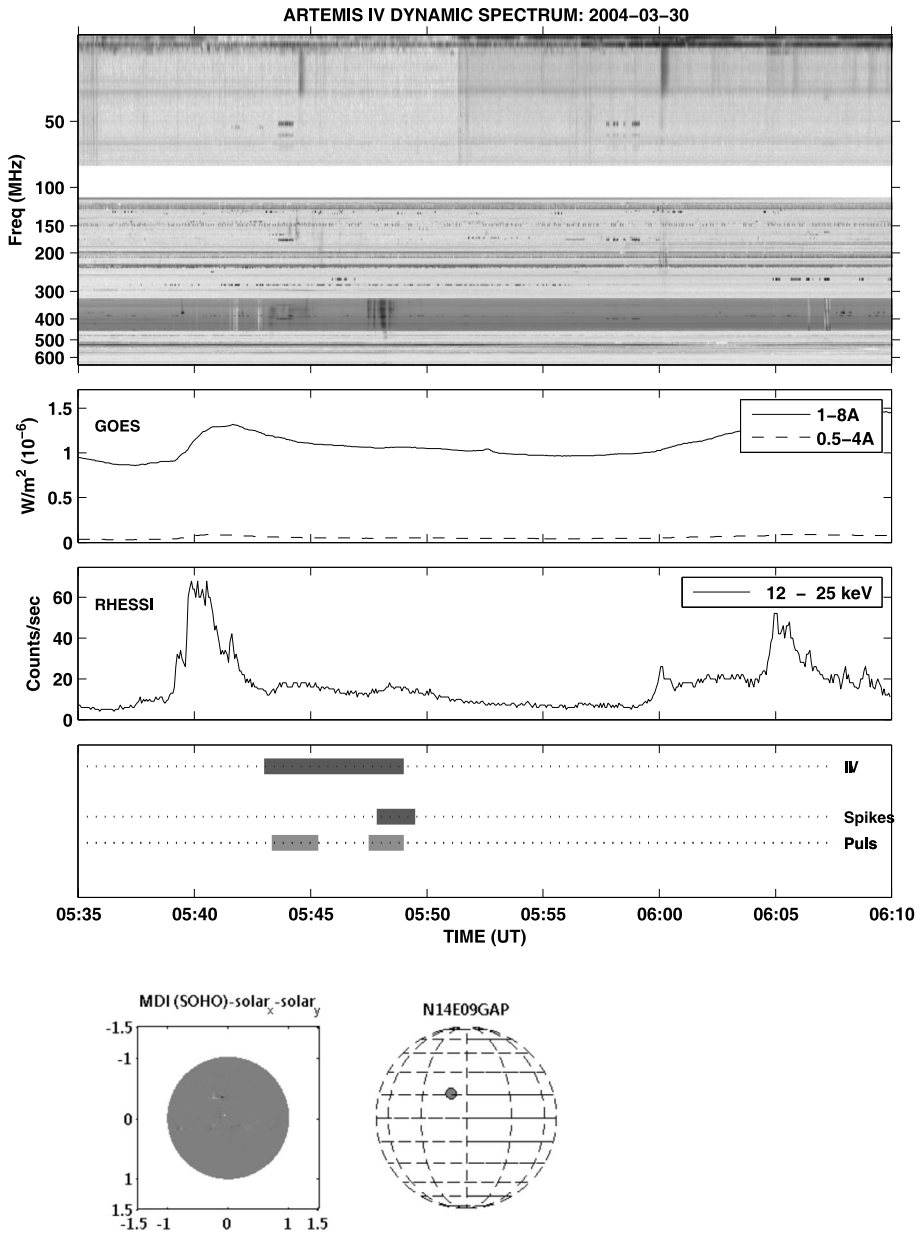


Figure 28 Event 18 on 30 March 2004.

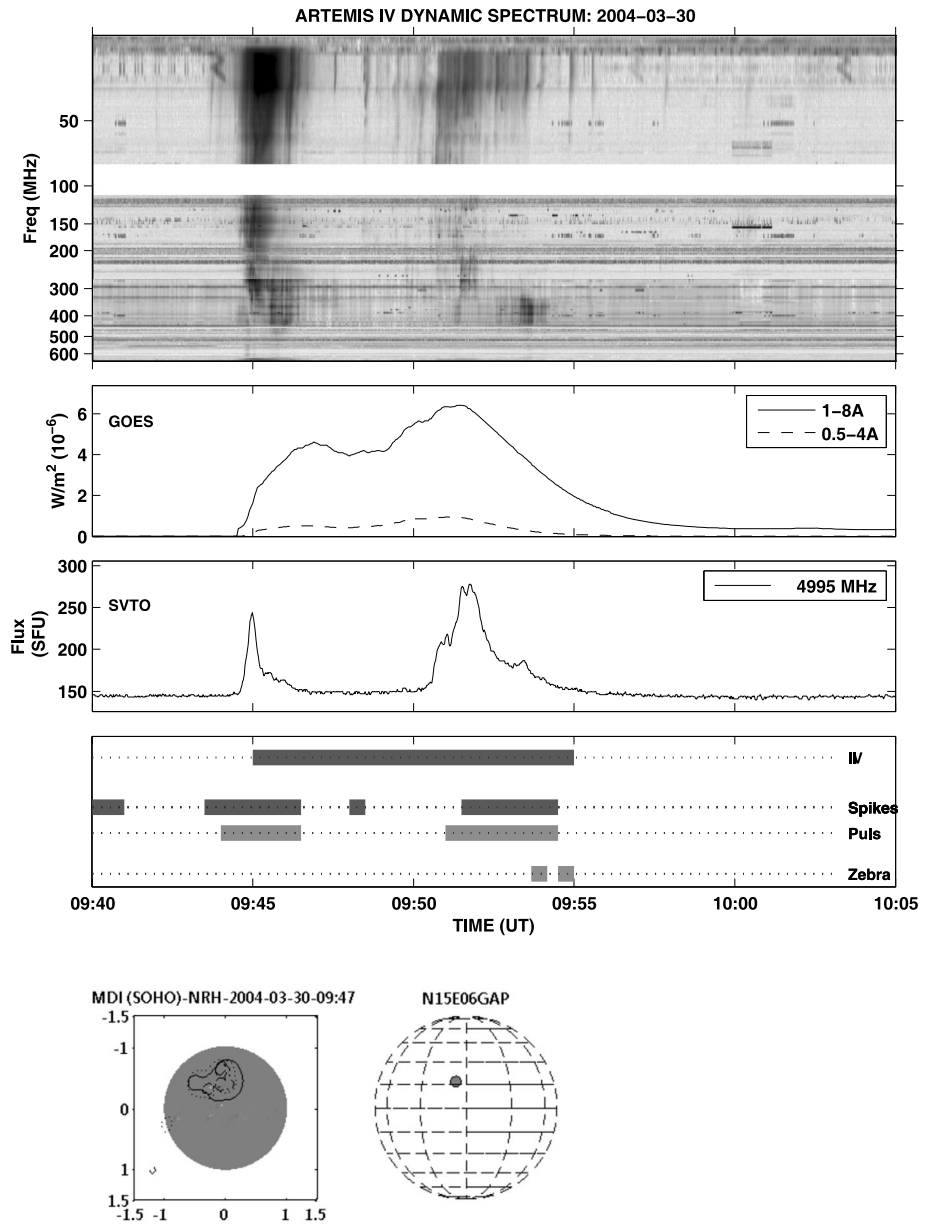


Figure 29 Event 19 on 30 March 2004.

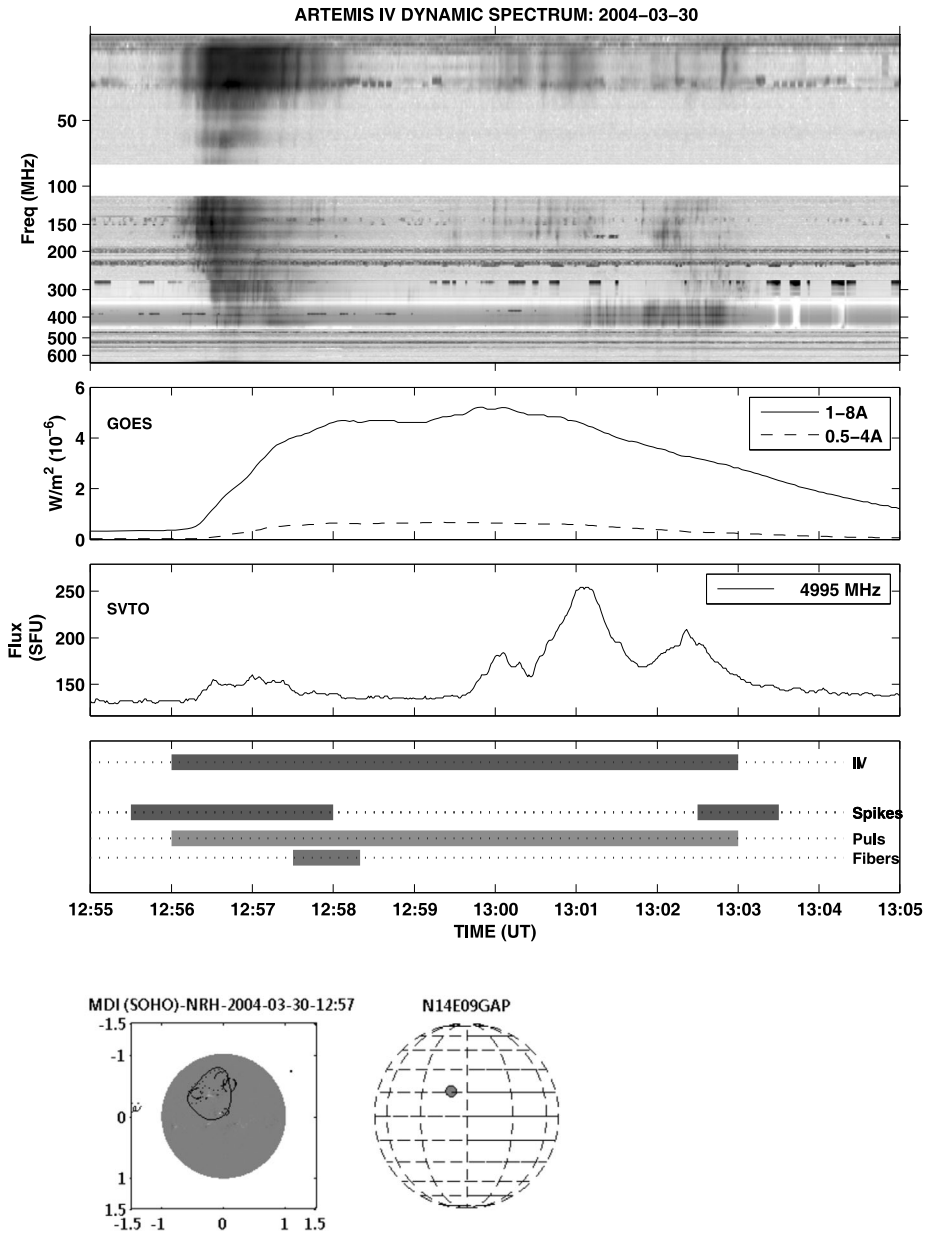


Figure 30 Event 20 on 30 March 2004.

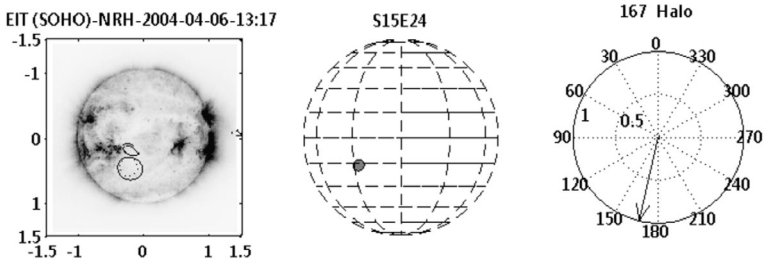
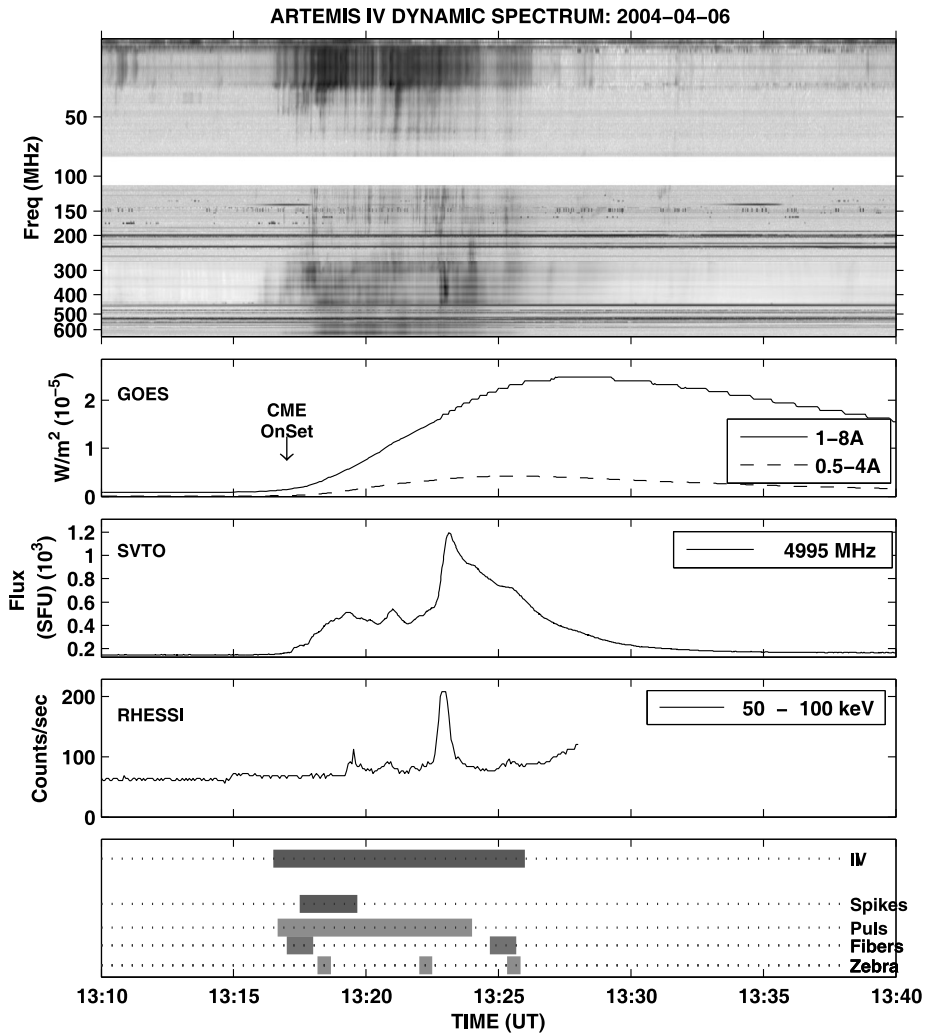


Figure 31 Event 21 on 06 April 2004.

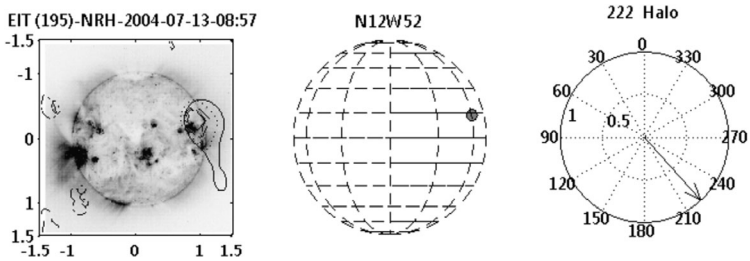
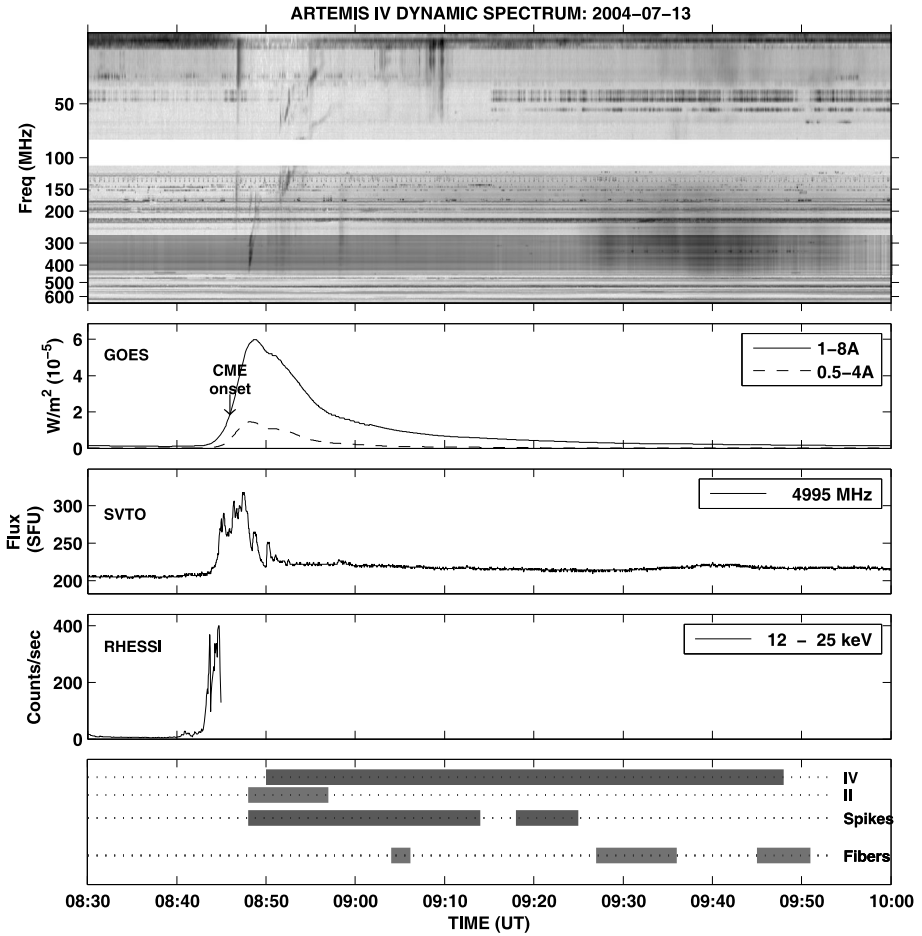


Figure 32 Event 22 on 13 July 2004.

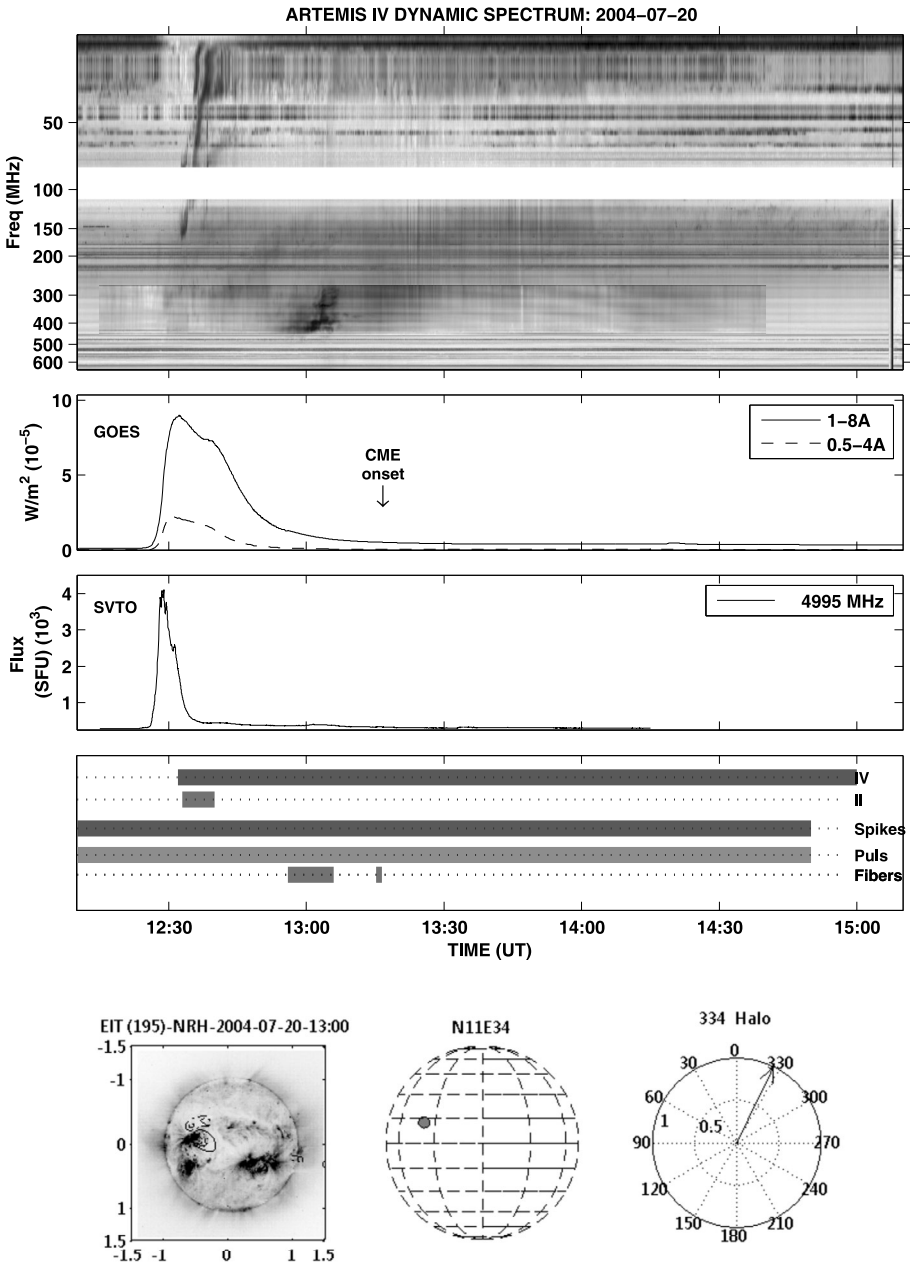


Figure 33 Event 23 on 20 July 2004.

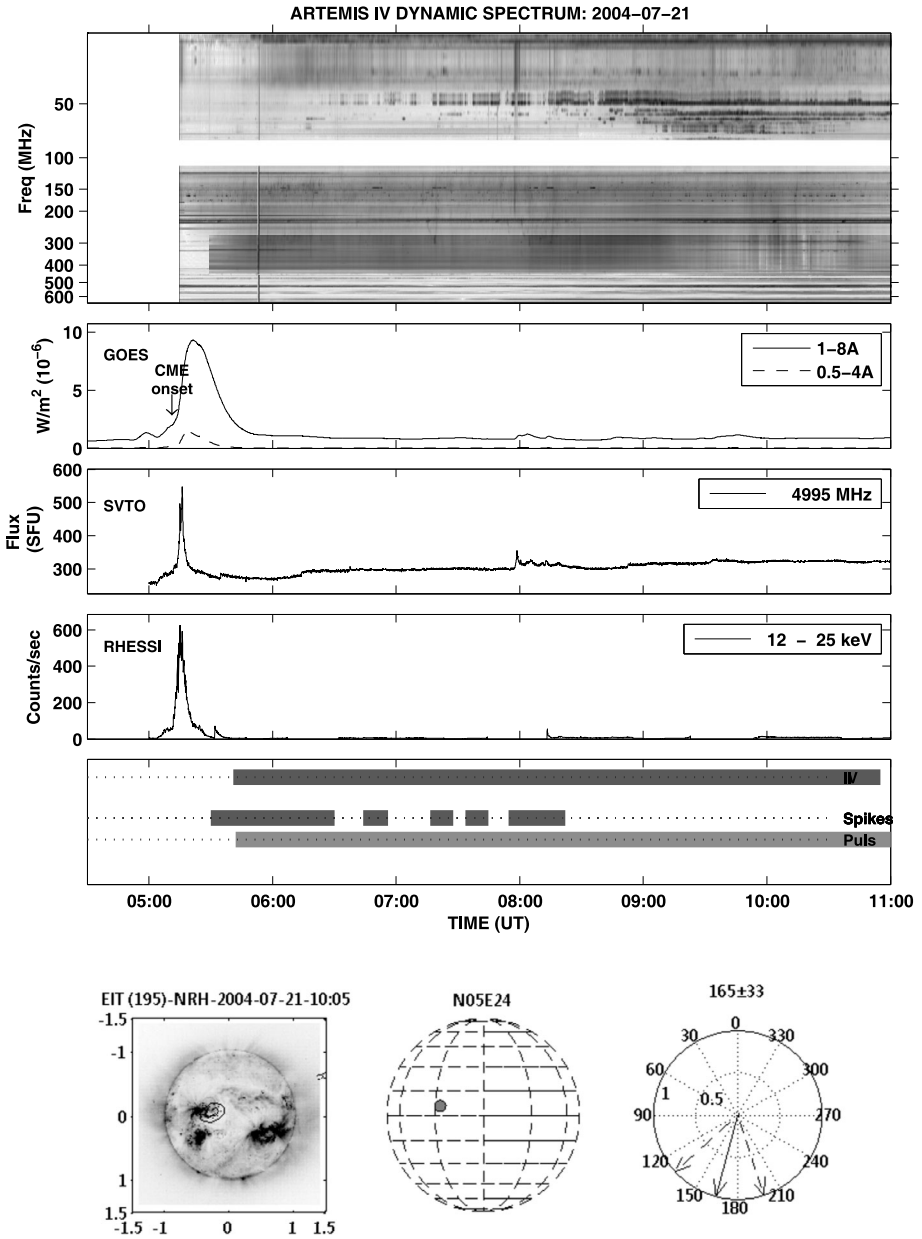


Figure 34 Event 24 on 21 July 2004.

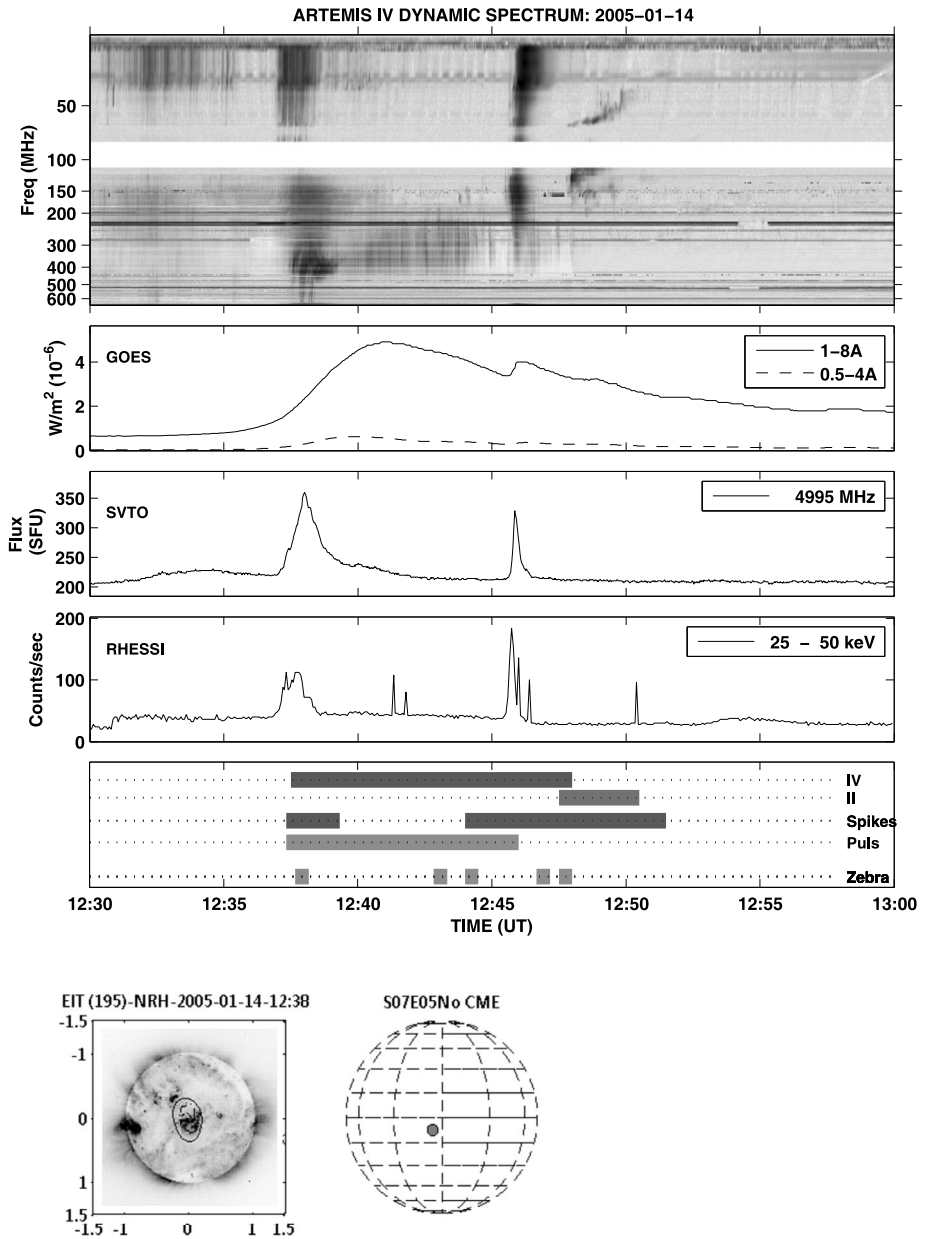


Figure 35 Event 25 on 14 January 2005.

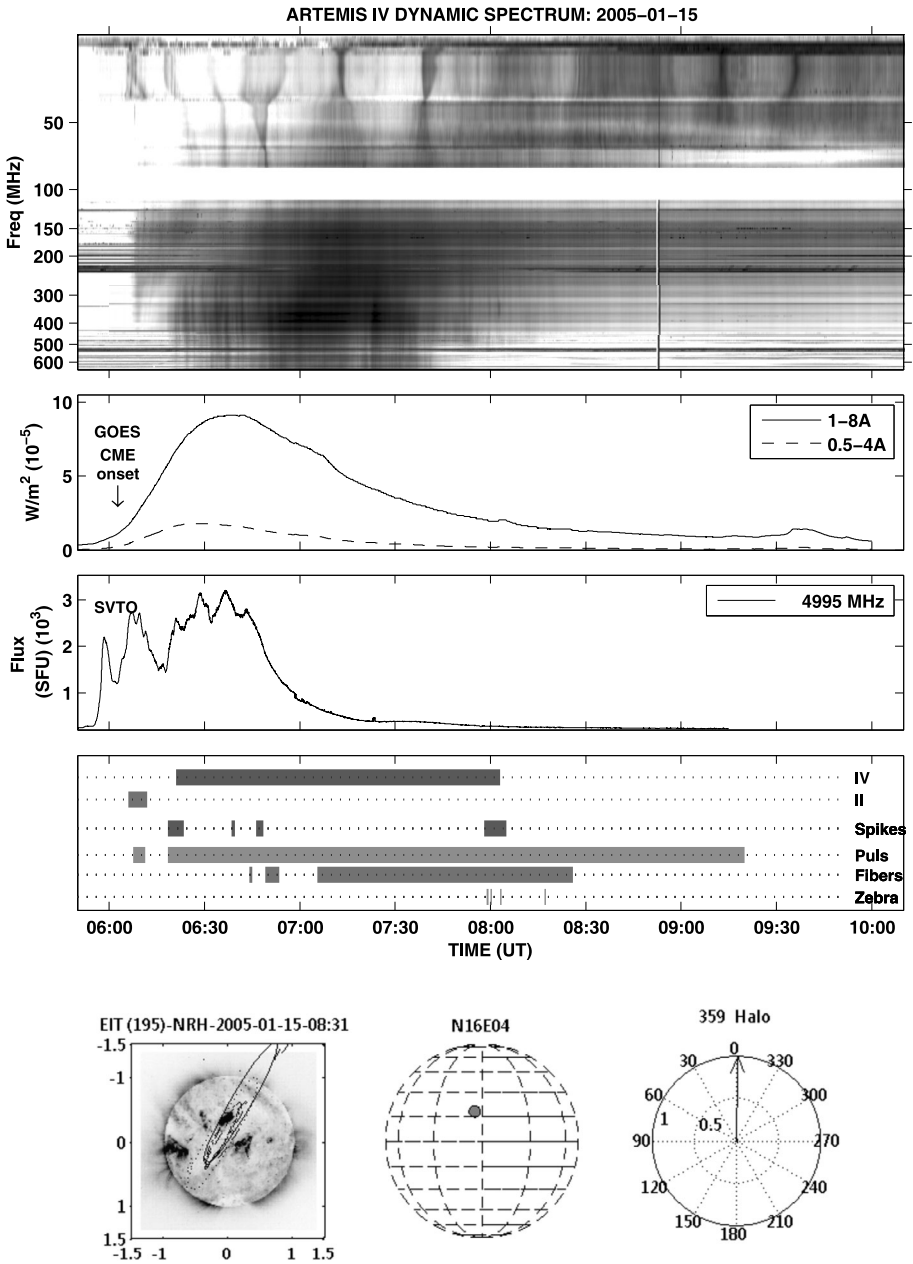


Figure 36 Event 26 on 15 January 2005.

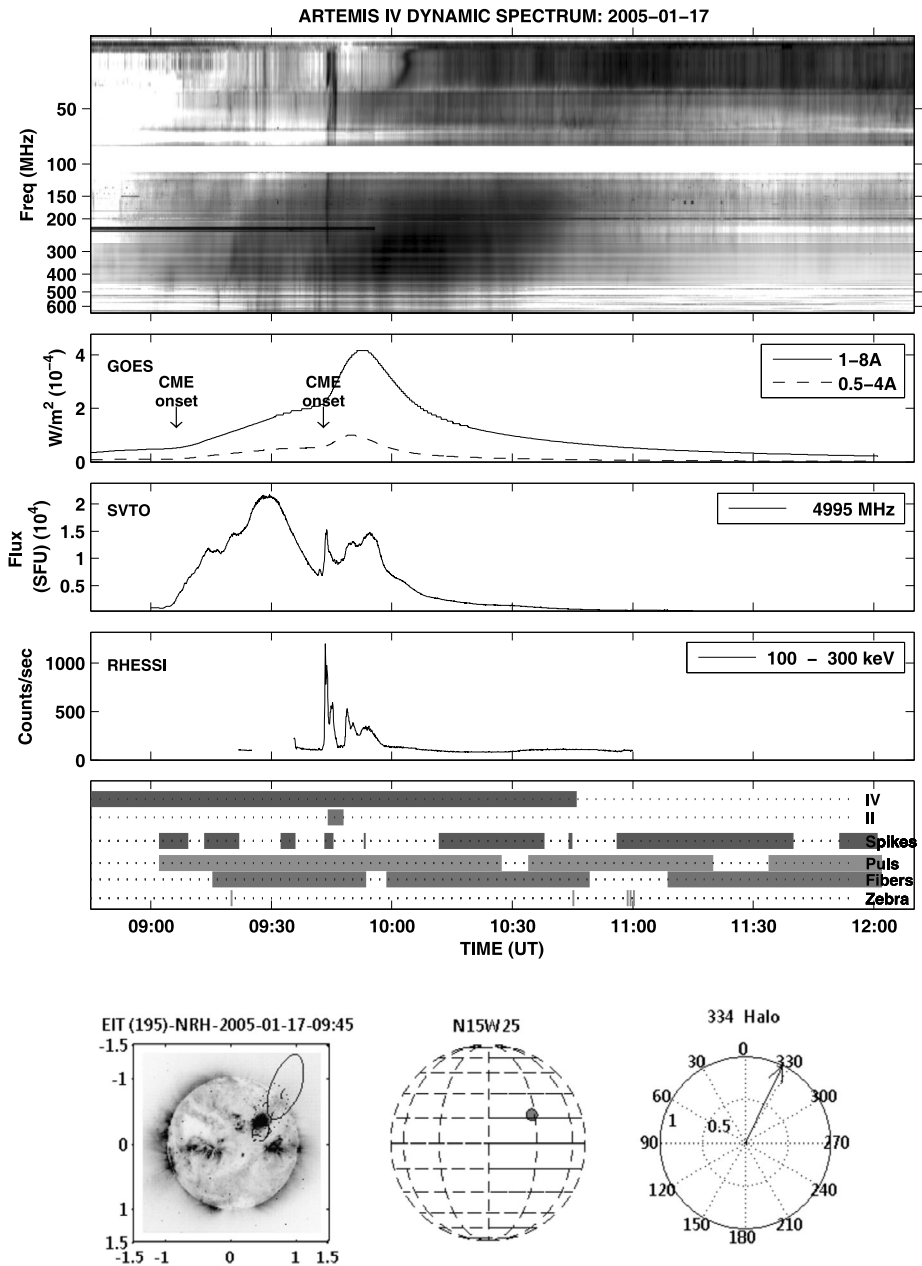


Figure 37 Event 27 on 17 January 2005.

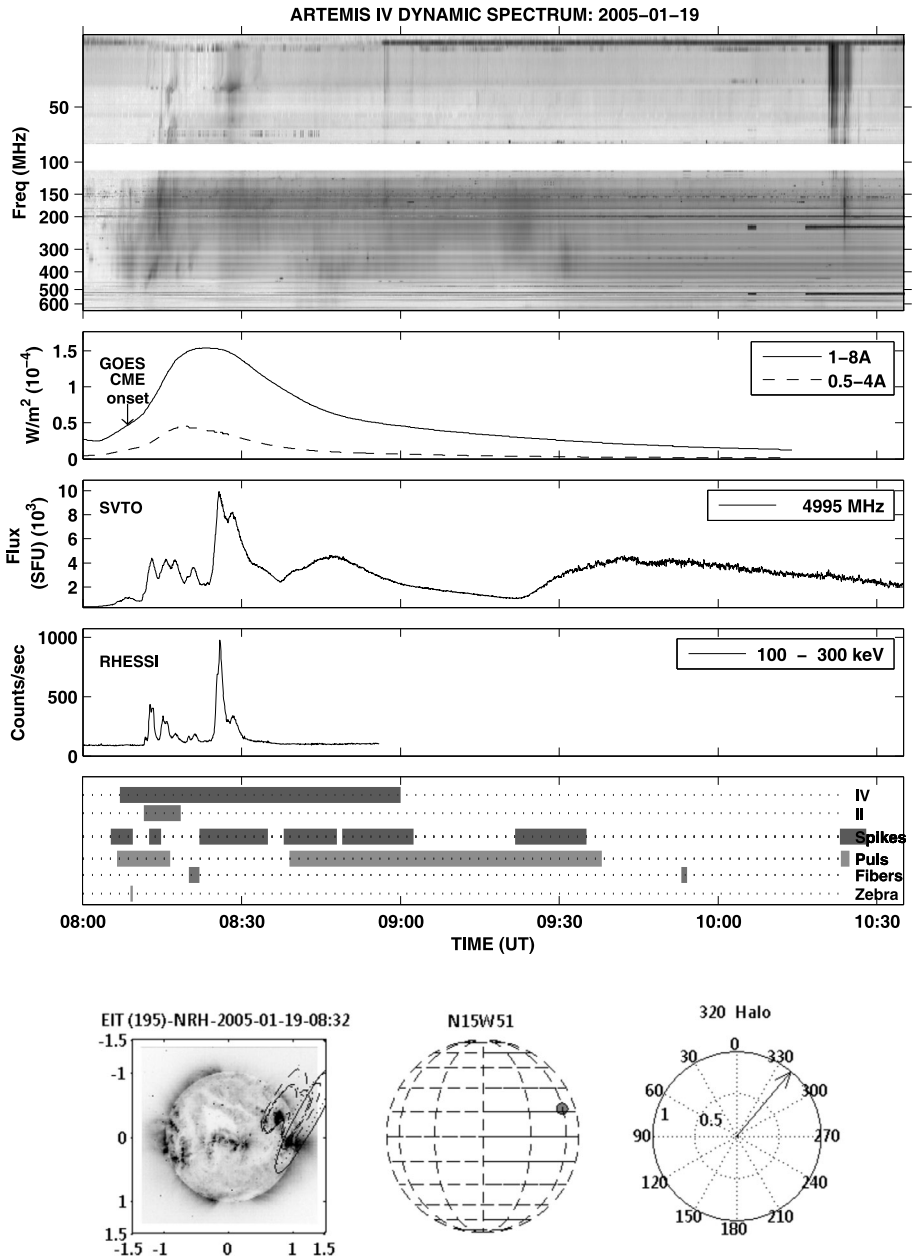


Figure 38 Event 28 on 19 January 2005.

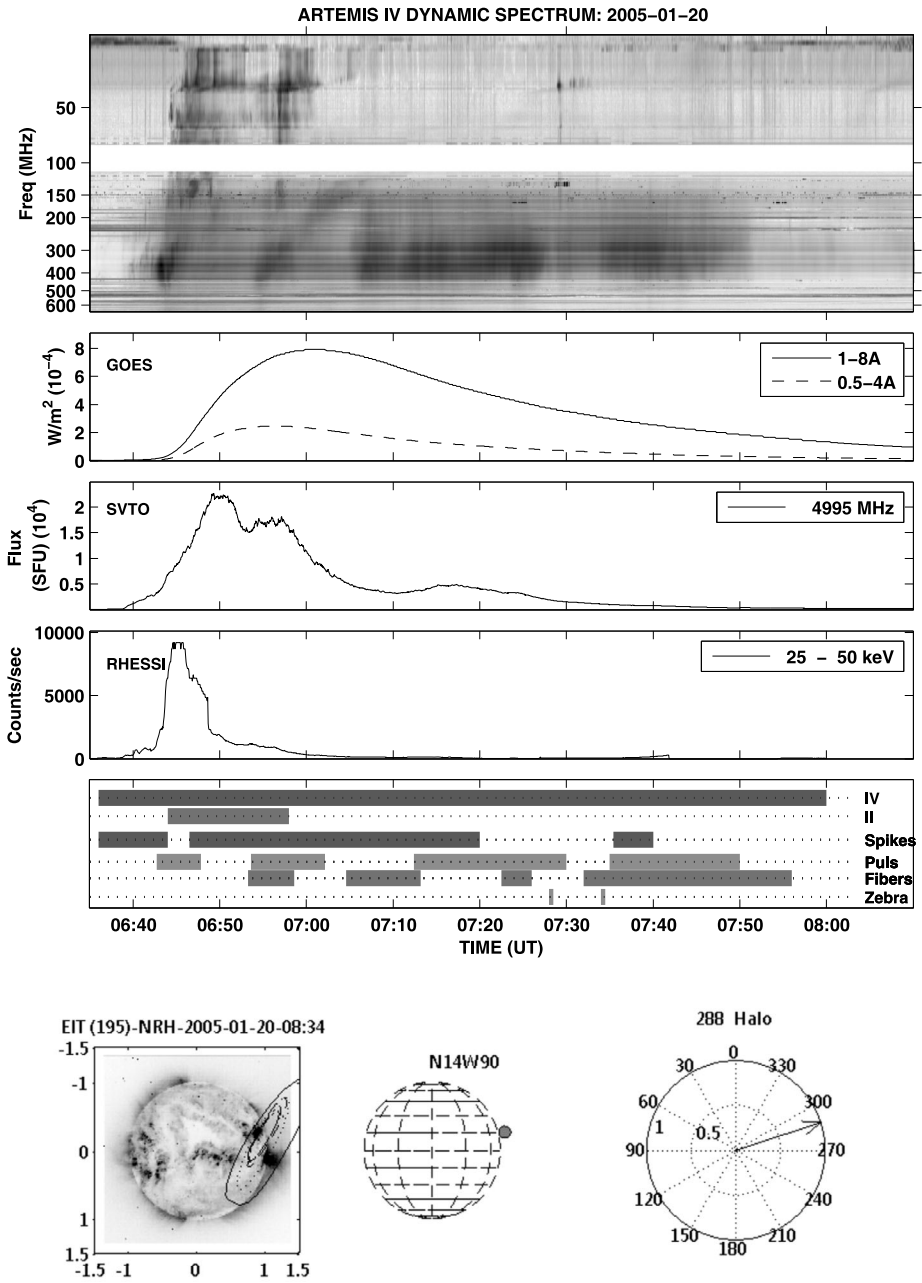


Figure 39 Event 29 on 20 January 2005.

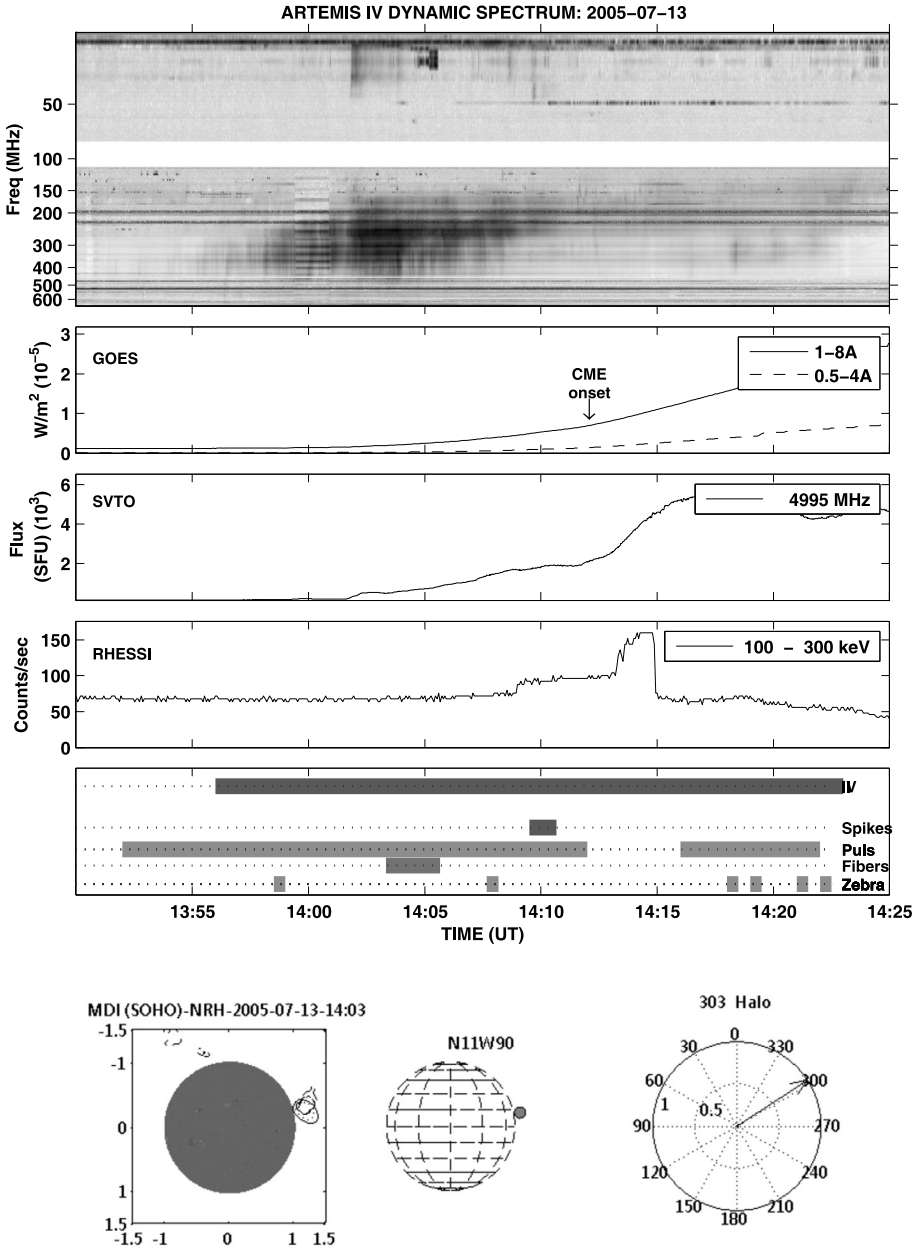


Figure 40 Event 30 on 13 July 2005.

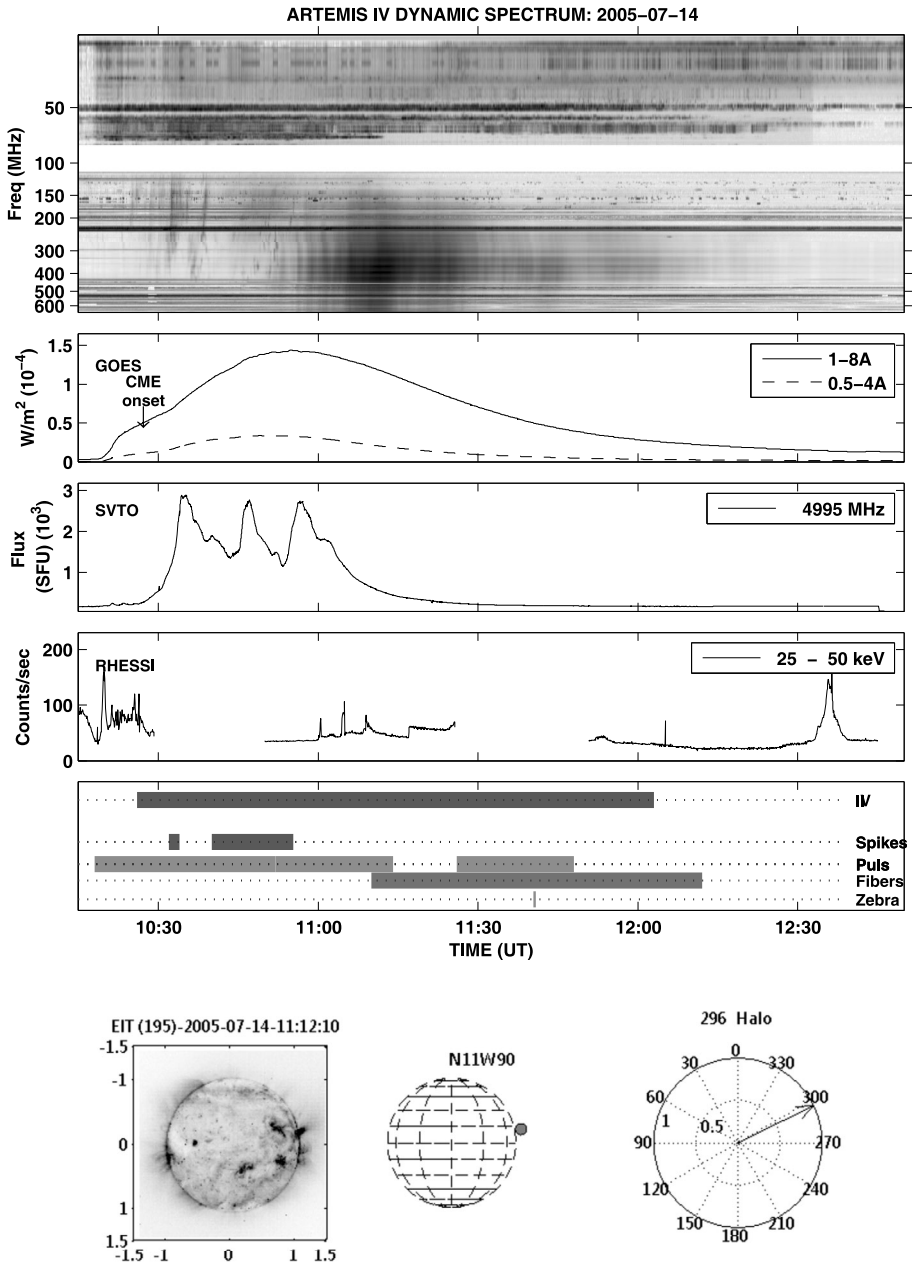


Figure 41 Event 31 on 14 July 2005.

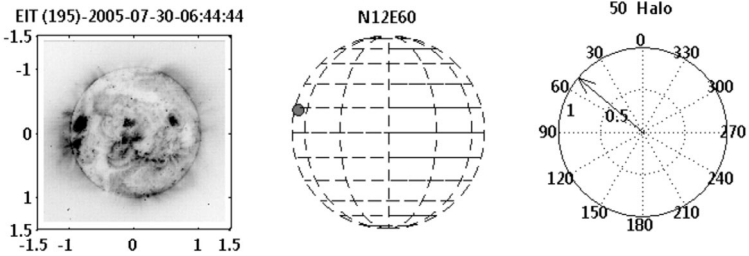
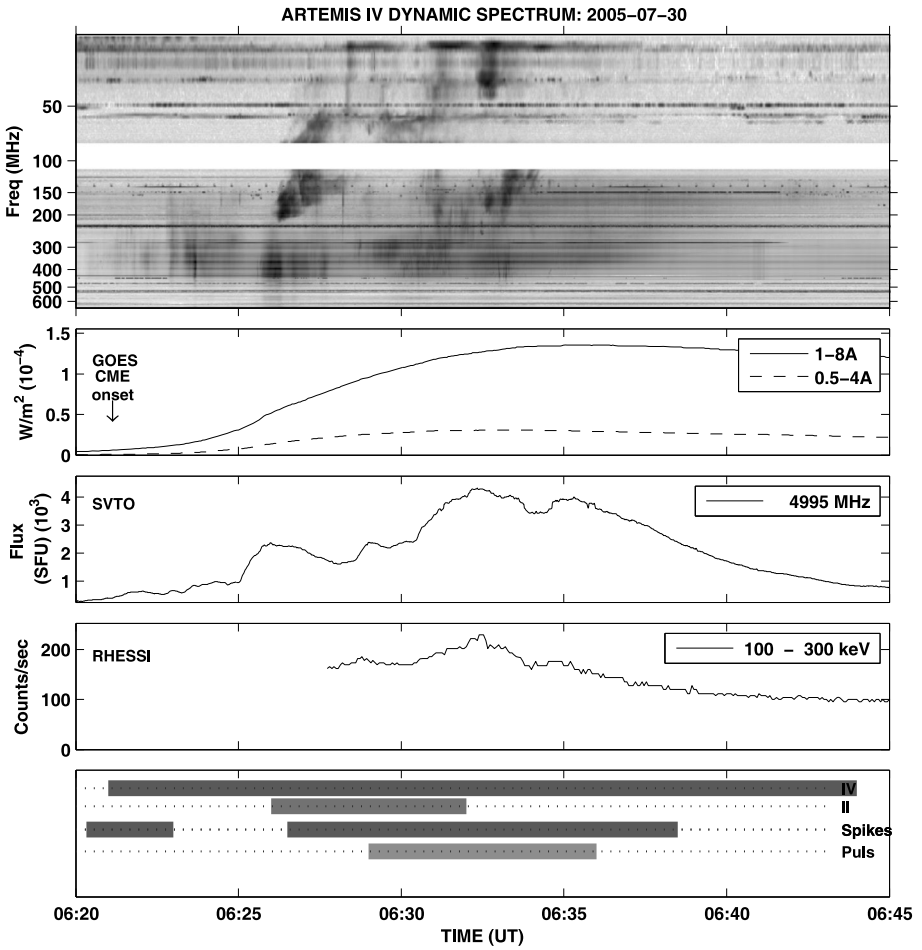


Figure 42 Event 32 on 30 July 2005.

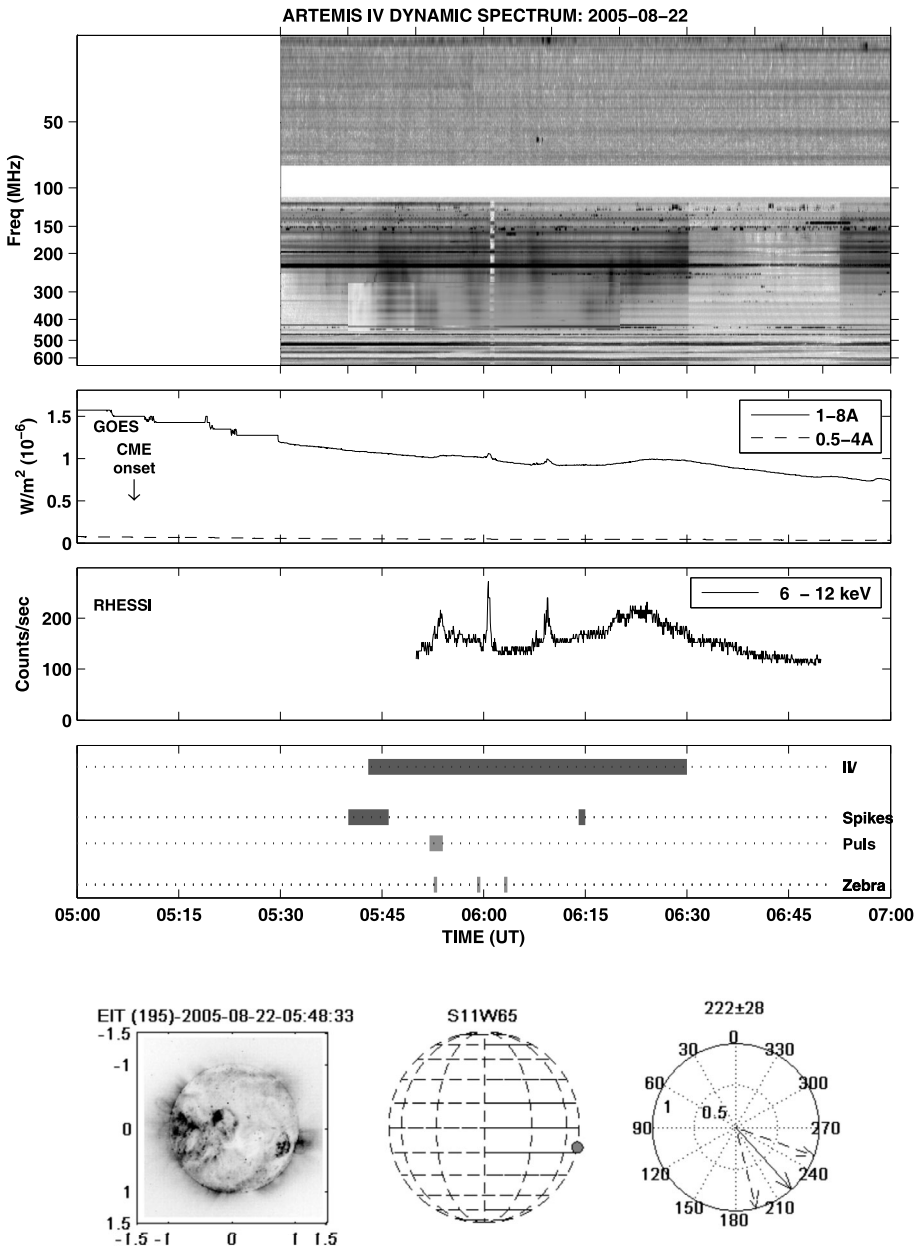
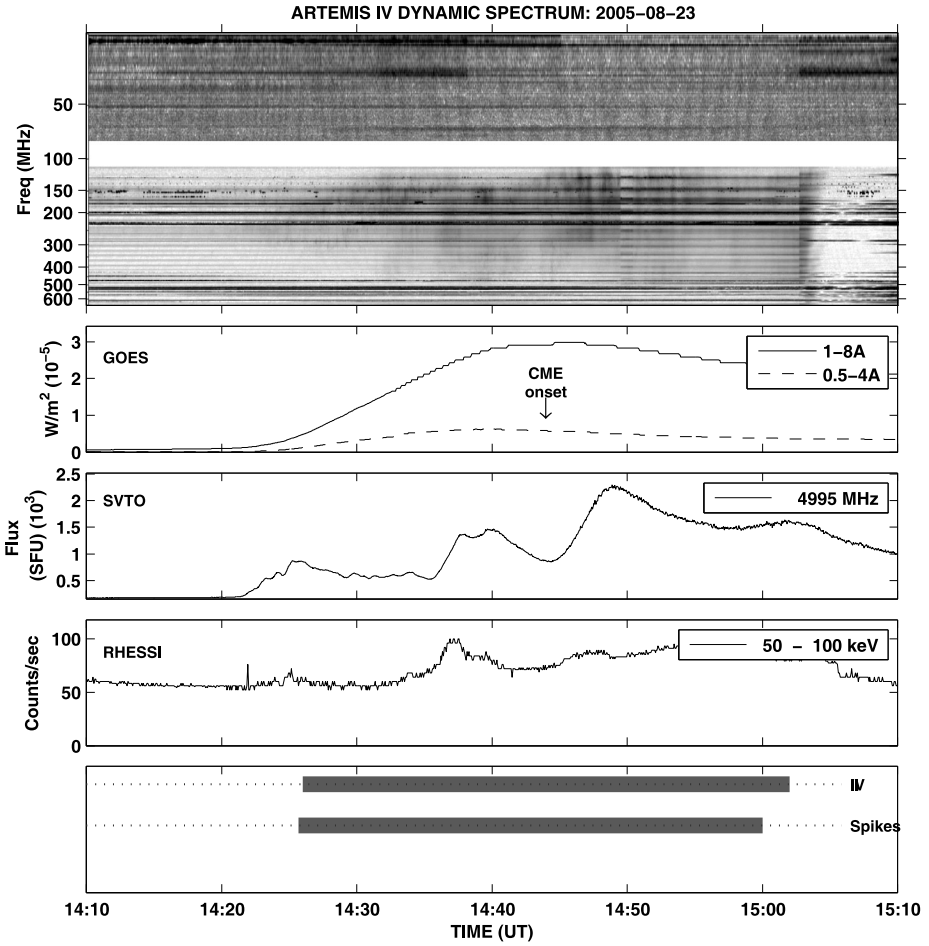


Figure 43 Event 33 on 22 August 2005.



EIT (195)-NRH-2005-08-23-14:51

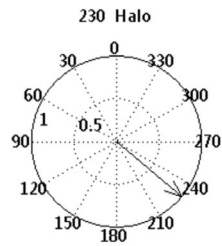
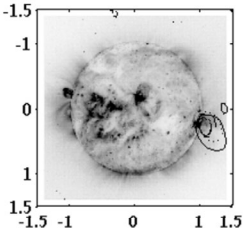


Figure 44 Event 34 on 23 August 2005.

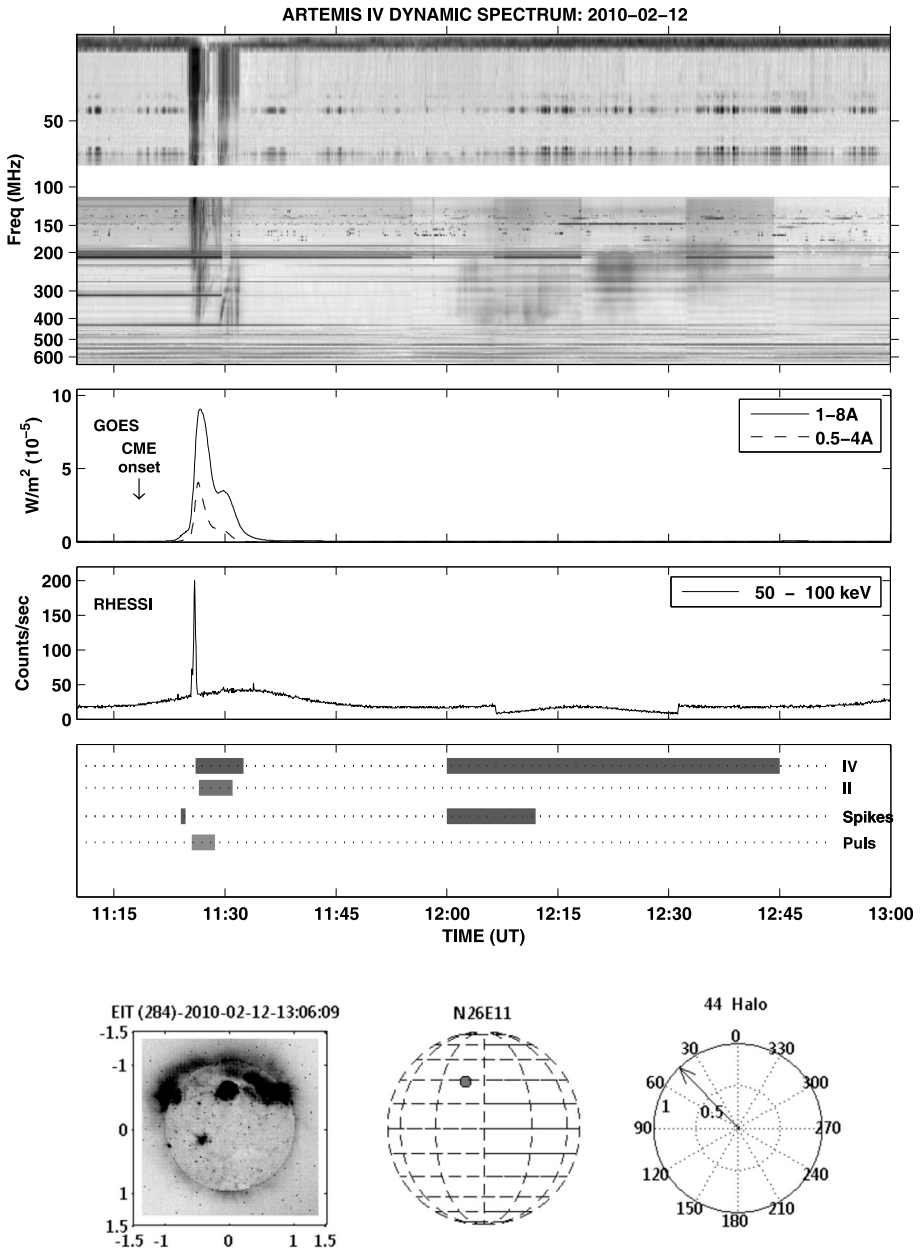


Figure 45 Event 35 on 12 February 2010.

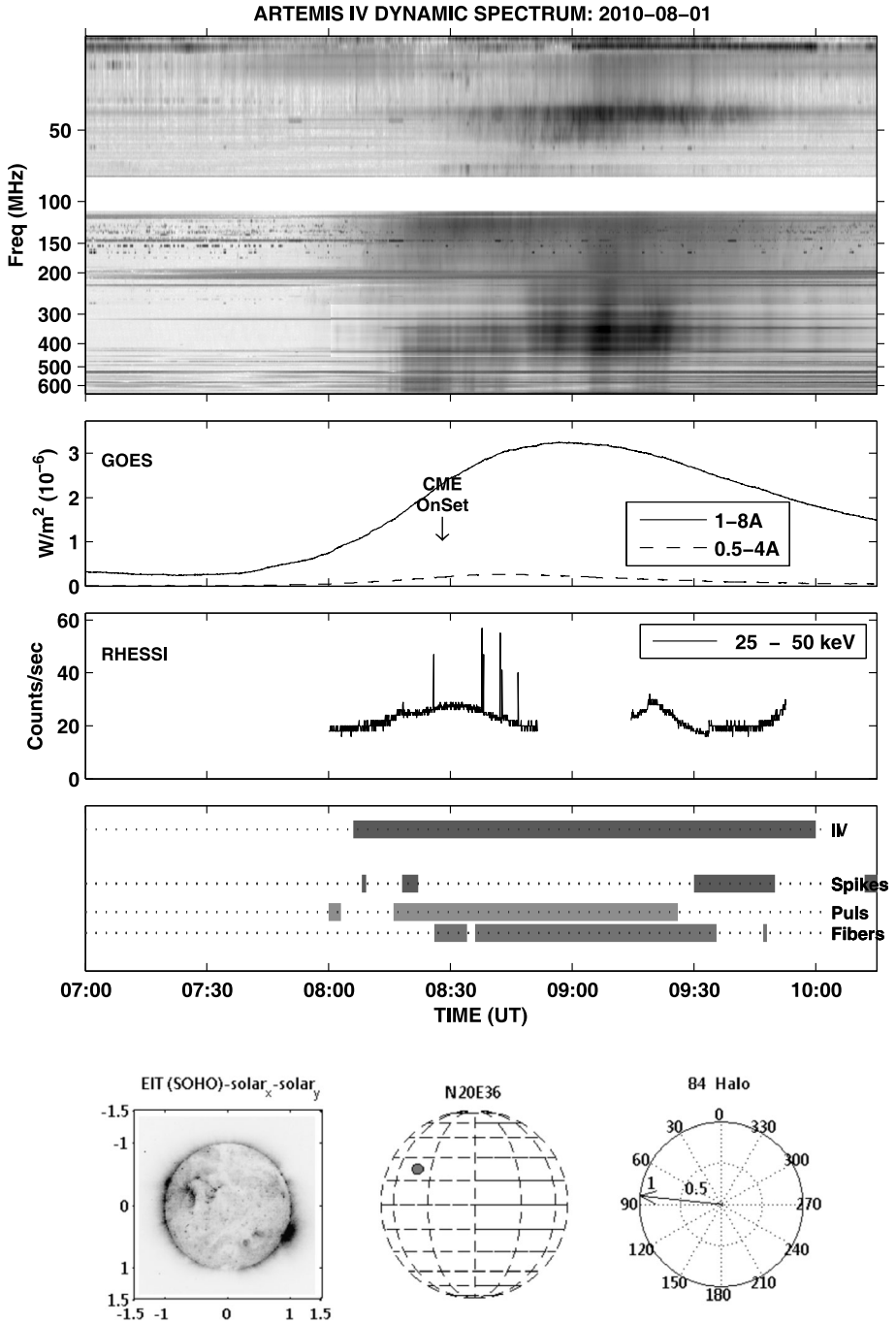


Figure 46 Event 36 on 01 August 2010.

References

- Allaart, M.A.F., van Nieuwkoop, J., Slottje, C., Sondaar, L.H.: 1990, *Solar Phys.* **130**, 183.
- Aurass, H.: 2007, *Adv. Space Res.* **39**, 1407.
- Aurass, H., Klein, K.L., Zlotnik, E.Y., Zaitsev, V.V.: 2003, *Astron. Astrophys.* **410**, 1001.
- Aurass, H., Rausche, G., Mann, G., Hofmann, A.: 2005, *Astron. Astrophys.* **435**, 1137.
- Bárta, M., Karlický, M.: 2005, *Hvar Obs. Bull.* **29**, 205.
- Benz, A.O.: 2003, In: Klein, L. (ed.) *Energy Conversion and Particle Acceleration the Solar Corona, Lecture Notes Phys.* **612**, Springer, Berlin, 80.
- Benz, A.O., Csillaghy, A., Aschwanden, M.J.: 1996, *Astron. Astrophys.* **309**, 291.
- Benz, A.O., Mann, G.: 1998, *Astron. Astrophys.* **333**, 1034.
- Benz, A.O., Perret, H., Saint-Hilaire, P., Zlobec, P.: 2006, *Adv. Space Res.* **38**, 951.
- Bernold, T.: 1980, *Astron. Astrophys. Suppl.* **42**, 43.
- Bouratzis, C., Preka-Papadema, P., Hillaris, A., Tsitsipis, P., Kontogeorgos, A., Kurt, V., Moussas, X.: 2010, *Solar Phys.* **267**, 343.
- Brueckner, G.E., Howard, R.A., Koomen, M.J., Korendyke, C.M., Michels, D.J., Moses, J.D., et al.: 1995, *Solar Phys.* **162**, 357.
- Caroubalos, C., Maroulis, D., Patavalis, N., Bougeret, J.L., Dumas, G., Perche, C., et al.: 2001, *Exp. Astron.* **11**, 23.
- Caroubalos, C., Hillaris, A., Bouratzis, C., Alissandrakis, C.E., Preka-Papadema, P., Polygiannakis, J., et al.: 2004, *Astron. Astrophys.* **413**, 1125.
- Caroubalos, C., Alissandrakis, C.E., Hillaris, A., Preka-Papadema, P., Polygiannakis, J., Moussas, X., et al.: 2006, In: Solomos, N. (ed.) *Recent Adv. Astron. Astrophys., Am. Inst. Phys.* **CS-848**, 864.
- Chen, B., Bastian, T.S., Gary, D.E., Jing, J.: 2011, *Astrophys. J.* **736**, 64.
- Chernov, G.P.: 1990, *Solar Phys.* **130**, 75.
- Chernov, G.P.: 2005, *Plasma Phys. Rep.* **31**, 314.
- Chernov, G.P.: 2006, *Space Sci. Rev.* **127**, 195. DOI.
- Chernov, G.P.: 2008, *Astron. Lett.* **34**, 486.
- Chernov, G.P., Yan, Y.H., Fu, Q.J.: 2003, *Astron. Astrophys.* **406**, 1071.
- Chernov, G.P., Markeev, A.K., Poquerusse, M., Bougeret, J.L., Klein, K.L., Mann, G., Aurass, H., Aschwanden, M.J.: 1998, *Astron. Astrophys.* **334**, 314.
- Chernov, G.P., Kaiser, M.L., Bougeret, J.L., Fomichev, V.V., Gorgutsa, R.V.: 2007, *Solar Phys.* **241**, 145.
- Delaboudinière, J.P., Artzner, G.E., Brunaud, J., Gabriel, A.H., Hochedez, J.F., Millier, F., et al.: 1995, *Solar Phys.* **162**, 291.
- Elgaroy, O.: 1986, *Solar Phys.* **104**, 41.
- Fárník, F., Garcia, H., Karlický, M.: 2001, *Solar Phys.* **201**, 357.
- Fernandes, F.C.R., Krishan, V., Andrade, M.C., Cecatto, J.R., Freitas, D.C., Sawant, H.S.: 2003, *Adv. Space Res.* **32**, 2545.
- Fishman, G.J., Meegan, C.A., Parnell, T.A., Wilson, R.B.: 1982, In: Lingenfelter, R.E., Hudson, H.S., Worrall, D.M. (eds.) *Gamma Ray Transients and Related Astrophys. Phenomena, Am. Inst. Phys.* **CS-77**, 443.
- Fishman, G.J., Meegan, C.A., Parnell, T.A., Wilson, R.B., Paciesas, W.: 1984, Woosley, S.E. (ed.): *Am. Inst. Phys.* **CS-115**, 651.
- Fu, Q.J., Yan, Y.H., Liu, Y.Y., Wang, M., Wang, S.J.: 2004, *Chin. J. Astron. Astrophys.* **4**, 176.
- Gopalswamy, N., Yashiro, S., Michalek, G., Stenborg, G., Vourlidas, A., Freeland, S., Howard, R.: 2009, *Earth Moon Planets* **104**, 295.
- Güdel, M., Benz, A.O.: 1988, *Astron. Astrophys. Suppl.* **75**, 243.
- Guidice, D.A., Cliver, E.W., Barron, W.R., Kahler, S.: 1981 In: *Bull. Amer. Astron. Soc.* **13**, 553.
- Hillarlis, A., Malandraki, O., Klein, K.L., Preka-Papadema, P., Moussas, X., Bouratzis, C., Mitsakou, E., Tsitsipis, P., Kontogeorgos, A.: 2011, *Solar Phys.* **273**, 493.
- Isliker, H., Benz, A.O.: 1994, *Astron. Astrophys. Suppl.* **104**, 145.
- Jiříčka, K., Karlický, M., Mészárosová, H.: 2002, In: Sawaya-Lacoste, H. (ed.) *Solspa 2001, Proc. Second Solar Cycle and Space Weather Euroconference, ESA SP-477*, 351.
- Jiříčka, K., Karlický, M., Mészárosová, H., Snížek, V.: 2001, *Astron. Astrophys.* **375**, 243.
- Karlický, M., Mészárosová, H., Jelínek, P.: 2013, *Astron. Astrophys.* **550**, A1.
- Karlický, M., Bárta, M., Jiříčka, K., Mészárosová, H., Sawant, H.S., Fernandes, F.C.R., Cecatto, J.R.: 2001, *Astron. Astrophys.* **375**, 638.
- Kerdran, A., Delouis, J.M.: 1997, In: Trotter, G. (ed.) *Coronal Phys. from Radio and Space Observations, Lecture Notes Phys.* **483**, Springer, Berlin, 192.
- Klassen, A., Aurass, H., Mann, G.: 2001, *Astron. Astrophys.* **370**, L41.
- Kontogeorgos, A., Tsitsipis, P., Moussas, X., Preka-Papadema, G., Hillaris, A., Caroubalos, C., et al.: 2006, *Space Sci. Rev.* **122**, 169.

- Kuijpers, J.: 1975, *Solar Phys.* **44**, 173.
- Lin, R.P. (The Hessi Team): 2001, In: Gladysheva, O.G., Kocharov, G.E., Kovaltsov, G.A., Usoskin, I.G. (eds.) *Internat. Cosmic Ray Conf.* **27**, 209.
- Lin, R.P., Dennis, B.R., Hurford, G.J., Smith, D.M., Zehnder, A., Harvey, P.R., et al.: 2002, *Solar Phys.* **210**, 3.
- Mann, G., Baumgaertel, K., Chernov, G.P., Karlický, M.: 1989, *Solar Phys.* **120**, 383.
- Messerotti, M., Zlobec, P., Padovan, S.: 2001, *Mem. Soc. Astron. Ital.* **72**, 633.
- Mészárosová, H., Karlický, M., Jiříčka, K.: 2005, *Hvar Obs. Bull.* **29**, 309.
- Mészárosová, H., Karlický, M., Sawant, H.S., Fernandes, F.C.R., Cecatto, J.R., de Andrade, M.C.: 2008, *Astron. Astrophys.* **491**, 555.
- Nindos, A., Aurass, H.: 2007, In: Klein, K.-L., MacKinnon, A.L. (eds.) *The High Energy Solar Corona: Waves, Eruptions, Particles, Lecture Notes Phys.* **725**, Springer, Berlin, 251.
- Nindos, A., Aurass, H., Klein, K.L., Trotter, G.: 2008, *Solar Phys.* **253**, 3.
- Ning, Z., Wu, H., Xu, F., Meng, X.: 2008, *Solar Phys.* **250**, 107.
- Oberoi, D., Everts, E.R., Rogers, A.E.E.: 2009, *Solar Phys.* **260**, 389.
- Pick, M., Vilmer, N.: 2008, *Astron. Astrophys. Rev.* **16**, 1.
- Rausche, G., Aurass, H., Mann, G., Karlický, M., Vocks, C.: 2007, *Solar Phys.* **245**, 327.
- Robbrecht, E., Berghmans, D.: 2004, *Astron. Astrophys.* **425**, 1097.
- Robbrecht, E., Berghmans, D., der Linden, R.A.M.V.: 2009, *Astrophys. J.* **691**(2), 1222.
- Slottje, C.: 1982, Ph.D. thesis, Univ. Utrecht.
- Webb, D.F., Howard, T.A.: 2012, *Living Rev. Solar Phys.* **9**, 3. DOI.
- Yashiro, S., Gopalswamy, N., St. Cyr, O.C., Lawrence, G., Michalek, G., Young, C.A., Plunkett, S.P., Howard, R.A.: 2001, *AGU Spring Meeting Abstracts*, 31.
- Yashiro, S., Gopalswamy, N., Michalek, G., St. Cyr, O.C., Plunkett, S.P., Rich, N.B., Howard, R.A.: 2004, *J. Geophys. Res.* **109**(18), 7105.
- Zhang, J., Dere, K.P., Howard, R.A., Kundu, M.R., White, S.M.: 2001, *Astrophys. J.* **559**, 452.
- Zlotnik, E.Y., Zaitsev, V.V., Aurass, H., Mann, G., Hofmann, A.: 2003, *Astron. Astrophys.* **410**, 1011.
- Zlotnik, E., Zaitsev, V., Aurass, H., Mann, G.: 2005, *Adv. Space Res.* **35**, 1774.
- Zlotnik, E., Zaitsev, V., Aurass, H., Mann, G.: 2009, *Solar Phys.* **255**, 273.